Supporting Information: Nickel (I) Aryl Species: Synthesis, Properties, and Catalytic Activity

Megan Mohadjer Beromi, Gourab Banerjee, Gary W Brudvig, Nilay Hazari*, and Brandon Q Mercado

The Department of Chemistry, Yale University, P. O. Box 208107, New Haven, Connecticut, 06520, USA. E-mail: nilay.hazari@yale.edu.

Table of Contents

SI. General Methods

Experiments were performed under an atmosphere of dinitrogen in an M-Braun glovebox or using standard Schlenk techniques, unless specified otherwise. Purging of the glovebox atmosphere was not performed between uses of pentane, benzene, toluene, diethyl ether, and THF; as such, trace amounts of the solvents may have been present in the box atmosphere and intermixed in the solvent bottles. All chemicals were used as received unless otherwise stated. Air- or moisture-sensitive liquids were transferred using stainless steel cannulae on a Schlenk line or in a glovebox. Solvents were dried via passage through a column of activated alumina and subsequently stored under dinitrogen. Deuterated solvents were obtained from Cambridge Isotope Laboratories. C_6D_6 and d_8-toluene were dried over sodium metal with benzophenone ketyl radical as an indicator. All deuterated solvents were vacuum-transferred prior to use. Powdered K_3PO_4 was purchased from Acros Organics, finely ground using a mortar and pestle, heated in an oven at 120 °C for at least 24 hours and stored in a glove box. NMR spectra were recorded on Agilent-400, -500 or -600 MHz spectrometers at ambient probe temperatures unless otherwise stated. Chemical shifts are reported in ppm, with respect to residual internal protio solvent for ^{1}H and ^{13}C NMR spectra and to an external standard for ^{31}P NMR spectra (85% H_3PO_4 at 0.0 ppm). Solution magnetic susceptibilities were determined by ^{1}H NMR spectroscopy via the Evans' method.[1] IR spectra were recorded in a glove box on a Bruker Alpha instrument equipped with Platinum-ATR attachment with a diamond-tip for solid-state measurements. Gas Chromatography was performed on a ThermoFisher Trace 1300 GC apparatus equipped with a flame ionization detector and a Supelco fused silica capillary column (5 Å molecular sieves, 30 m x 0.53 mm) using the following parameters: flow rate 1.23 mL/min constant flow, column temperature 50 °C (held for 5 min), 20 °C/min increase to 300 °C (held for 5 min), total time 22.5 min. GC yields were calculated based on calibration curves generated using the independently synthesized biaryl product of interest. 1-(4'-methoxyphenyl)naphthalene and 2-methyl-4'-methoxy-1,1'-biphenyl standards were synthesized using (XPhos)Pd(η^3-1-^{t}BuIndenyl)(Cl)[2] (XPhos = 2-Dicyclohexylphosphino-2',4',6'-triisopropylbiphenyl) or (IPr*^{OMe})Pd(η^3-1-^{t}BuIndenyl)(Cl)[2] (IPr*^{OMe} = N,N'-Bis(2,6-bis(diphenylmethyl)-4-methoxyphenyl)imidazol-2-ylidene) and compared to literature NMR data to check purity.[3] Naphthalen-1-yl sulfamate, 4-trifluoromethylphenyl sulfamate, 4-methoxyphenyl sulfamate, and TEMPOH were prepared according to literature procedures.[4] (dppf)Ni^{0}(C_2H_4) (**10**)[5] was prepared

according to literature precedent. X-Band EPR spectra were recorded on a Bruker ELEXSYS E500 EPR spectrometer equipped with a SHQ resonator and an Oxford ESR-900 helium-flow cryostat with the following settings: microwave frequency, 9.4 GHz; modulation frequency, 100 kHz; modulation amplitude, 10 G; sweep time, 84 s; conversion time, 41 ms; time constant 20 ms. 1 mM solutions of the samples of interest were prepared in the glovebox using toluene for a total of 200 μL of solution per tube. The tubes were sealed in the glovebox and immediately frozen in liquid nitrogen. Spectra were simulated using the "pepper" function in EasySpin version 5.0.3.[6] Robertson Microlit Laboratories, Inc. performed the elemental analyses (inert atmosphere).

SII. NMR Identification of Ni(I) Aryl Complexes

General Procedure for the NMR-Scale In Situ Synthesis of Ni(I) Aryl Complexes

To a J-Young tube containing a capillary of cobaltocene in C_6D_6 as well as a capillary of PPh_3 in C_6D_6 was added (dppf)Ni^{I}Br (**2**) (0.00316 mmol, 2.2 mg) and 500 µL of C_6D_6. The tube was capped and agitated until **2** had dissolved. The appropriate arylmagnesium bromide Grignard reagent (1.5 equiv, 0.00474 mmol) was added via micropipette, and the tube was capped tightly and agitated by inversion twice. ^{1}H and ^{31}P NMR spectra were immediately taken, with the following parameters used for ^{1}H NMR spectroscopy: nt=256 scans, d1=0.5 s, at=1.0 s, sweep width (-75, 75 ppm). The same procedure was followed when using (dppf)Ni^{I}Cl (**1**) as the starting material, and the resulting spectra are consistent with those observed when using **2** as the starting material.

NMR evidence for the new nickel(I) aryl species was primarily based on the ^{1}H NMR shift of the phenyl proton resonances on the phosphorus nuclei of the dppf ligand relative to the starting material (12.5 ppm). The ^{1}H NMR spectra showing the unique phenyl proton resonance used to identify each complex, except for (dppf)Ni^{I}(Ph) (**7**), are given in Figure S1. The lifetime of the *in-situ* formed nickel(I) aryl species was monitored by ^{1}H NMR spectroscopy until complete degradation of the resonances for (dppf)Ni^{I}(*o*-tolyl) (**4)**, (dppf)Ni^{I}(2,6-xylyl) (**5**), and (dppf)Ni^{I}(2,4,6-mesityl) (**6**) was observed. The data quantifying the extent of decomposition as a function of time for each complex is shown in Figure S2A. ^{1}H NMR spectroscopy was utilized to quantify the decay using the relative integrations between the cobaltocene internal standard and the phenyl proton resonance peak at various times. The complex **7** decayed too quickly to analyse using ^{1}H NMR spectroscopy, while the decay of **3** was extremely slow under the same conditions. Representative NMR spectra for tracking the decay of **5** are shown in Figure S2B.

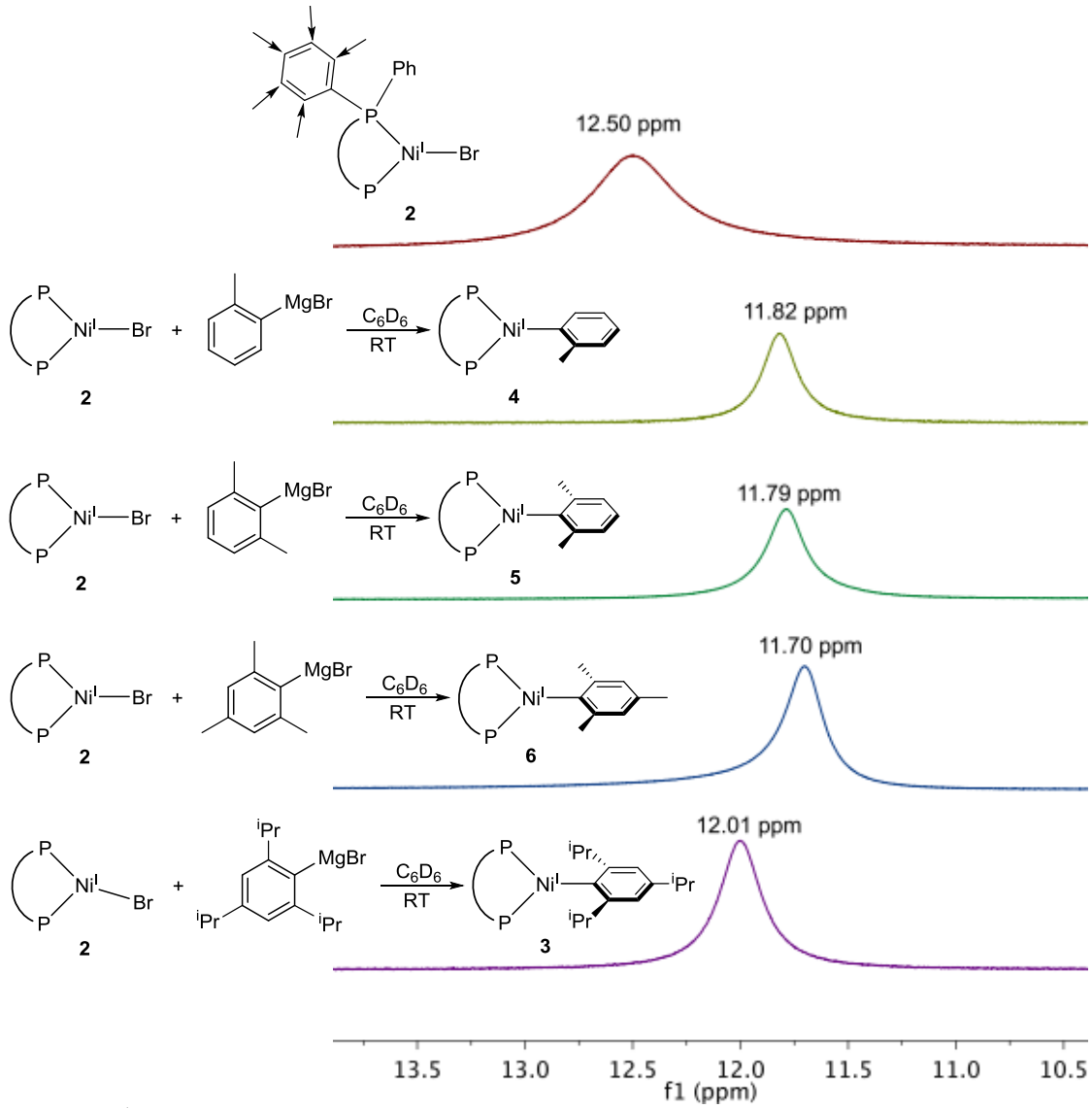

Figure S1. ^{1}H NMR spectra leading to the identification of unique nickel(I) aryl species. The chemical shifts of phenyl proton resonances (denoted with arrows in the structure of **2**) were compared to that of the starting material in each case. Chemical shifts were standardized to a cobaltocene internal standard.

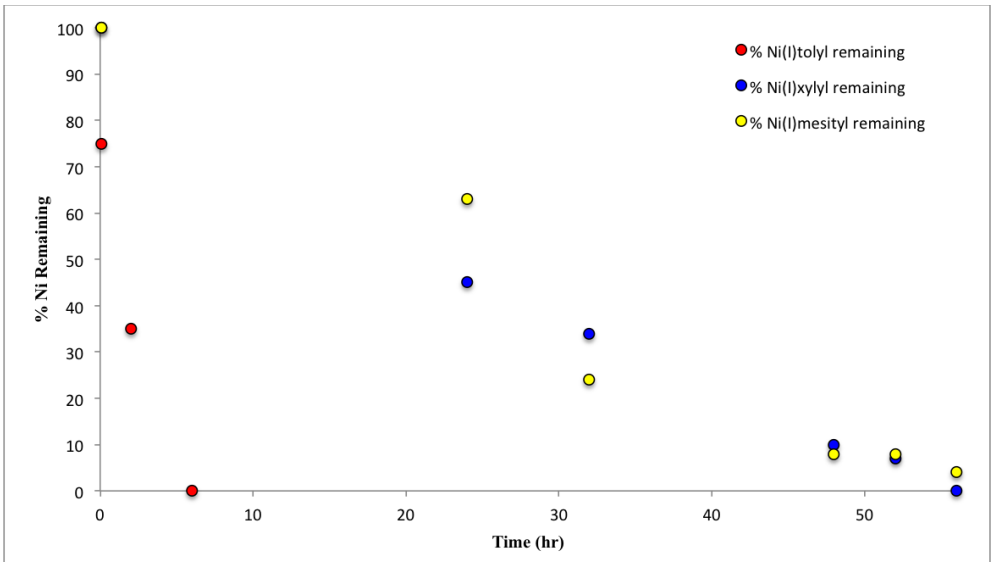

Figure S2A. Solution lifetimes of *in-situ* formed nickel(I) aryl species determined by ^{1}H NMR spectroscopy.

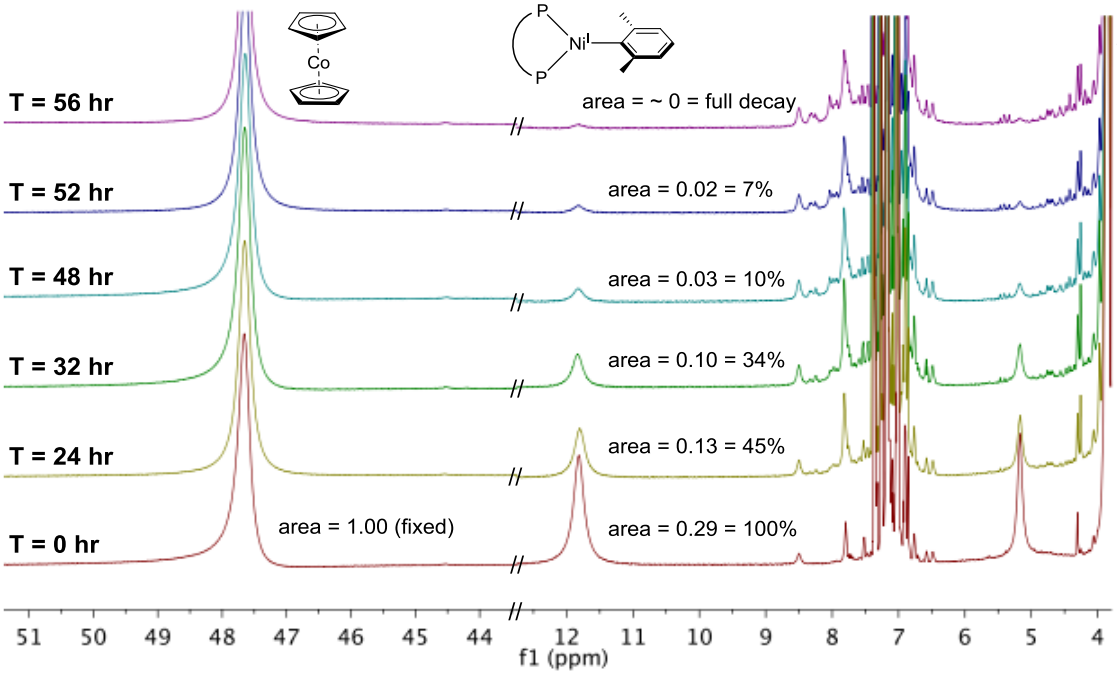

Figure S2B. Representative ^{1}H NMR spectra for the determination of the solution lifetime of (dppf)Ni^{I}(2,6-xylyl) **(5)**.

SIII. Synthesis and Characterization of (dppf)Ni^{I}(2,4,6-$^{i}Pr_3C_6H_2$) (3) and (dppf)Ni^{II}(2,4,6-$^{i}Pr_3C_6H_2$)(Br) (9)

*Synthesis and Characterization of **3***

To a 100 mL Schlenk flask containing a stir bar was added (dppf)Ni^{I}Cl (**1**) (0.308 mmol, 200 mg). The flask was sealed and taken out of the glovebox and attached to a Schlenk line. 30 mL of pentane was added via cannula transfer. 2,4,6-triisopropylphenylmagnesium bromide (5 equiv, 1.54 mmol, 3.08 mL) was then added using a gas-tight syringe. The solution was stirred vigorously at room temperature for 1 hour, after which the dark orange filtrate was separated from a grey solid by filtration using a filter cannula. The solvent was removed from the filtrate *in vacuo* to afford an orange, sticky residue. The residue was dissolved in minimal diethyl ether and recrystallized at -35 °C in a glovebox freezer to afford bright orange crystals of **3** (43% yield, 110 mg). Crystals suitable for X-ray diffraction were grown from a concentrated solution in diethyl ether at -35 °C.

^{1}H NMR (500 MHz, C_6D_6): δ 12.00 (br s, 10H); 5.27 (br s, 8H); 4.38 (br s, 15 H); 2.79 (br s, 9H); 1.55 (br s, 6H); 1.05 (br s, 3H). The full spectrum of **3** is provided in Figure S3A.

ATR-IR (cm^{-1}): 3049, 3014, 2946, 2920, 2857, 1476, 1458, 1433, 1162, 1095, 1023, 818, 740, 693, 634, 536, 506, 485, 453, 422. The full ATR-IR spectrum of **3** is provided in Figure S3B.

Magnetic susceptibility (C_6D_6): 1.643 μ_B.

An authentic X-band EPR spectrum of **3** was recorded in frozen toluene and is shown in Figure S3C. The EPR parameters specific to the experiment as well as the simulation parameters are provided in the caption of Figure S3C. The residual signal not covered by the simulation is included in grey to indicate that the missing fit cannot be attributed to other nickel-containing paramagnetic species.

No elemental analysis was obtained on this compound due to its instability.

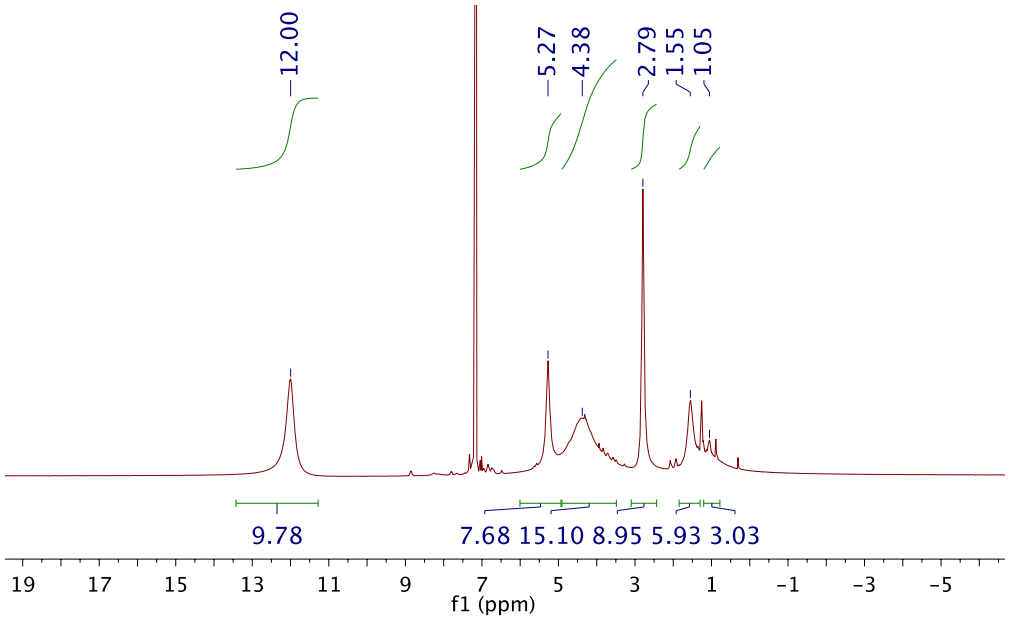

Figure S3A. ^{1}H NMR spectrum of (dppf)Ni(2,4,6-^{i}Pr$_3$C$_6$H$_2$) (**3**) in C_6D_6.

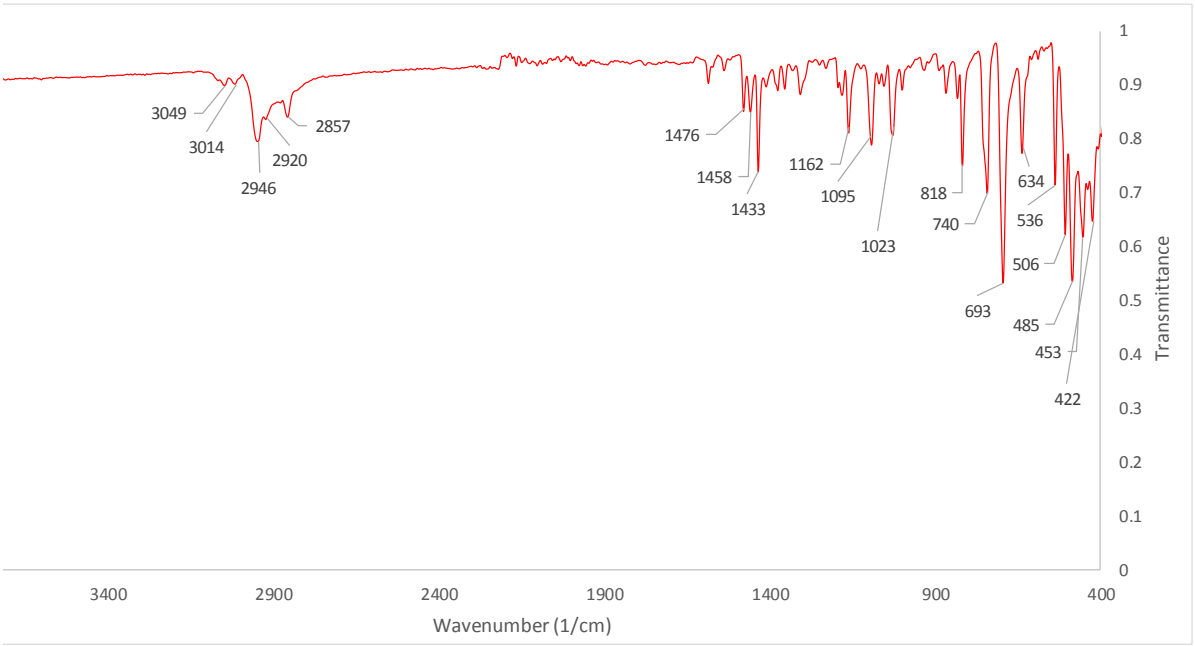

Figure S3B. Solid-state ATR-IR spectrum of (dppf)Ni(2,4,6-^{i}Pr$_3$C$_6$H$_2$) (**3**).

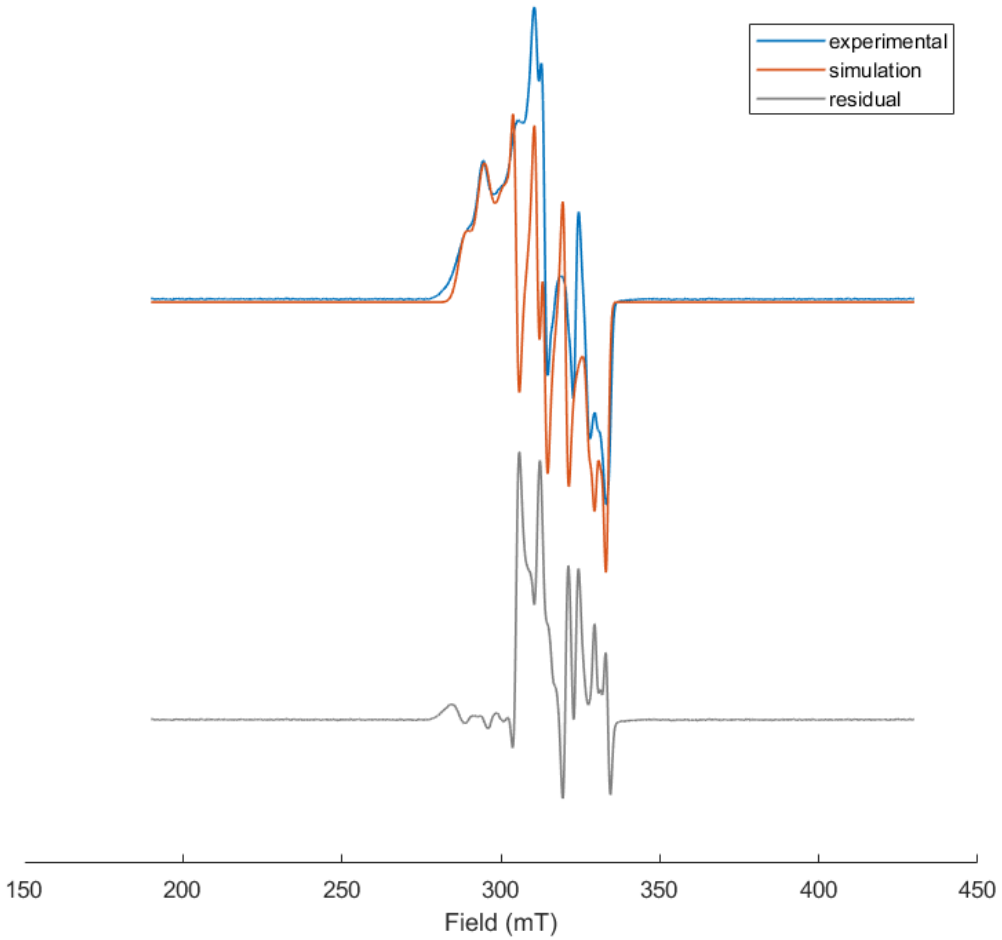

Figure S3C. Low temperature (7 K) X-Band EPR spectrum of (dppf)Ni(2,4,6-$^{i}Pr_3C_6H_2$) (**3**) (blue) and the spectral simulation (red). Residual signal appears in grey. The spectrum is modelled as a rhombic species with g_x = 2.03, g_y = 2.12 and g_z = 2.29. The hyperfine splitting arises from two inequivalent phosphorus nuclei, with anisotropic hyperfine values of [47, 62, 185] MHz and [129, 210, 218] MHz. Line broadening was simulated using the gStrain function with values of [0.016, 0.016, 0.043]. MW Frequency: 9.37 GHz, MW Power: 1 mW.

*Comments About the Synthesis of **3** and Other Nickel(I) Aryl Complexes*

A substantial excess of Grignard reagent is needed in the synthesis of **3** due to the ability of the nickel(I) aryl product to disproportionate in the presence of unreacted nickel(I) halide. The disproportionation event produces a nickel(II) species and an unstable nickel(0) species (see *Section SVII*). As such, transmetalation must be fast and quantitative, which is achieved through the use of a large excess of Grignard reagent. In the synthesis of the nickel(I) aryl species with smaller aryl groups, we noticed even greater instability of the products when THF was used. As such, the synthesis proceeded by removing most of the THF solvent from the Grignard reagent *in vacuo* and redissolving the residue in d_8-toluene. In these cases, the amount of Grignard reagent was limited to 1.5 equivalents to avoid residual THF from degrading the product.

*Synthesis and Characterization of **9***

The compound was synthesized by modification of the previously described literature method for the preparation of (dppf)Ni^{II}(*o*-tolyl)(Br).[7,8] (dppf)$Ni^{II}Br_2$ (100 mg, 0.129 mmol) was added to a 100 mL Schlenk flask containing a stir bar. 10 mL of THF was cannula transferred into the flask, and the contents were stirred until dissolution. The flask was cooled to 0 °C in an ice bath, after which 2,4,6-triisopropylmagnesium bromide (0.5 M, 258 μL, 0.129 mmol, 1 equiv.) was added dropwise using a gas-tight syringe. The solutions turned from dark green to orange after stirring vigorously for 30 mins. The flask was allowed to warm to room temperature, after which the THF was removed under vacuum to yield an orange residue. 5 mL of methanol was added to the flask, and the heterogeneous mixture was sonicated for 3 minutes until a uniform suspension was obtained. The flask was cooled in an ice bath for 15 minutes, and the resulting bright yellow solid was isolated by vacuum filtration and analyzed by ^{1}H, ^{31}P, and ^{13}C NMR spectroscopy.

Yield: 39% (45.0 mg)

Due to fluxional processes, the ^{1}H NMR spectrum was obtained at low temperature.

^{1}H NMR (*d_8*-toluene, 500 MHz, -50 °C): δ 9.49 (br s, 1H), 9.16 (br s, 1H), 8.84 (t, 2H), 7.64 (m, 1H), 7.28 (m, 3H), 7.20 (m, 1H), 6.87-6.73 (m, 8H), 6.52 (s, 1H), 5.53-5.48 (m, 2H), 4.66 (m, 1H), 4.17 (s 1H), 3.77 (app s, 2H), 3.65 (d, 2H), 3.46 (s, 1H), 3.43 (s, 1H), 2.80 (m, 2H), 1.97 (d, 3H), 1.39 (s, 1H), 1.29 (m, 9H), 1.02 (d, 6H).

$^{31}P\{^{1}H\}$ NMR (C_6D_6, 202 MHz, 25 °C): δ 29.15 (d, J = 24 Hz); 10.56 (d, J = 22 Hz).

$^{13}C\{^{1}H\}$ NMR (C_6D_6, 126 MHz, 25 °C): δ 151.75, 145.14, 137.63, 136.74, 134.33, 131.28, 130.49, 129.57, 127.11, 122.43, 120.36, 77.76, 76.29, 74.13, 73.94, 71.59, 70.68, 38.52, 34.82, 34.28, 26.26, 25.88, 25.31, 25.09, 24.45, 23.68.

The ^{1}H, $^{31}P\{^{1}H\}$ and $^{13}C\{^{1}H\}$ spectra are given in Figure S4.

Elemental Analysis: % Calc'd(Found): C: 65.66(65.41); H: 5.74(5.86); N: <0.02(<0.02).

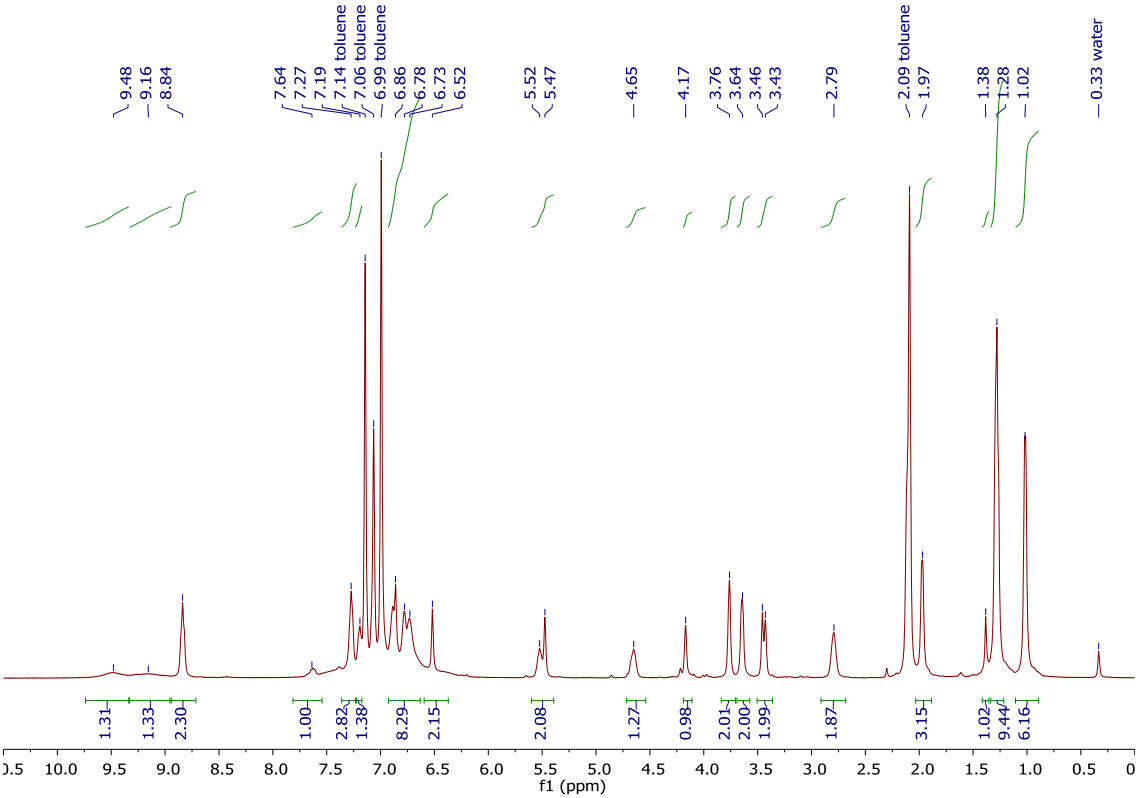

Figure S4A. ^{1}H NMR spectrum of (dppf)Ni^{II}(^{i}Pr$_3$C$_6$H$_2$)(Br) (**9**) in d_8-toluene at -50 °C.

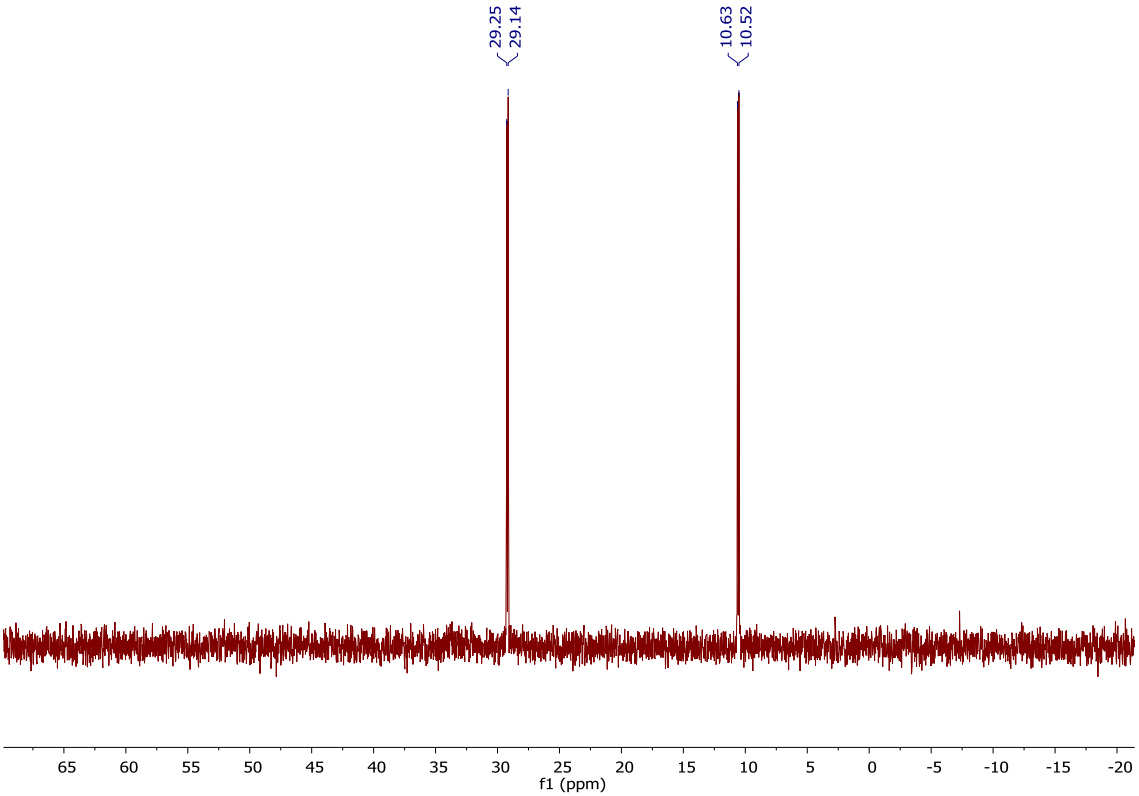

Figure S4B. ^{31}P{^{1}H} NMR spectrum of (dppf)Ni^{II}(^{i}Pr$_3$C$_6$H$_2$)(Br) (**9**) in C_6D_6 at room temperature.

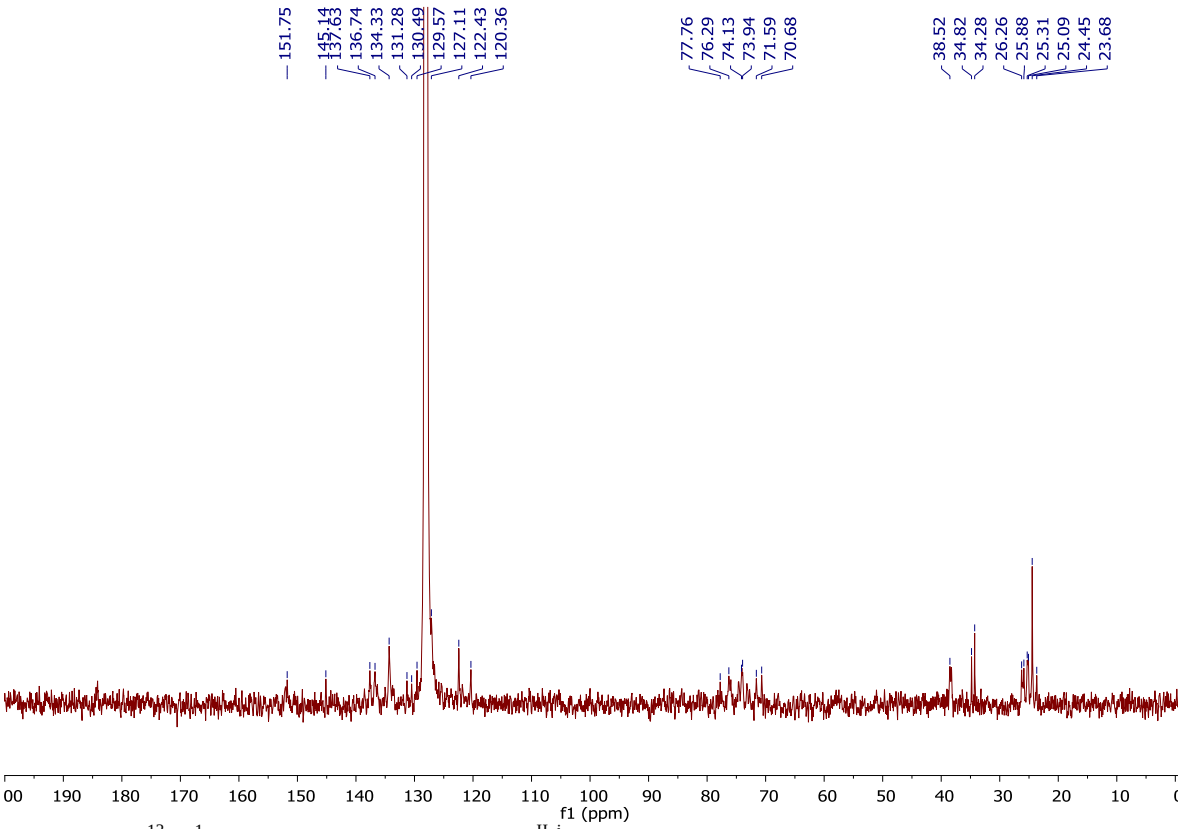

Figure S4C. $^{13}C\{^{1}H\}$ NMR spectrum of (dppf)$Ni^{II}(^{i}Pr_3C_6H_2)$(Br) (**9**) in C_6D_6 at room temperature.

SIV. EPR Identification of Ni(I) Aryl Complexes

General Procedure for the EPR Identification of Ni(I) Aryl Complexes

To a vial was added (dppf)Ni^{I}Br (**2**) (0.00316 mmol, 2.2 mg), which was dissolved in 500 µL of toluene. The appropriate arylmagnesium bromide Grignard reagent (1.5 equiv, 0.00474 mmol) was added via micropipette, and the vial was agitated to mix. 32 µL of the reaction mixture was added to an EPR tube containing 168 µL of toluene to make a 1 mM solution. The EPR tube was sealed with a septum, brought out of the glove box and immediately frozen in liquid nitrogen. An EPR spectrum was then recorded.

For the identification of (dppf)Ni^{I}(Ph) (**7**), the same reaction procedure was followed, except the nickel solution, EPR tube containing toluene, and Grignard reagent were frozen in a cold well in the glovebox cooled by liquid nitrogen. The solutions were warmed to just above the freezing point, after which the appropriate amount of Grignard reagent was added to the nickel solution via micropipette. 32 µL of the reaction mixture was then added to the toluene in the cooled EPR tube and the tube was sealed, quickly brought out of the glovebox, and frozen immediately in liquid nitrogen. An EPR spectrum was then recorded.

The EPR spectra of the nickel(I) aryl species are given in Figure S5A-E along with spectral simulations. EPR parameters specific to each spectrum as well as simulation parameters are provided in the captions of each figure. The parameters for each species are also tabulated in Table S1.

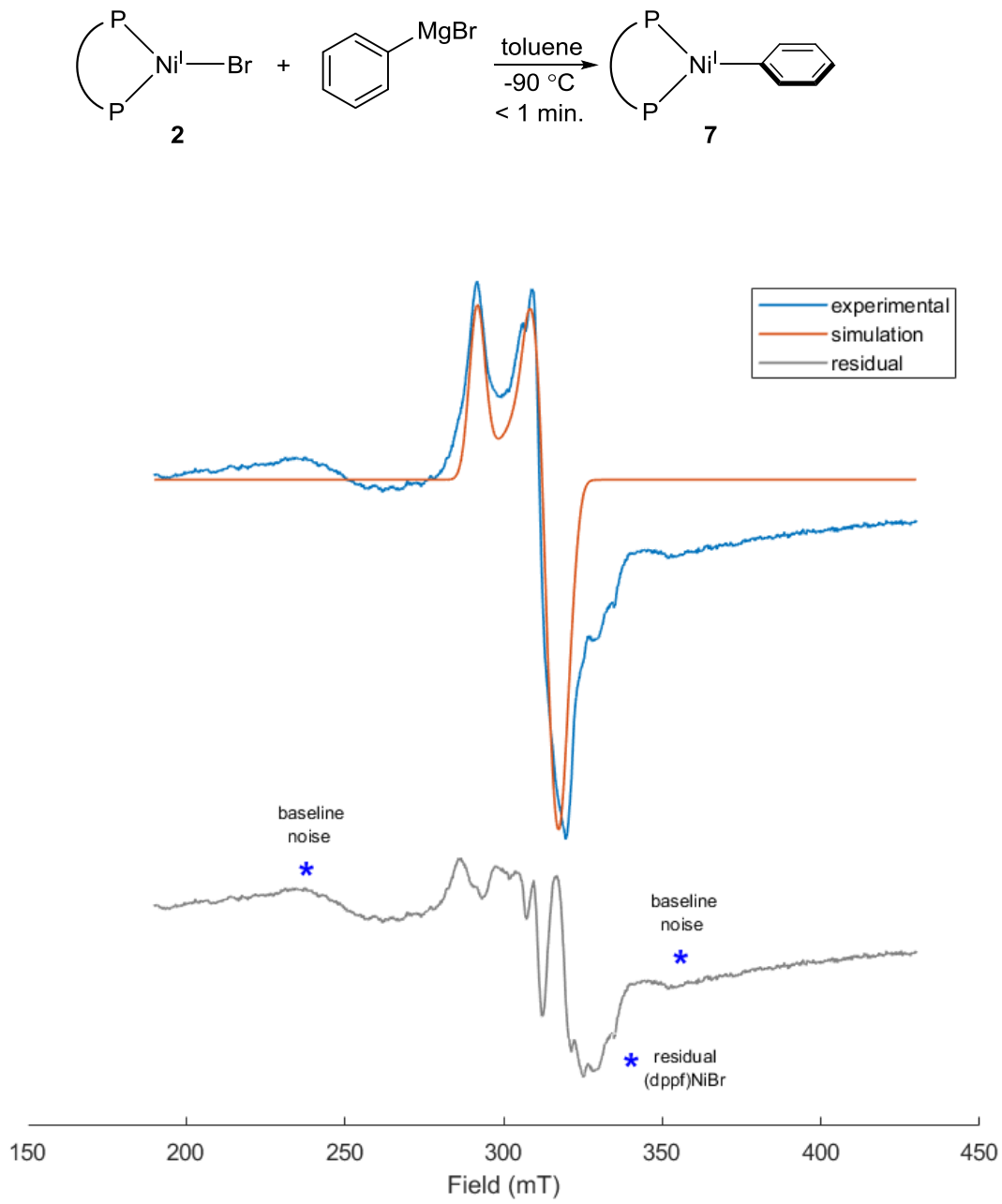

Figure S5A: Low temperature (7 K) X-Band EPR spectrum of **7** (blue) and the spectral simulation (red). Residual signal appears in grey. The spectrum is modelled as an approximately axial species with $g_{\perp}$ = 2.12 and $g_{\parallel}$ = 2.29. The hyperfine splitting arises from two approximately equivalent phosphorus nuclei, with anisotropic hyperfine tensors of [101, 51] MHz for each phosphorus nucleus. Line broadening was simulated using the gStrain function with values of [0.034, 0.040]. The residual signal is attributed to **2** that was not fully transmetalated before freezing the EPR tube, or baseline noise that is significant due to the low concentration of paramagnetic material. MW Frequency: 9.37 GHz, MW Power: 20 mW.

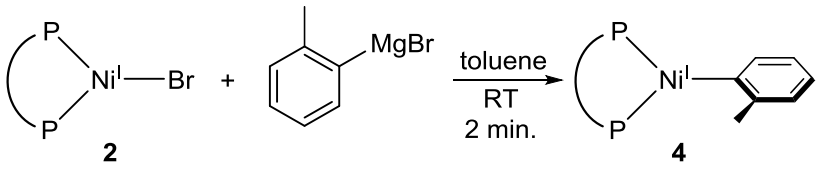

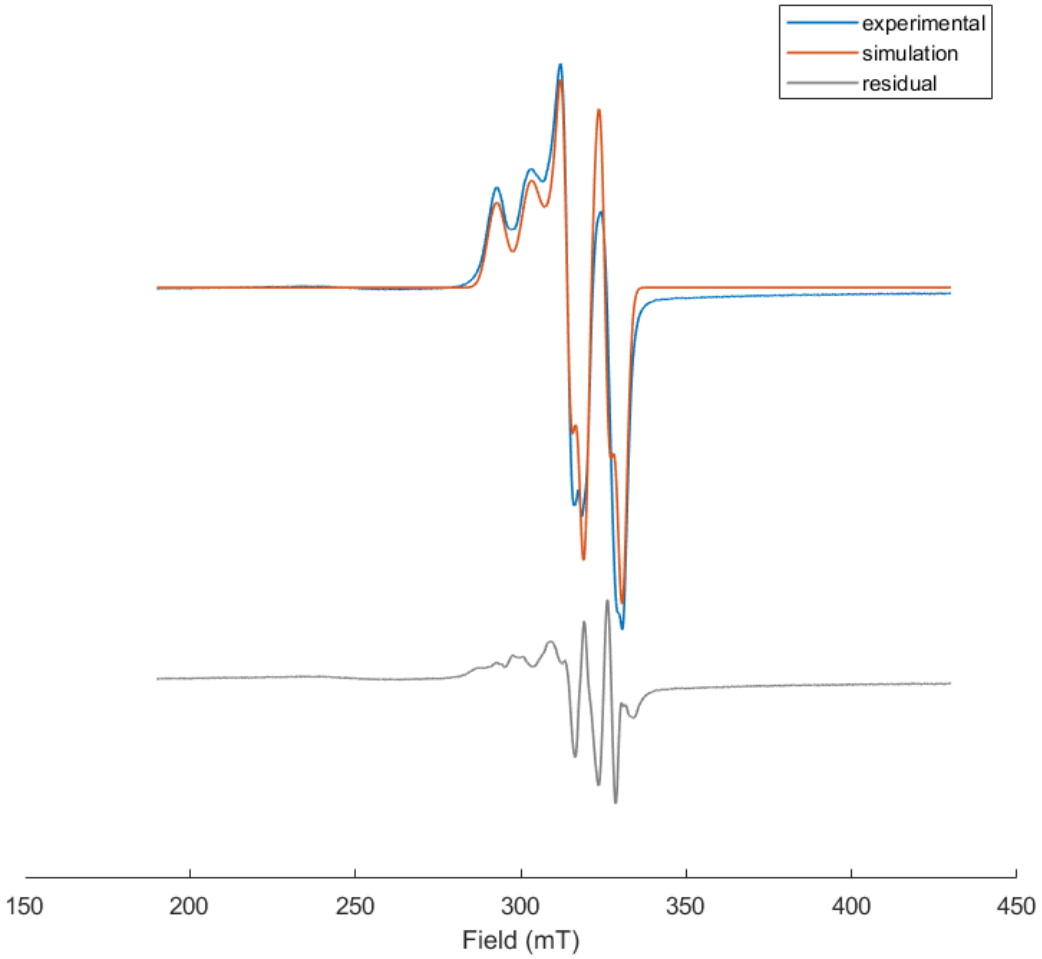

Figure S5B: Low temperature (7 K) X-Band EPR spectrum of **4** (blue) and the spectral simulation (red). Residual signal appears in grey. The spectrum is modelled as an approximately axial species with $g_{\perp}$ = 2.08 and $g_{\parallel}$ = 2.25. The hyperfine splitting arises from two inequivalent phosphorus nuclei, with anisotropic hyperfine values of [336, 323] MHz and [106, 75] MHz. Line broadening was simulated using the gStrain function with values of [0.025, 0.040]. MW Frequency: 9.37 GHz, MW Power: 10 mW.

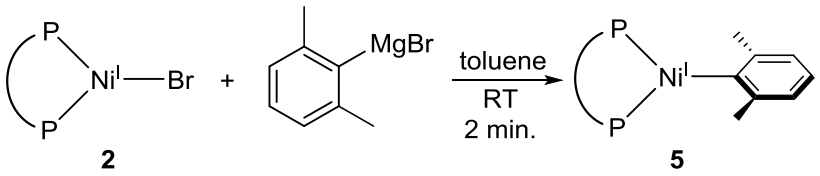

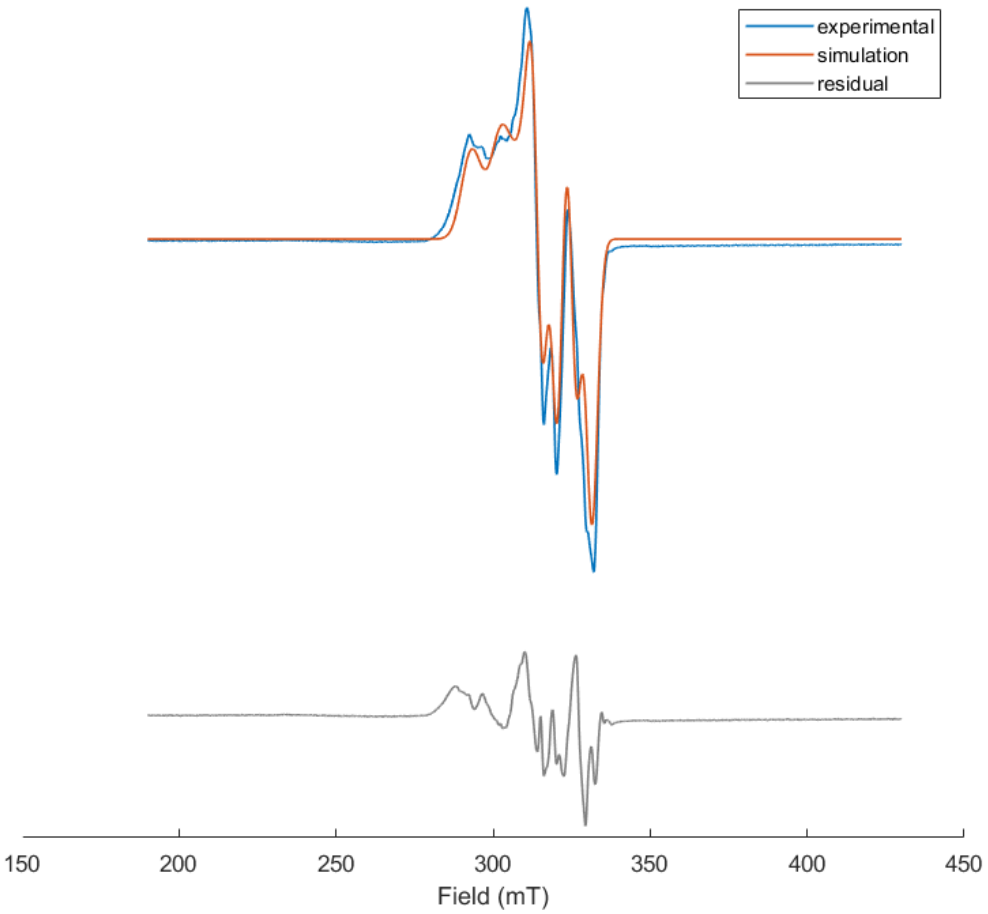

Figure S5C: Low temperature (7 K) X-Band EPR spectrum of **5** (blue) and the spectral simulation (red). Residual signal appears in grey. The spectrum is modelled as a slightly rhombic species with $g_x = 2.07$ $g_y = 2.08$ and $g_z = 2.25$. The hyperfine splitting arises from two inequivalent phosphorus nuclei, with anisotropic hyperfine values of [316, 295] MHz and [136, 82] MHz. Line broadening was simulated using the gStrain function with values of [0.030, 0.030, 0.050]. MW Frequency: 9.38 GHz, MW Power: 10 mW. Spectrum is the average of 4 scans.

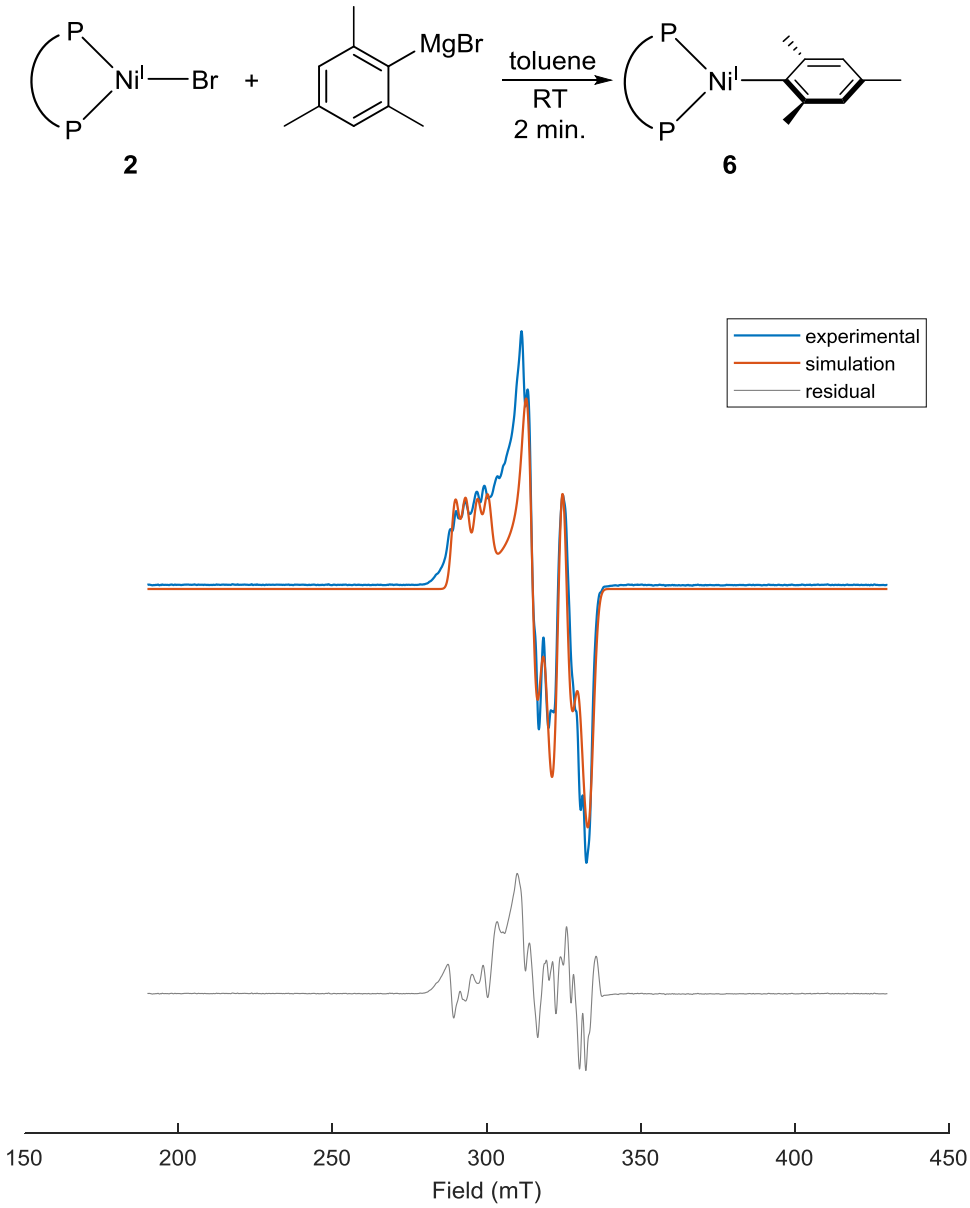

Figure S5D: Low temperature (8.5 K) X-Band EPR spectrum of **6** (blue) and the spectral simulation (red). Residual signal appears in grey. The spectrum is modelled as a rhombic species with g_x = 2.06 and g_y = 2.08 and g_z = 2.27. The hyperfine splitting arises from two inequivalent phosphorus nuclei, with anisotropic hyperfine values of [326, 227] MHz and [134, 106] MHz. Line broadening was simulated using the gStrain function with values of [0.022, 0.021, 0.022]. MW Frequency: 9.37 GHz, MW Power: 0.01 mW. Spectrum is the average of 4 scans.

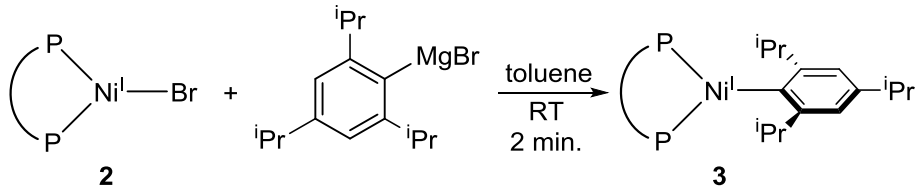

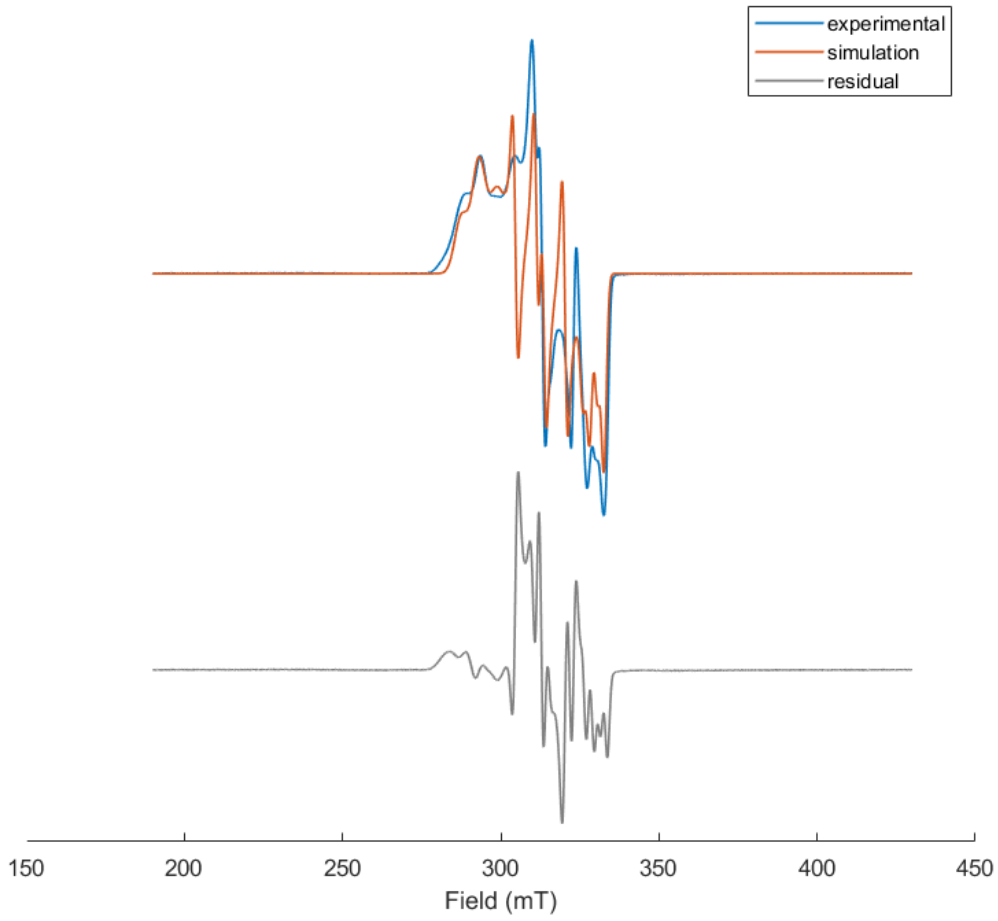

Figure S5E: Low temperature (7 K) X-Band EPR spectrum of **3** (blue) and the spectral simulation (red). Residual signal appears in grey. The spectrum is modelled as a rhombic species with g_x = 2.03 and g_y = 2.15 and g_z = 2.29. The hyperfine splitting arises from two inequivalent phosphorus nuclei, with anisotropic hyperfine values of [57, 201, 188] MHz and [128, 270, 165] MHz. Line broadening was simulated using the gStrain function with values of [0.012, 0.012, 0.038]. MW Frequency: 9.37 GHz, MW Power: 1 mW.

Table S1. Simulation Parameters for EPR Spectra of Nickel(I) Aryl Species. Hyperfine values are given in MHz.

Species	g_x	g_y	g_z	$A^{P1}{}_x$	$A^{P1}{}_y$	$A^{P1}{}_z$	$A^{P2}{}_x$	$A^{P2}{}_y$	$A^{P2}{}_z$
7	2.12	2.12	2.29	101	101	51	101	101	51
4	2.08	2.08	2.25	336	336	323	106	106	75
5	2.07	2.08	2.25	316	316	295	136	136	82
6	2.06	2.08	2.27	326	326	227	134	134	106
3 (*in situ*)	2.04	2.15	2.29	57	201	188	128	270	165
3 (authentic)	2.03	2.15	2.28	47	197	198	101	270	169

SV. Degradation of Ni(I) Aryl Complexes

*Solution Stability of (dppf)Ni^{I}(2,4,6-^{i}Pr$_3$C$_6$H$_2$) (**3**) without COD Present*

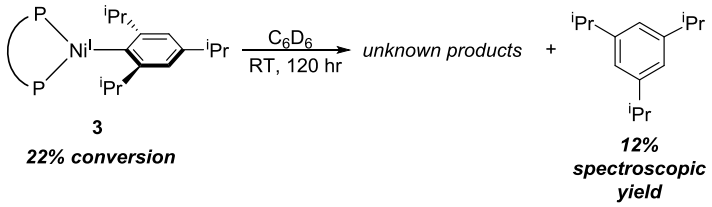

The solution stability of isolated **3** was probed in C_6D_6. To a J-Young tube containing a capillary of cobaltocene in C_6D_6 as well as a capillary of PPh_3 in C_6D_6 was added **3** (0.00316 mmol, 2.6 mg). 500 µL of C_6D_6 was added to the J-Young tube via micropipette, after which the tube was capped and agitated to mix the contents. ^{1}H and ^{31}P NMR spectra were immediately recorded, and the reaction was monitored intermittently for 120 hours. The following parameters were used for ^{1}H NMR spectroscopy: nt=256 scans, d1=0.5 s, at=1.0 s, sweep width (-75, 75 ppm).

When **3** is left to stand in C_6D_6, slow decomposition is observed by ^{1}H NMR spectroscopy (Figure S6A). After 24 hours, only 7% of **3** is lost, and after 120 hours, only 22% is lost. Corresponding to this 22% loss in nickel is the formation of 1,3,5-triisopropylbenzene in 12% yield. Unfortunately, the only phosphorus-containing product identified by ^{31}P NMR spectroscopy is the free dppf ligand, although another unidentified species appears at ~23 ppm (Figure S6B).

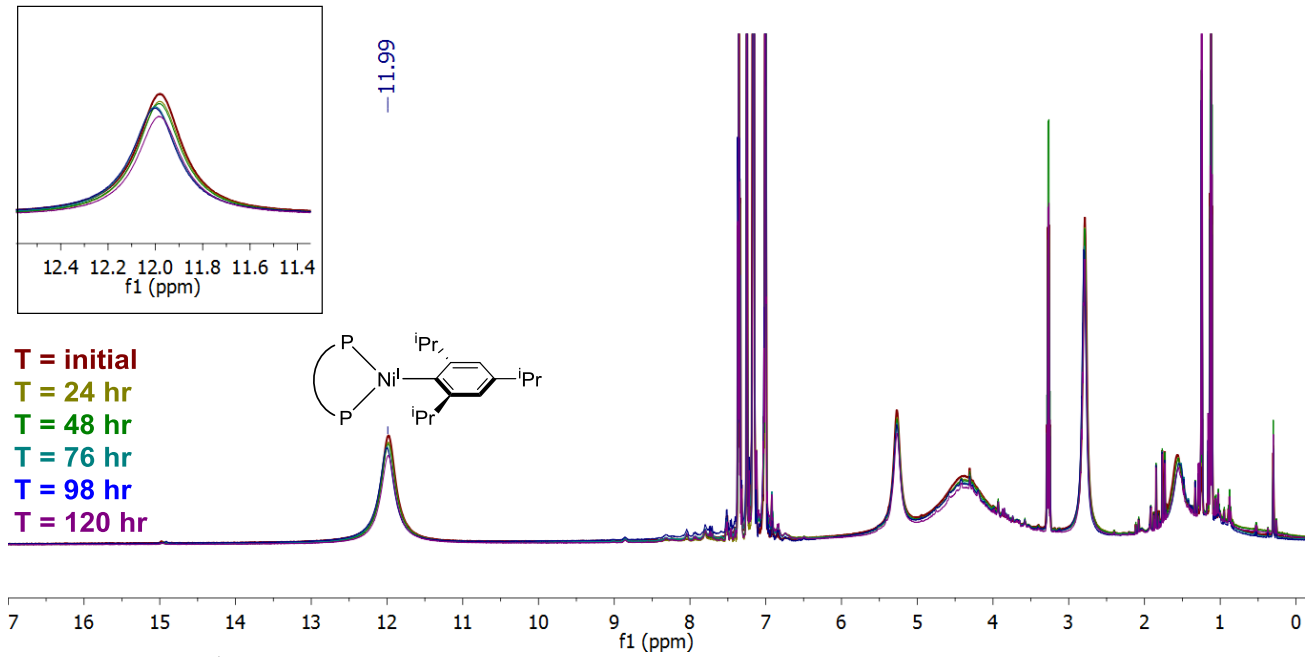

Figure S6A. Full ^{1}H NMR spectrum indicating the slow degradation of **3** in C_6D_6 over 120 hours. Inset: expanded view of the region in which the phenyl protons of **3** used to quantify degradation appear.

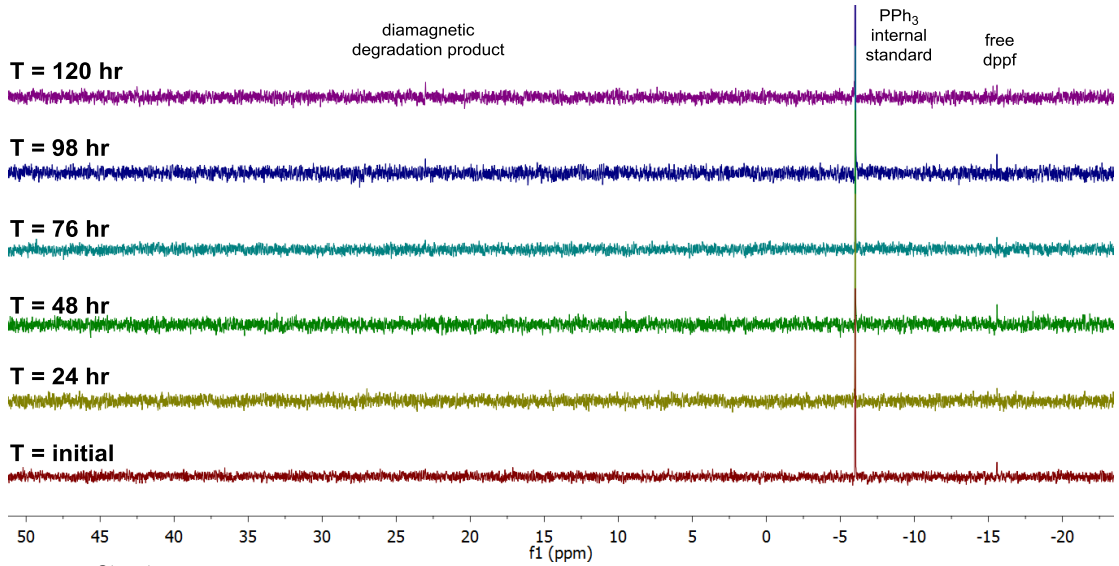

Figure S6B. $^{31}P\{^{1}H\}$ NMR spectra of **3** in C_6D_6 over 120 hours indicating the formation of a small amount of an unknown diamagnetic product as well as free dppf.

*Solution Stability of (dppf)Ni^{I}(2,4,6-^{i}Pr$_3$C$_6$H$_2$) (**3**) in the Presence of COD*

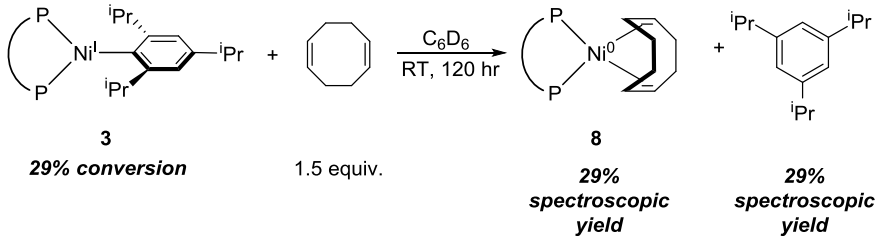

In order to identify the nickel-containing decomposition products of the solution degradation of **3**, COD was used as a trapping agent. To a J-Young tube containing a capillary of cobaltocene in C_6D_6 as well as a capillary of PPh_3 in C_6D_6 was added **3** (0.00316 mmol, 2.6 mg). 500 µL of C_6D_6 was added to the J-Young tube via micropipette. COD (1.5 equiv., 0.00474 mmol, 0.6 µL) was added via micropipette directly to the tube, after which the tube was capped and agitated to mix the contents. ^{1}H and ^{31}P NMR spectra were immediately recorded, and the reaction was monitored intermittently for 120 hours. The following parameters were used for ^{1}H NMR spectroscopy: nt=256 scans, d1=0.5 s, at=1.0 s, sweep width (-75, 75 ppm).

When **3** is left to stand in C_6D_6 with COD, slow decomposition is observed by NMR spectroscopy (Figure S7A). By ^{31}P NMR spectroscopy, the degraded nickel is trapped in the form of (dppf)Ni^{0}(COD) (**8**) over the course of the reaction (Figure S7B). After 120 hours, 29% of the nickel(I) aryl is decomposed, which corresponds to the generation **8** in 29% yield. Further, 1,3,5-triisopropylbenzene is also produced in 29% yield with the production of **8**. The use of COD definitively indicates that the fate of the nickel is a zerovalent, dppf-ligated species.

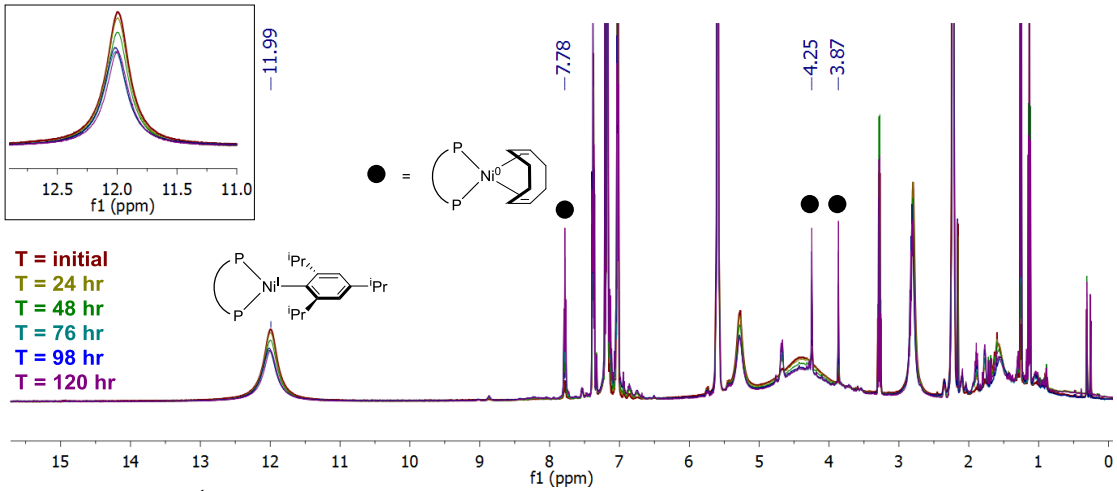

Figure S7A. Full ^{1}H NMR spectrum indicating the slow degradation of **3** in C_6D_6 over 120 hours with the simultaneous appearance of **8**, seen in the increase in peaks marked with black dots in the spectrum. Inset: expanded view of the region in which the phenyl protons of **3** appear, which was used to quantify degradation.

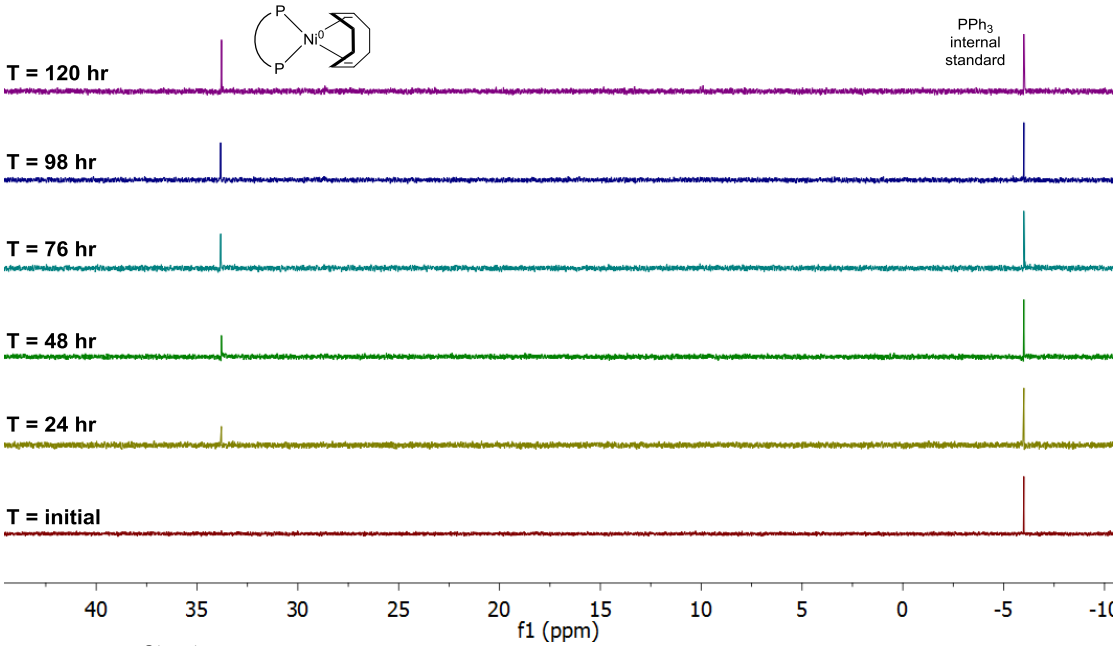

Figure S7B. ^{31}P{^{1}H} NMR spectra indicating the formation of **8** as a function of time when **3** is left to stand in C_6D_6.

Identification of Mono- vs. Biaryl Degradation Products

The reaction mixtures from the *in situ* formation and decomposition of (dppf)Ni^{I}(Ph) (**7**), (dppf)Ni^{I}(*o*-tolyl) (**4**), (dppf)Ni^{I}(2,6-xylyl) (**5**), (dppf)Ni^{I}(2,4,6-mesityl) (**6**), and (dppf)Ni^{I}(2,4,6-$^{i}Pr_3C_6H_2$) (**3**) were analyzed by GC in all cases except **3**, which was analyzed using ^{13}C NMR spectroscopy. Each nickel(I) aryl species was prepared as detailed in *General Procedure for the NMR-Scale Synthesis of Ni(I) Aryl Complexes* after which the reaction mixture was left to stand in J-Young tubes for their previously determined lifetimes in all cases except **3**, which was allowed to decompose for 48 hours before analysis. For **7**, the reaction was performed in d_8-toluene in order to be able to identify the monoaryl product, benzene. For the samples analyzed by GC, the tubes were then uncapped and 200-300 μL of reaction mixture was added to a ~5 cm plug of silica and eluted with ethyl acetate. The identity of aryl and biaryl products was verified by comparison of the retention times of the peaks of interest to that of authentic aryl or biaryl species. For **3**, the crude reaction mixture was analyzed by ^{13}C NMR spectroscopy (151 MHz, 3800 scans) and compared to authentic samples and literature.[9]

For the smaller nickel(I) aryl species, both monoaryl and biaryl products can be identified. For the bulkiest nickel(I) aryl species, the predominant product evident by ^{13}C NMR spectroscopy is the monoaryl product, 1,3,5-triisopropylbenzene, with no evidence for the biaryl product, 2,2',4,4',6,6'-hexaisopropyl-1,1'-biphenyl. Taken together, the presence of biaryl products in all cases except for **3** may suggest that binuclear events are hindered by the added steric bulk on the aryl ligand, which may contribute to its enhanced lifetime. All compiled spectra with annotations are shown in Figure S8.

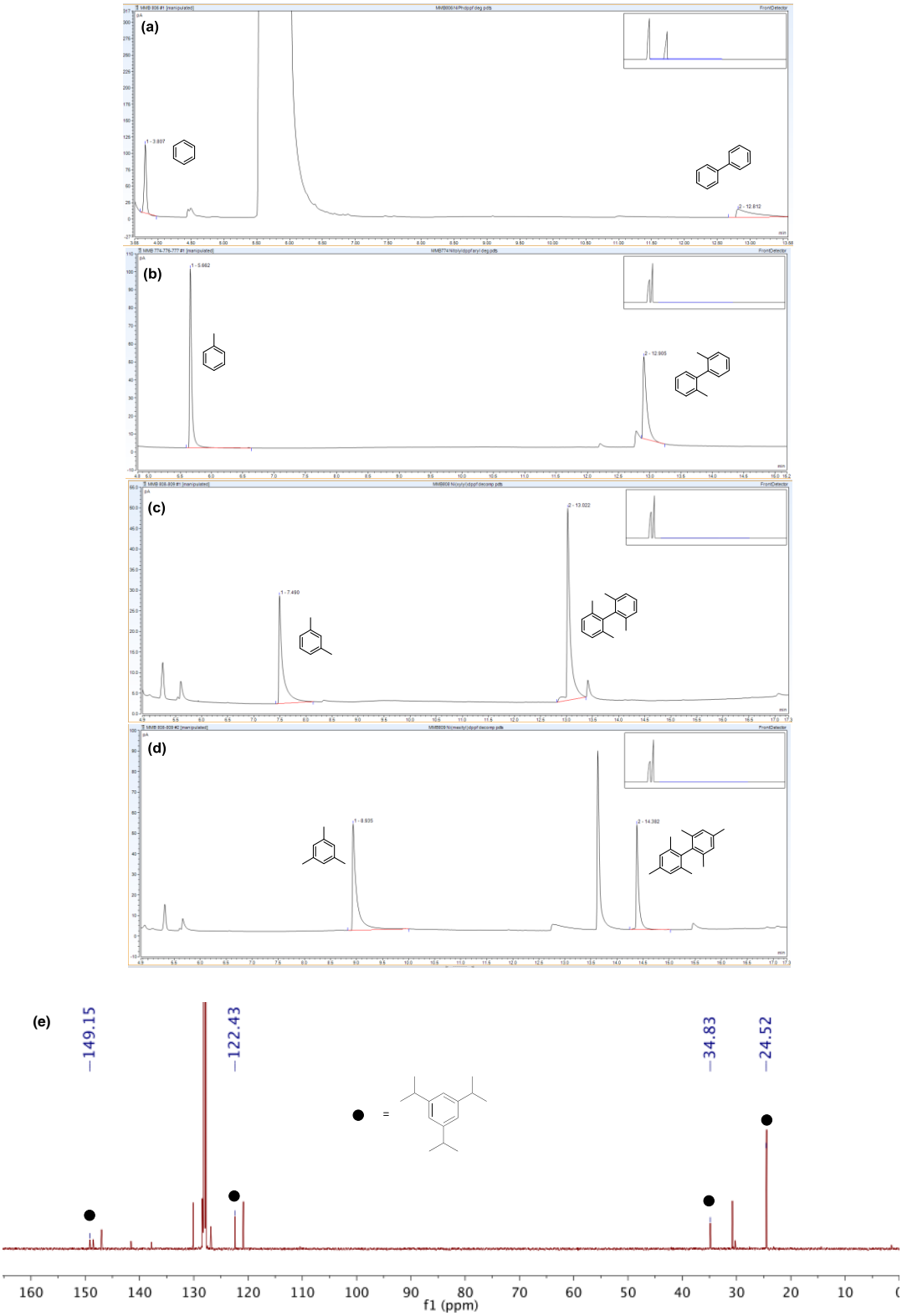

Figure S8. Compiled gas chromatograms and $^{13}C\{^{1}H\}$ NMR spectrum and corresponding assignments of aryl and biaryl products resulting from the degradation of (a) (dppf)Ni^{I}(Ph) (**7**), (b) (dppf)Ni^{I}(*o*-tolyl) (**4**), (c) (dppf)Ni^{I}(2,6-xylyl) (**5**), (d) (dppf)Ni^{I}(2,4,6-mesityl) (**6**), and (e) (dppf)Ni^{I}(2,4,6-$^{i}Pr_3C_6H_2$) (**3**).

Decomposition Rate as a Function of Nickel Concentration for a Small and Large Aryl Species

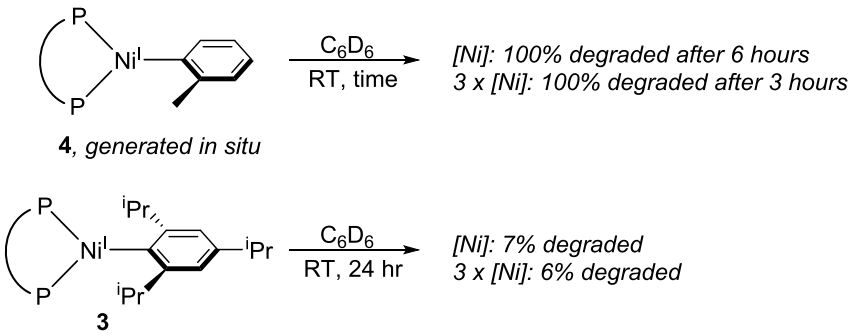

In order to determine the impact of nickel concentration on the rate of decomposition of nickel(I) aryl species, the decomposition of *in situ* generated **4** and authentic **3** were analyzed at three times the nickel concentration used to determine their native lifetimes (see *Section SII*). To a J-Young tube containing a capillary of cobaltocene in C_6D_6 as well as a capillary of PPh_3 in C_6D_6 was added **1** (0.00948 mmol, 6.1 mg) and *o*-tolylmagnesium bromide (1.2 M, 0.00948 mmol, 7.9 µL) or authentic **3** (0.00948 mmol, 7.8 mg). The contents were dissolved in 500 µL C_6D_6, after which the nickel(I) aryl species were analyzed by paramagnetic ^{1}H NMR spectroscopy at various time points, using the following parameters: nt=256 scans, d1=0.5 s, at=1.0 s, sweep width (-75, 75 ppm).

The decomposition of the nickel(I) species containing a relatively small aryl group, **4**, was accelerated when the nickel concentration was tripled. After 3 hours and triple the concentration of nickel, all of the signals corresponding to that of **4** were consumed (Figure S9). This is significantly faster than the decomposition rate seen in the native case of 6 hours (see Figure S2A). Such rate acceleration in the presence of more nickel is consistent with a binuclear event resulting in decomposition; this is further supported by the observation of the biaryl 2,2'-dimethylbiphenyl by GC analysis (see Figure S8, (b)).

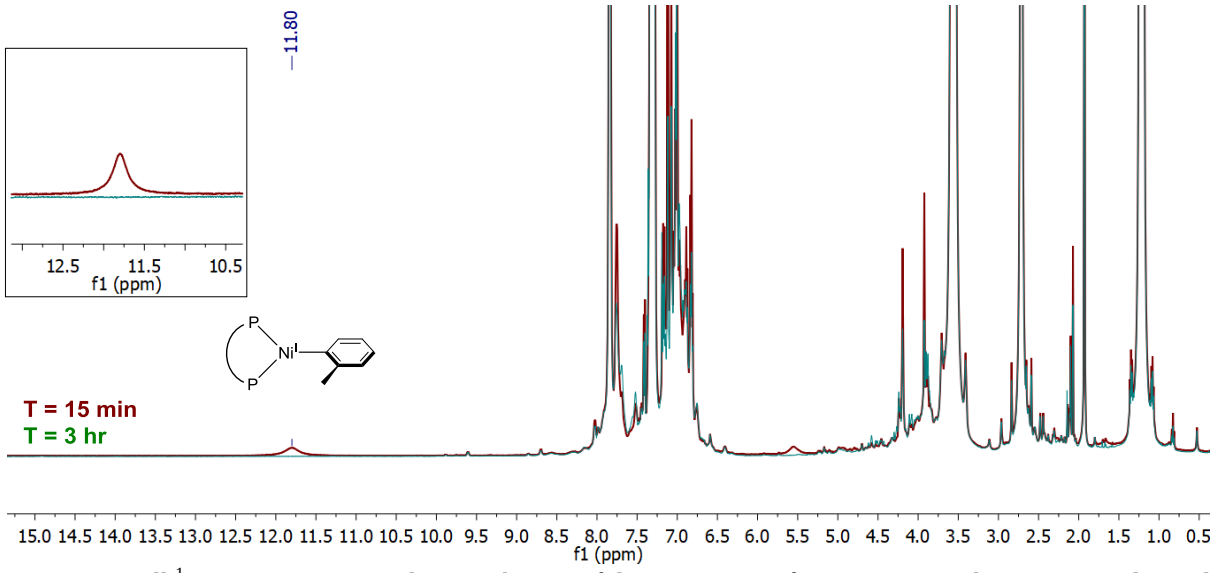

Figure S9. Full ^{1}H NMR spectrum indicating the rate of decomposition of *in situ* generated **4** in C_6D_6 at elevated concentration over 3 hours. Inset: expanded view of the region in which the phenyl protons of **4** used to quantify degradation appear.

In contrast, the decomposition of the nickel(I) species containing the largest aryl group, **3**, is not accelerated with an increase in nickel concentration. After 24 hours, the triply concentrated solution of **3** was only approximately 6% degraded (Figure S10), which is consistent with the 7% degradation seen in the native case (see Figure S6A and discussion). The lack of decomposition rate acceleration with increase in nickel concentration implies that a binuclear event resulting in the decomposition of **3** is not occurring. In support of this, analysis of the aryl decomposition products indicates that only the monoaryl product, 1,3,5-triisopropylbenzene, can be identified (see Figure S8, (e)).

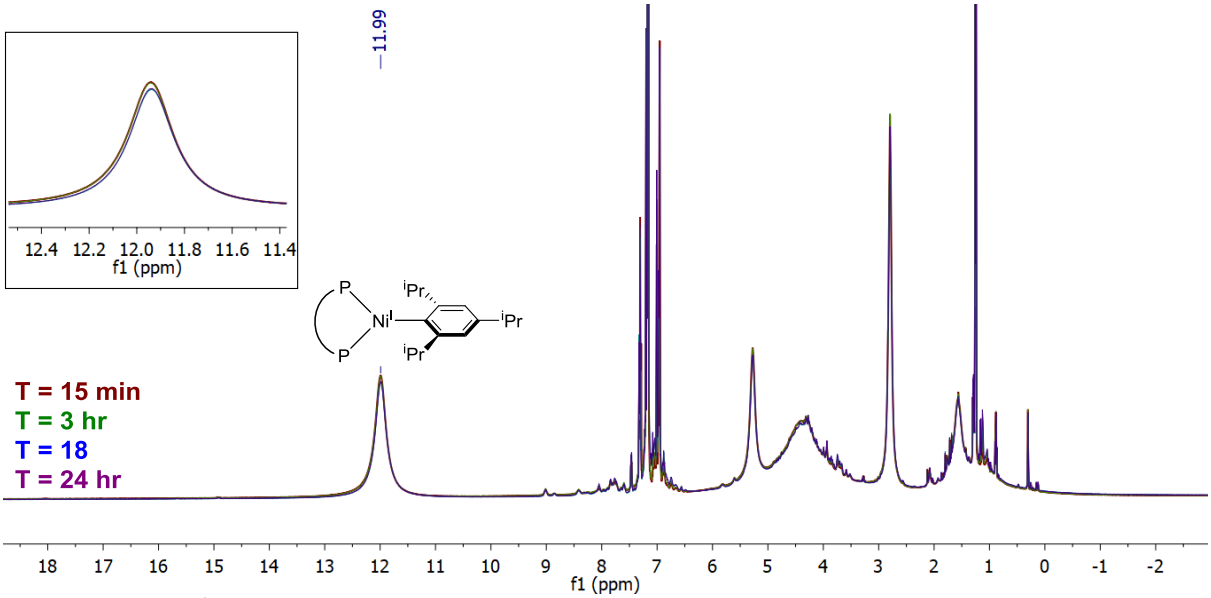

Figure S10. Full ^{1}H NMR spectrum indicating the rate of decomposition of *in situ* generated **3** in C_6D_6 at elevated concentration over 24 hours. Inset: expanded view of the region in which the phenyl protons of **3** used to quantify degradation appear.

*Instability of (dppf)Ni(2,4,6-$^{i}Pr_3C_6H_2$) (**3**) at Elevated Temperature*

In order to gain further information about the stability of **3**, its decomposition was monitored at 50 °C using ^{1}H and ^{31}P NMR spectroscopy. **3** (0.00316 mmol, 2.6 mg) was dissolved in 500 µL of C_6D_6 in a J-Young tube containing a capillary of cobaltocene in C_6D_6 as well as a capillary of PPh_3 in C_6D_6. The tube was capped and added to an oil bath at 50 °C for two hours, after which the first time point was taken. ^{1}H NMR spectroscopy showed complete consumption of the nickel(I) aryl species (Figure S11). This rate of decomposition is significantly increased from room temperature, in which there is essentially no degradation of the nickel(I) aryl species in the same timeframe.

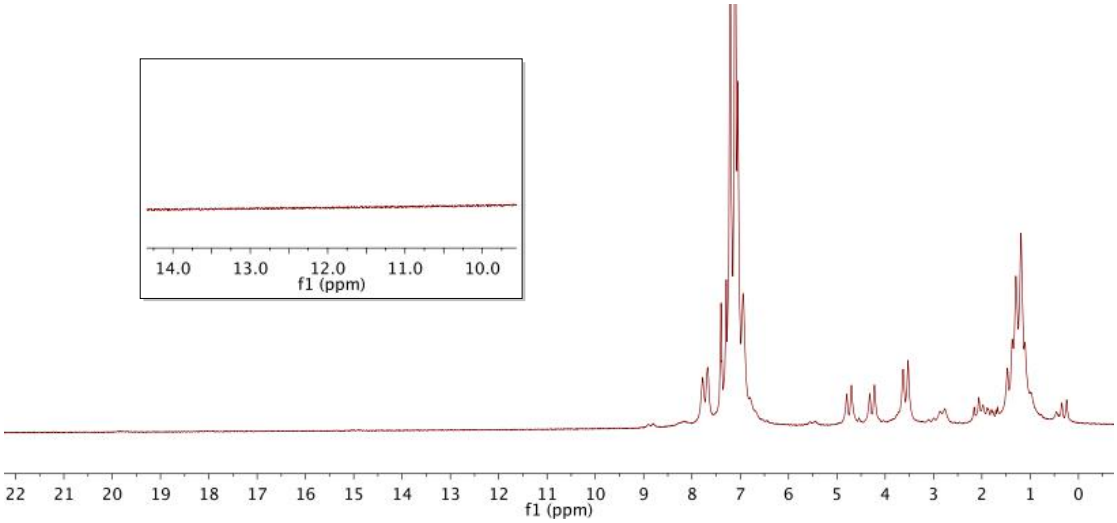

Figure S11. ^{1}H NMR spectrum of the solution containing **3** after 2 hours of heating, showing complete consumption of paramagnetic material. Inset: expansion of the region in which the phenyl protons appear, indicating no residual nickel(I) aryl species after 2 hours of heating.

SVI. Transmetalation of Ni(I) Halides with Boronic Acids

General Procedure for the Transmetalation of Ni(I) Halides with Boronic Acids

To a J-Young tube containing a capillary of cobaltocene in C_6D_6 as well as a capillary of PPh_3 in C_6D_6 was added the boronic acid of interest (20 equiv, 0.0632 mmol), and K_3PO_4 (36 equiv, 0.114 mmol, 24 mg). (dppf)Ni^ICl (**1**) (0.00316 mmol, 2.0 mg) was weighed into a vial, and 500 µL of C_6D_6 was added via micropipette. The vial was capped and agitated until dissolution of **1**, after which the nickel solution was added to the J-Young tube. Initial ^1H and ^{31}P NMR spectra were taken, with the following parameters used for ^1H NMR spectroscopy: nt=256 scans, d1=0.5 s, at=1.0 s, sweep width (-75, 75 ppm). The reaction was tracked by ^1H and ^{31}P NMR at room temperature at various time points for 24 hours, the spectra of which are shown in Figure S12 and S13. The tube was agitated by inversion before each time point.

*Transmetalation of (dppf)Ni^ICl (**1**) with 2,6-Xylylboronic Acid and K_3PO_4*

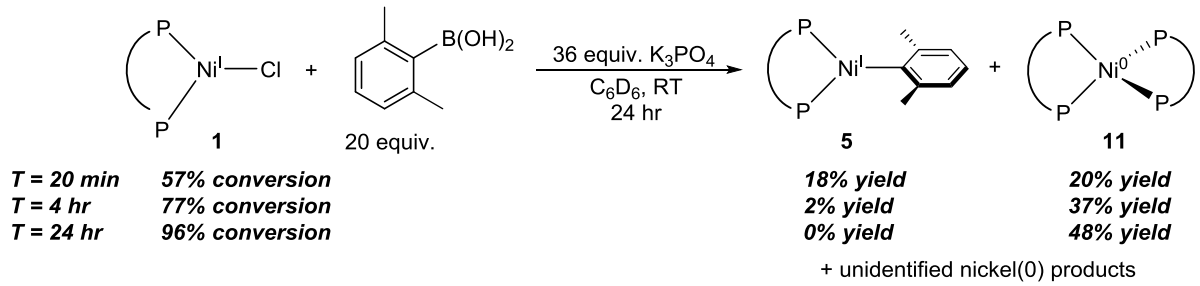

Reaction of **1** with 2,6-xylyl boronic acid produces a paramagnetic nickel species with a distinct spectroscopic signature at 11.83 ppm in the ^1H NMR spectrum (Figure S12A), which we attribute to the phenyl proton resonances of **5** (see Figure S1). Over the course of the reaction, this species never exceeds the amount of **1** starting material, and both starting material and product decrease over the course of the reaction. Concomitant with this decrease in **1** and **5** is the formation of (dppf)$_2Ni^0$ (**11**),[10] as detected by ^{31}P NMR spectroscopy (Figure S12B). Quantification by integration of each nickel species present after 24 hours of reaction indicates that 4% of **1** remains, while 48% of the nickel is in the form of **11**. As two equivalents of (dppf)Ni^0 are needed to produce an equivalent of **11** along with an equivalent of nickel(0), the maximum yield of **11** in this reaction is 50%.

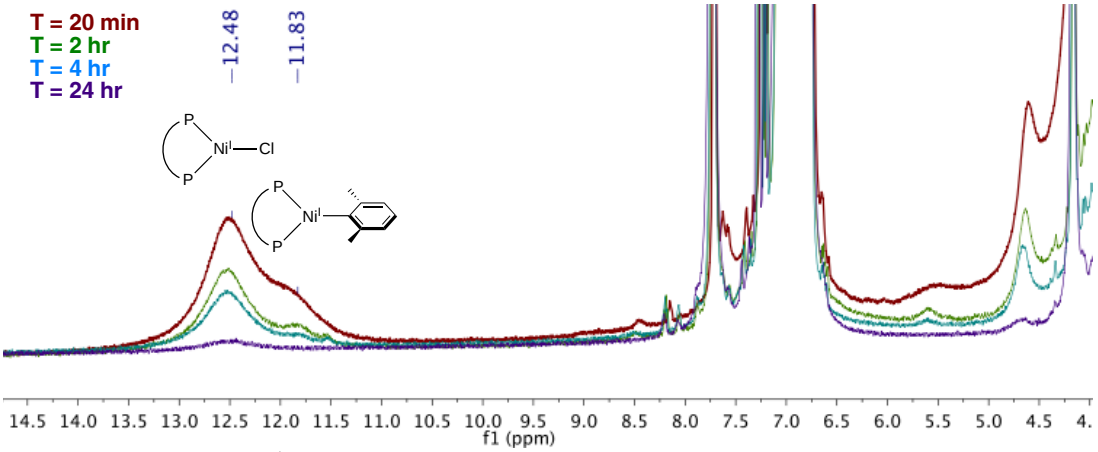

Figure S12A. Truncated ^{1}H NMR spectrum showing the presence of **5** and subsequent degradation of all paramagnetic nickel(I) species.

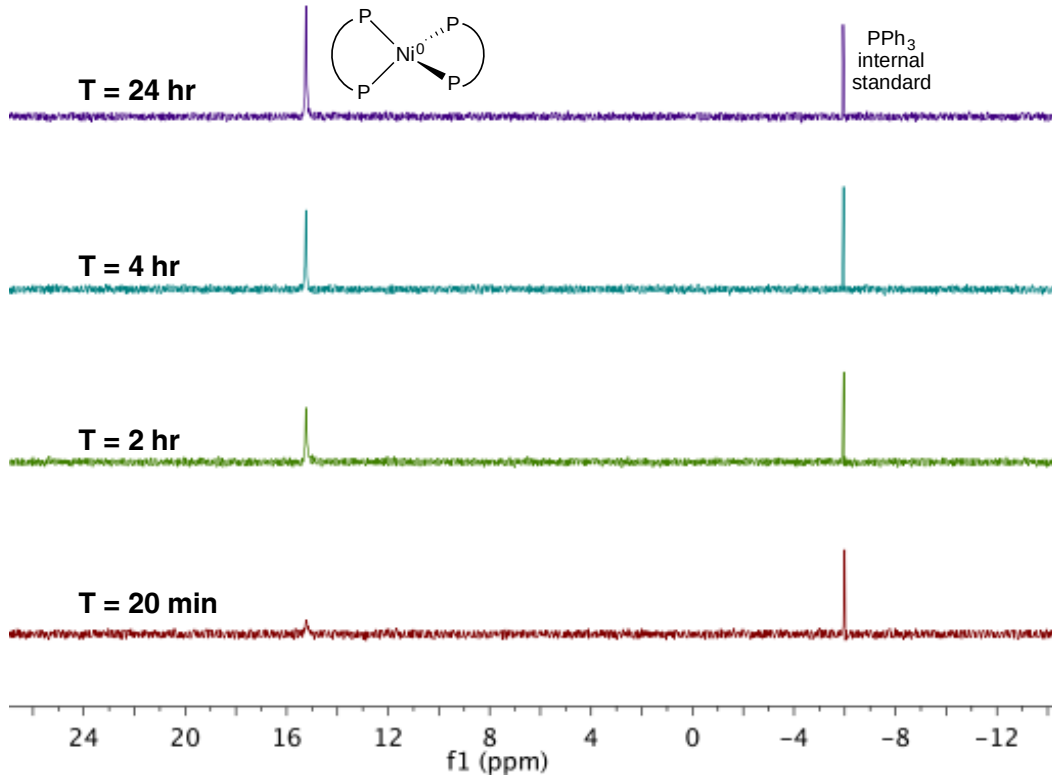

Figure S12B. ^{31}P{^{1}H} NMR spectra showing the appearance of **11** over the course of 24 hours.

*Transmetalation of (dppf)Ni^{I}Cl (**1**) with 2,4,6-Mesitylboronic Acid and K_3PO_4*

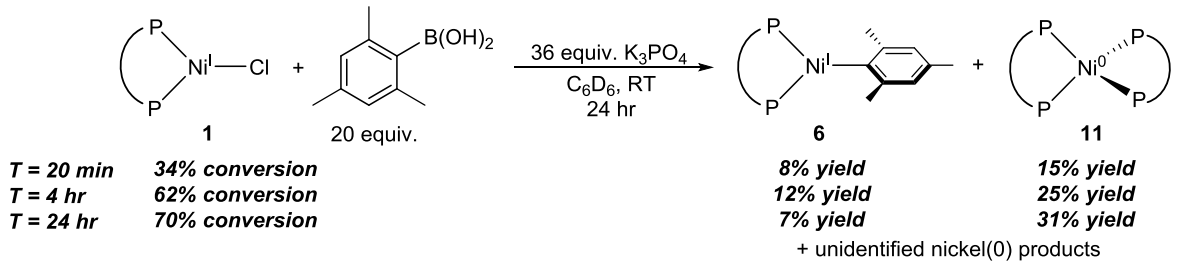

Similar to the reactivity seen with 2,6-xylylboronic acid, reaction of **1** with 2,4,6-mesitylboronic acid produces a paramagnetic nickel species with a distinct spectroscopic signature at 11.71 ppm by ^{1}H NMR spectrsocopy (Figure S13A), which we attribute to the phenyl proton resonances of **6** (see Figure S1). An appreciable build-up of **6** is not seen, and over the course of the reaction the maximum yield of **6** is only approximately 12%. However, the amounts of both **6** and **1** decrease over the course of the reaction and subsequently form **11**, as analyzed by ^{31}P NMR spectroscopy (Figure S13B). Quantification by integration of each nickel species present after 24 hours of reaction indicates that 30% of **1** remains, while 31% of the nickel is in the form of **11**.

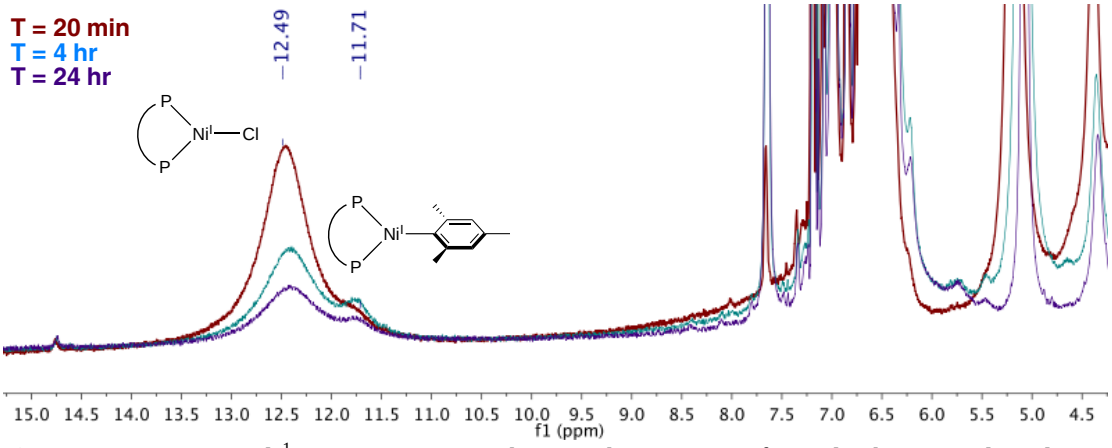

Figure S13A. Truncated ^{1}H NMR spectrum showing the presence of **6** and subsequent degradation of all paramagnetic nickel(I) species.

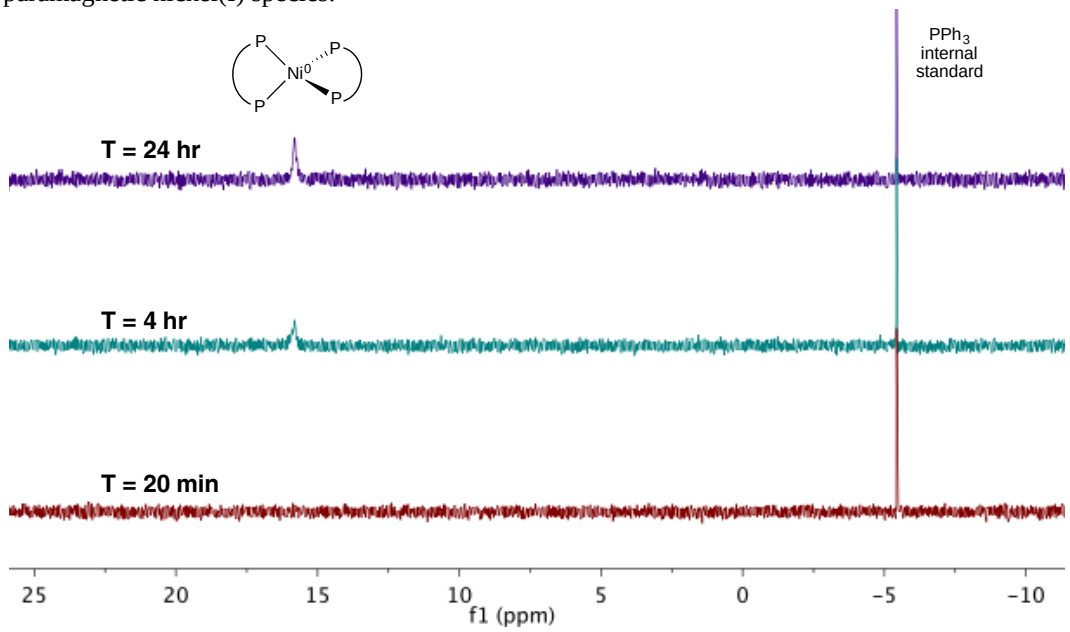

Figure S13B. ^{31}P{^{1}H} NMR spectra showing the appearance of **11** over the course of 24 hours.

*Stability of (dppf)Ni(2,4,6-$^{i}Pr_3C_6H_2$) (**3**) in the Presence of Boronic Acid*

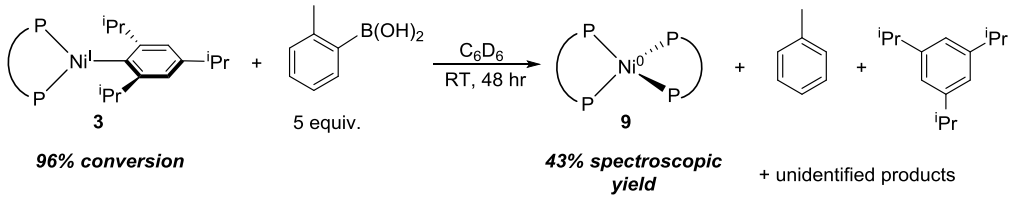

To a J-Young tube containing a capillary of cobaltocene in C_6D_6 as well as a capillary of PPh_3 in C_6D_6 was added *o*-tolylboronic acid (5 equiv, 0.0158 mmol, 2.1 mg). **3** (0.00316 mmol, 2.6 mg) was added to a vial and dissolved in 500 µL of C_6D_6. The solution was then added to the J-Young tube, and the tube was capped and initial ^{1}H and ^{31}P NMR spectra recorded, with the following parameters used for ^{1}H NMR spectroscopy: nt=256 scans, d1=0.5 s, at=1.0 s, sweep width (-75, 75 ppm). Spectra were taken intermittently over two days with agitation of the tube before each time point. After 48 hours the contents of the J-Young tube was exposed to air and ran through a pipet column containing approximately 5 cm of silica using an eluent of ethyl acetate. The mixture was then analyzed by GC.

The ^{1}H and ^{31}P NMR spectra of the reaction are shown in Figure S14. By ^{1}H NMR spectroscopy, degradation occurs at a rate such that, after 48 hours of reaction, only 4% of the starting nickel(I) aryl remains (Figure S14A). Over the course of the reaction **11** is generated as the sole zerovalent nickel product, as indicated by ^{31}P NMR spectroscopy (Figure S14B). GC analysis indicates that two aryl products, toluene and 1,3,5-triisopropylbenzene, are generated. Quantification after 24 hours indicates that 72% of the starting nickel(I) aryl species is consumed, and **11** is produced in 27% yield. Further, 43% of the nickel resides in the form of **11** at the end of the reaction, where the maximum yield of **11** is 50%. The toluene seen by GC is presumably due to protodeborylation of the boronic acid and is a byproduct of the excess boronic acid used in the reaction.

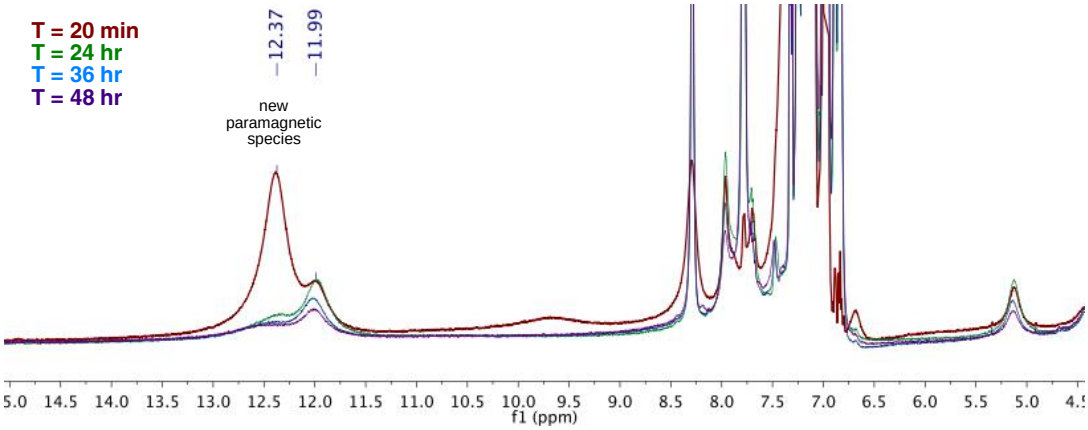

Figure S14A. Truncated ^{1}H NMR spectrum showing the presence of a new paramagnetic nickel species and subsequent degradation over 48 hours.

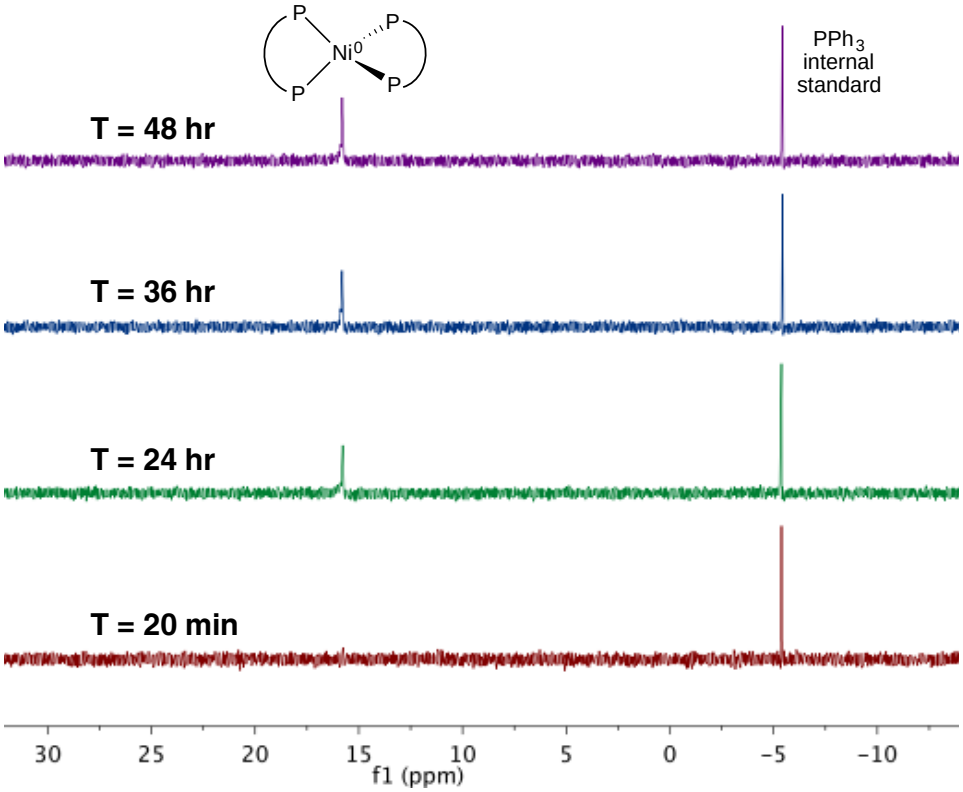

Figure S14B. ^{31}P{^{1}H} NMR spectra showing the appearance of **11** over the course of 48 hours.

*Stability of (dppf)Ni(2,4,6-$^{i}Pr_3C_6H_2$) (**3**) in the Presence of Base*

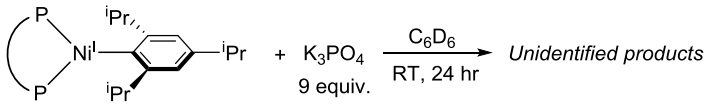

3

36% conversion

To a J-Young tube containing a capillary of cobaltocene in C_6D_6 as well as a capillary of PPh_3 in C_6D_6 was added K_3PO_4 (9 equiv, 0.0284 mmol, 6.0 mg). In a vial, **3** (0.00316 mmol, 2.6 mg) was dissolved in 500 µL of C_6D_6, and the solution was added to the J-Young tube. The tube was capped and initial ^{1}H and ^{31}P NMR spectra were recorded, with the following parameters used for ^{1}H NMR spectroscopy: nt=256 scans, d1=0.5 s, at=1.0 s, sweep width (-75, 75 ppm). Spectra were taken intermittently over one day with agitation of the tube before each time point. The ^{1}H and ^{31}P NMR spectra are given in Figure S15A and B, respectively.

Reaction of the nickel(I) aryl species with excess base results in an acceleration in the rate of decay. Under standard conditions with no additives, only 7% of the starting nickel(I) aryl is lost; however, when base is present in the reaction mixture, 36% of the nickel(I) aryl is lost in the same time frame, although the products were not identified.

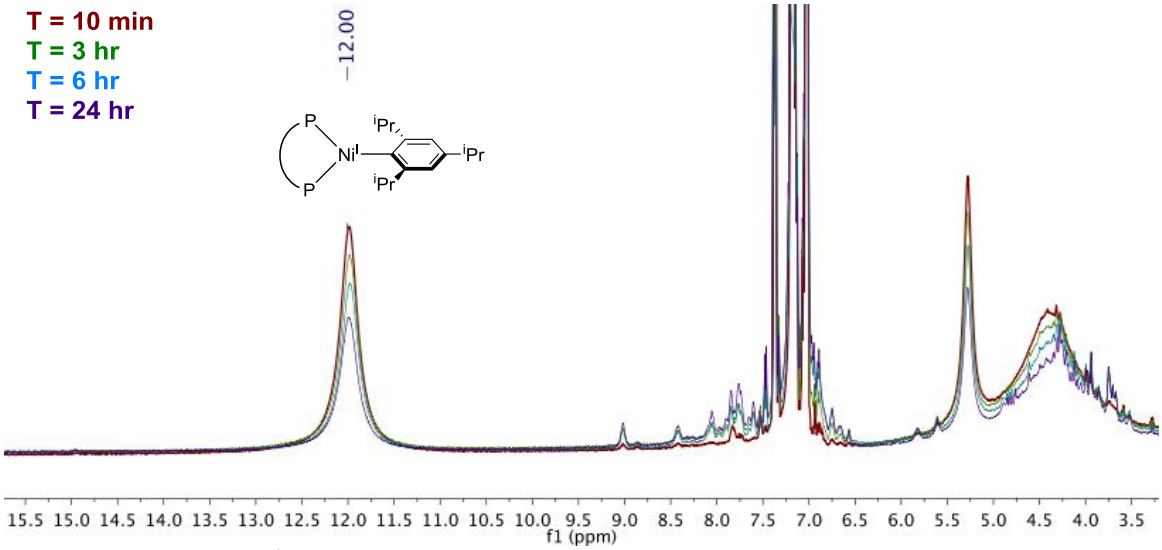

Figure S15A. Truncated ^{1}H NMR spectrum showing the increased rate of degradation of **3** over 24 hours in the presence of base.

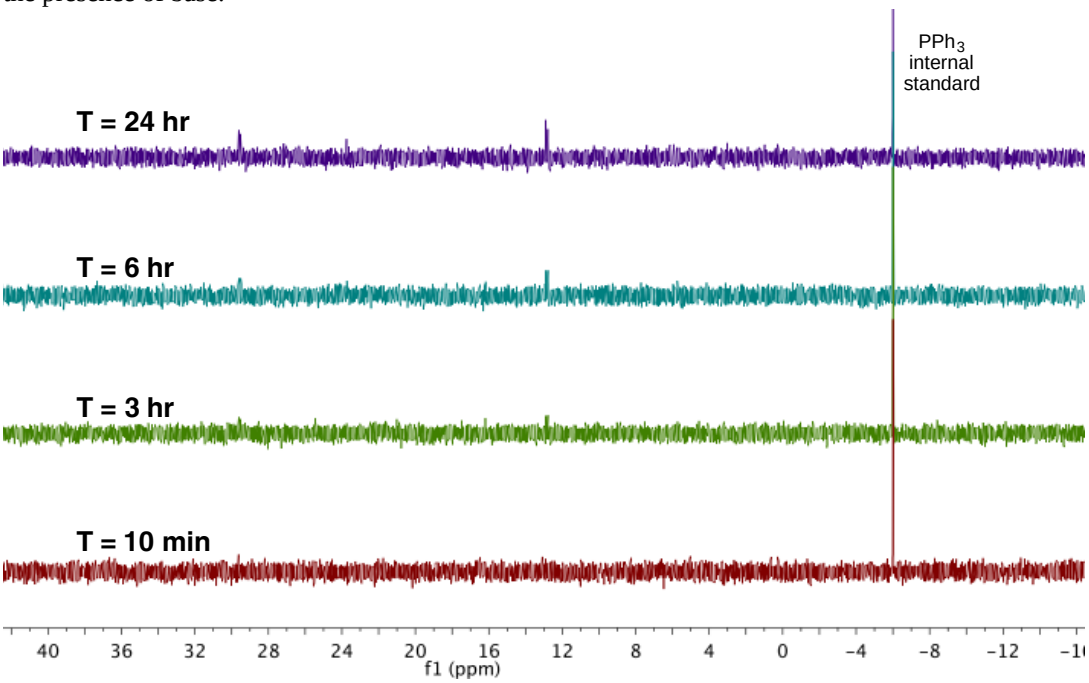

Figure S15B. ^{31}P{^{1}H} NMR spectra course showing the appearance of a unidentified nickel species over the course of 24 hours.

*Stability of (dppf)Ni(2,4,6-$^{i}Pr_3C_6H_2$) (**3**) in the Presence of Boronic Acid and Base*

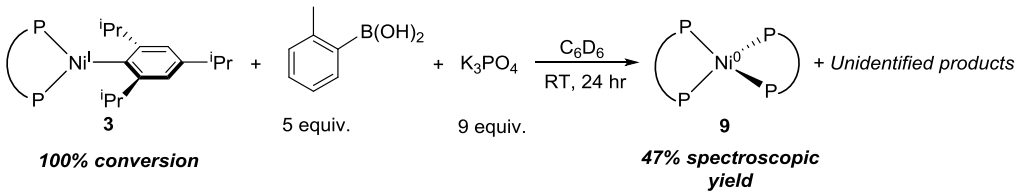

To a J-Young tube containing a capillary of cobaltocene in C_6D_6 as well as a capillary of PPh_3 in C_6D_6 was added *o*-tolylboronic acid (5 equiv, 0.0158 mmol, 2.1 mg) and K_3PO_4 (9 equiv, 0.0284 mmol, 6.0 mg). In a vial, **3** (0.00316 mmol, 2.6 mg) was dissolved in 500 µL of C_6D_6, and the solution was added to the J-Young tube. The tube was capped and initial ^{1}H and ^{31}P NMR spectra were recorded, with the following parameters used for ^{1}H NMR spectroscopy: nt=256 scans, d1=0.5 s, at=1.0 s, sweep width (-75, 75 ppm). Spectra were taken intermittently over one day with agitation of the tube before each time point. The ^{1}H and ^{31}P NMR spectra are given in Figure S16 A and B, respectively.

Compared to the degradation rate seen in the reaction of **3** with the individual components of transmetalation, reaction of **3** with both boronic acid and base results in rapid decomposition of the nickel(I) aryl to closed shell nickel species. Namely, **11** is produced in 13% yield within 10 minutes of reaction time, and reaches a maximum yield of 47% after 24 hours.

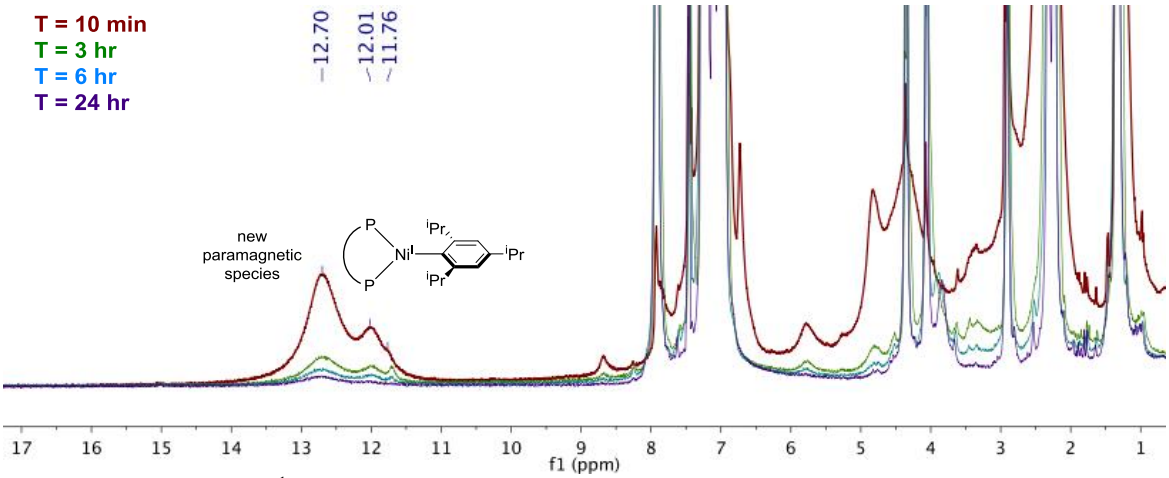

Figure S16A. Truncated ^{1}H NMR spectrum showing the increased rate of degradation of **3** over 24 hours and the appearance of a new, unstable paramagnetic species.

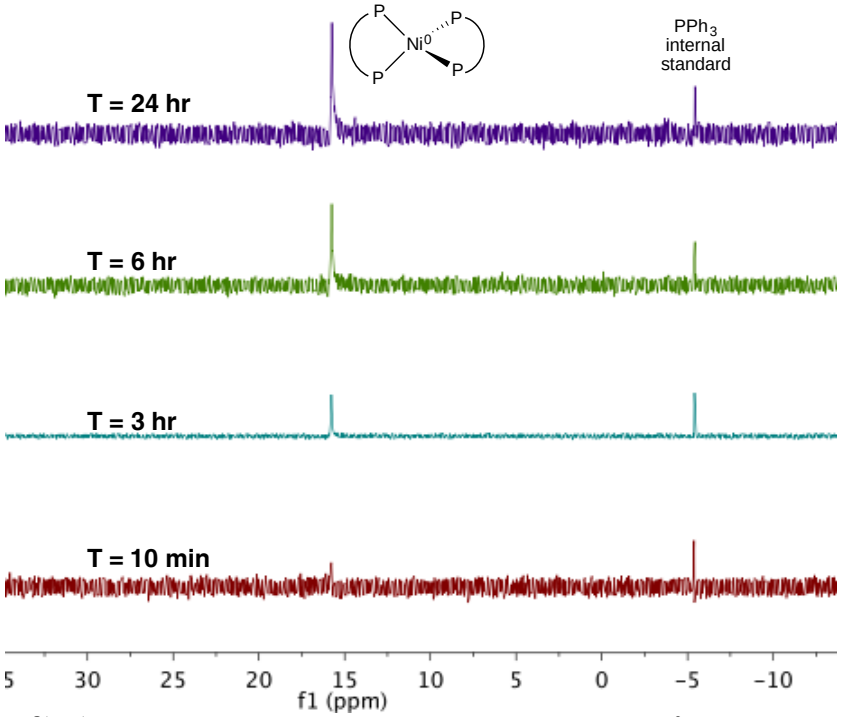

Figure S16B. ^{31}P{^{1}H} NMR spectra showing the appearance of $(dppf)_2Ni^0$ (**11**) over the course of 24 hours.

SVII. Stoichiometric Reactivity of Nickel(I) Aryl Species

*Reaction of (dppf)Ni^{I}(2,4,6-^{i}Pr$_3$C$_6$H$_2$) (**3**) with 2,6-Lutidinium Chloride*

To a J-Young tube containing a capillary of cobaltocene in C_6D_6 as well as a capillary of PPh_3 in C_6D_6 was added 2,6-lutidinium chloride (2 equiv., 0.00735 mmol, 1.1 mg). In a vial, **3** (0.00368 mmol, 3.0 mg) was dissolved in 500 µL of C_6D_6. The nickel solution was then added to the J-Young tube, after which the tube was capped and taken out of the glovebox. The tube was sonicated for 1 hour to dissolve the 2,6-lutidinium chloride, ensuring that the water bath stayed at room temperature while sonicating. After one hour, ^{1}H and ^{31}P NMR spectra were recorded, with the following parameters used for ^{1}H NMR spectroscopy: nt=256 scans, d1=0.5 s, at=1.0 s, sweep width (-75, 75 ppm).

The ^{1}H NMR indicated full conversion to **1**, evidenced by the peaks at 12.5 ppm and 4.4 ppm, which correspond to the phenyl protons on one phosphorus of the dppf (integration = 10 H) and the protons on both cyclopentadienyl rings (integration = 8 H), respectively (Figure S17A). Notably, 1,3,5-triisopropylbenzene is formed in quantitative yield as well.

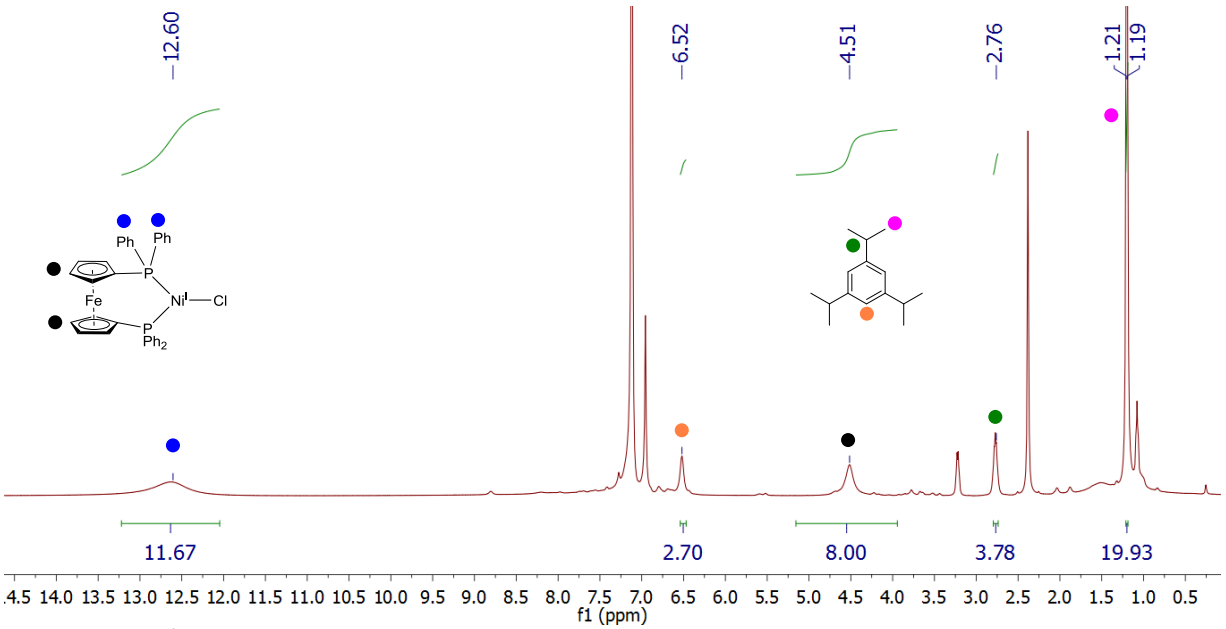

Figure S17A. ^{1}H NMR spectrum of the products of the reaction of **3** with 2,6-lutidinium chloride at room temperature for one hour.

The experiment was repeated without a superstoichiometric amount of 2,6-lutidinium chloride. With one equivalent of 2,6-lutidinium chloride, complete conversion to **1** does not occur, presumably because of the marked insolubility of 2,6-lutidinium chloride in C_6D_6. As a consequence, only a fraction of the starting **3** was converted to **1**, as determined by ^{1}H NMR

spectroscopy (Figure S17B). Disproportionation of the two Ni(I) centers then occurs to yield (dppf)Ni^{II}(2,4,6-$^{i}Pr_3C_6H_2$)(Cl) (the chloride analogue of **9**) and an unidentified Ni(0) product, as determined by ^{31}P NMR spectroscopy (Figure S17C).

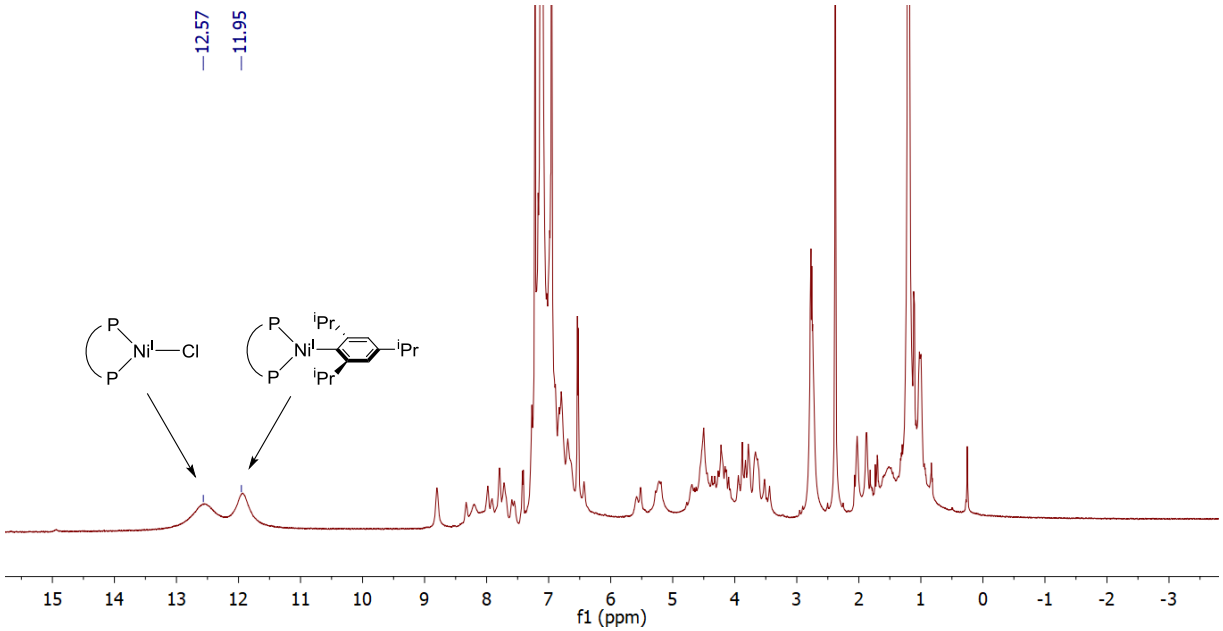

Figure S17B. ^{1}H NMR spectrum of the products of the reaction of **3** with one equivalent of 2,6-lutidinium chloride at room temperature for one hour.

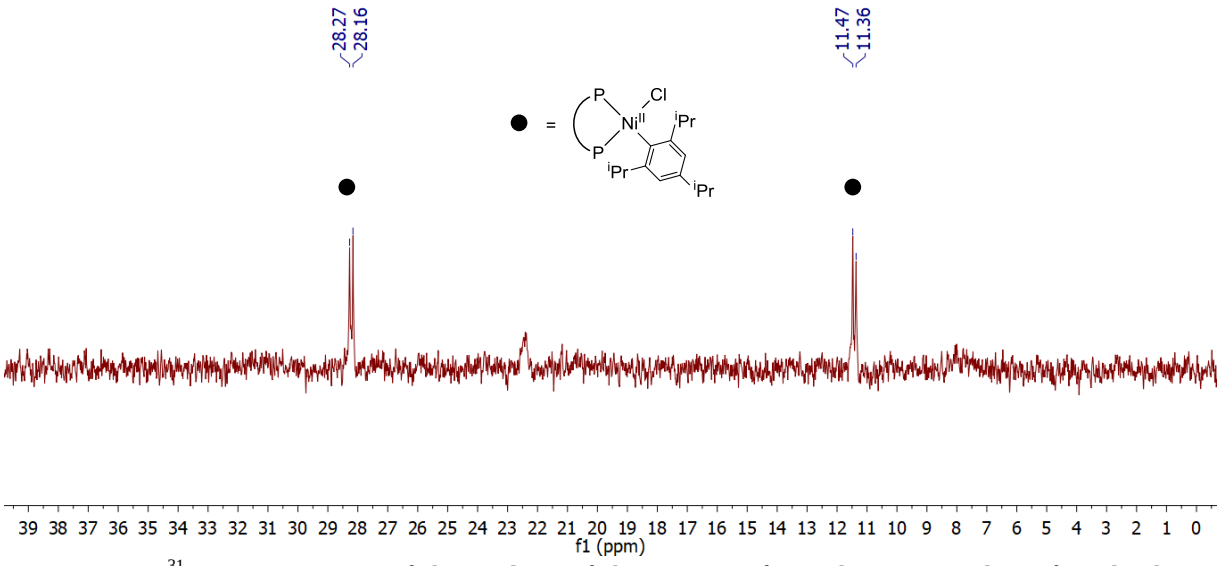

Figure S17C. ^{31}P NMR spectrum of the products of the reaction of **3** with one equivalent of 2,6-lutidinium chloride at room temperature for one hour.

In order to assess the outcome of the protonation reaction with a non-coordinating anion on the acid, **3** was reacted with 2,6-lutidinium tetrakis(3,5-bis(trifluoromethyl)phenyl)borate. To a J-Young tube containing a capillary of cobaltocene in C_6D_6 as well as a capillary of PPh_3 in C_6D_6 was added 2,6-lutidinium BAr^F_4 (BAr^F_4 = tetrakis(3,5-bis(trifluoromethyl)phenyl)borate) (2 equiv., 0.00735 mmol, 7.1 mg). In a vial, **3** (0.00368 mmol, 3.0 mg) was dissolved in 500 µL of C_6D_6. The nickel solution was added to the J-Young tube, after which the tube was capped and taken out of the glovebox. The tube was sonicated for 1 hour to dissolve the 2,6-lutidinium BAr^F_4, ensuring that the water bath stayed at room temperature while sonicating. After one hour, ^1H and ^{31}P NMR spectra were recorded, with the following parameters used for ^1H NMR spectroscopy: nt=256 scans, d1=0.5 s, at=1.0 s, sweep width (-75, 75 ppm).

The ^1H NMR spectrum indicated that several signals attributed to new, unidentified paramagnetic species arise after one hour at room temperature (Figure S18A). Further, 1,3,5-triisopropylbenzene is formed. As indicated by the ^{31}P NMR spectroscopy, free ligand is released in the reaction (Figure S18B). Taken with the data from the reaction of **3** with 2,6-lutidinium chloride, it appears that protonation of the nickel(I) aryl species to produce the monoaryl product occurs readily, and the resulting identity and stability of the nickel species produced after protonation is a function of the coordinating anion from the acid. These experiments provide insight into the mechanism of the reaction of **3** with boronic acid; protonation of the nickel(I) aryl species by the boronic acid and coordination of the boronate anion leads to an unstable nickel(I) halide species that degrades over the course of the reaction to zerovalent products.

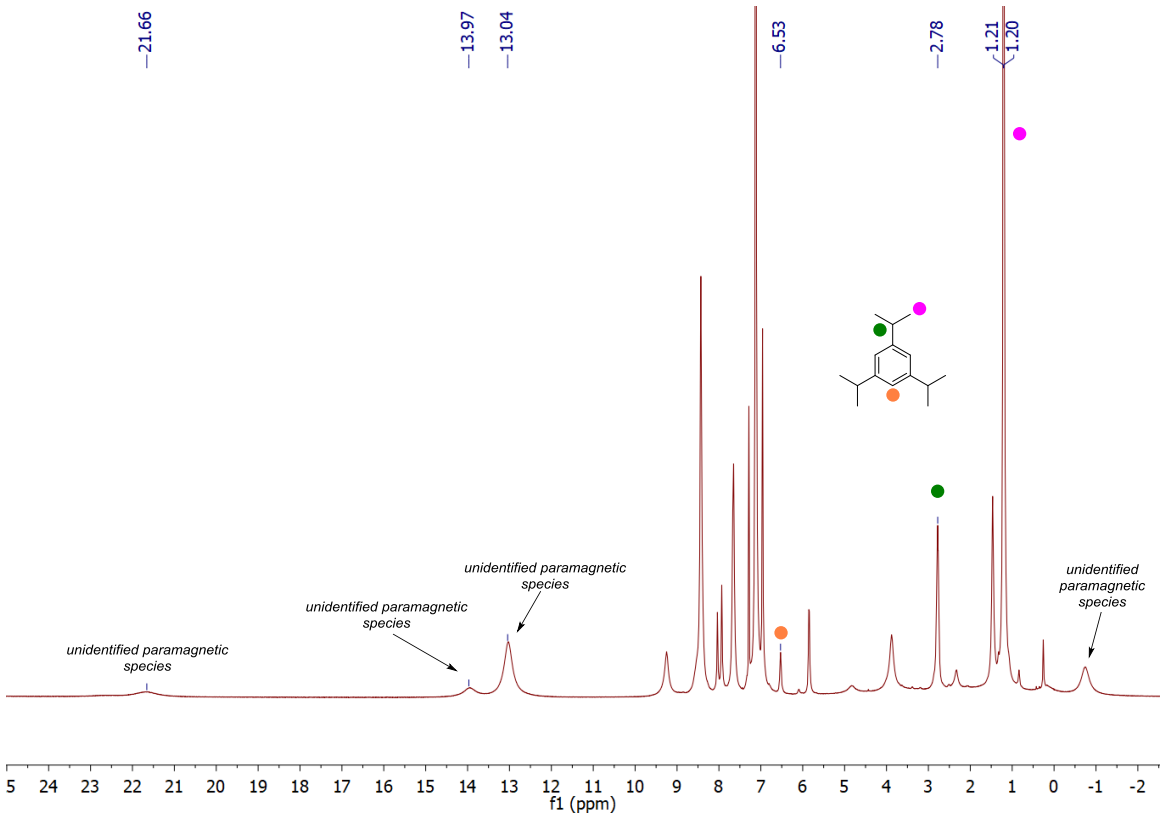

Figure S18A. ^{1}H NMR spectrum of the products of the reaction of **3** with 2,6-lutidinium BAr^{F}_{4} at room temperature for one hour.

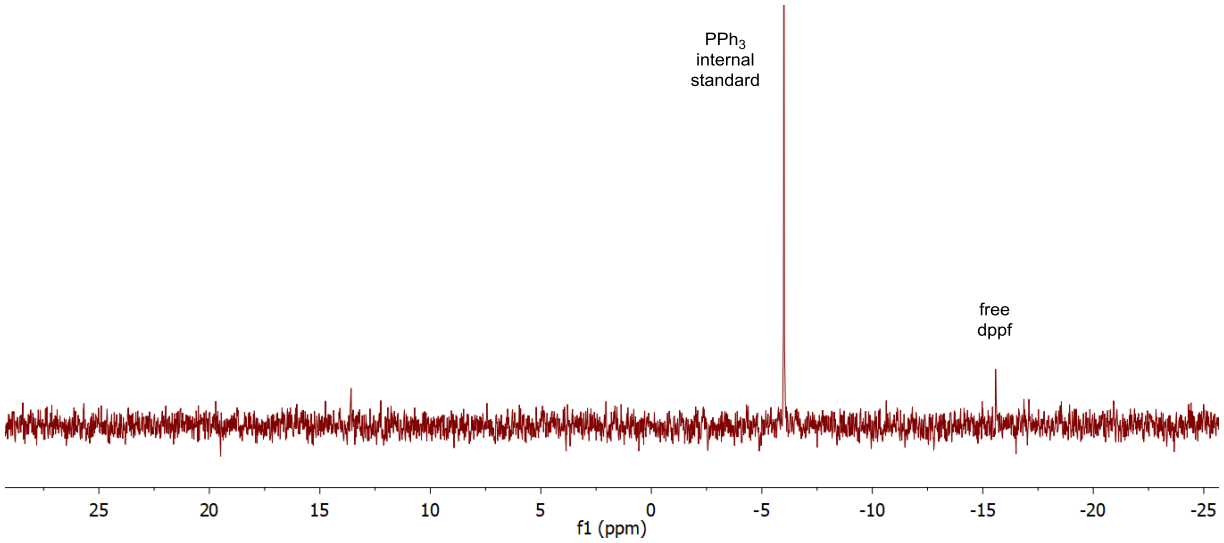

Figure S18B. ^{31}P NMR spectrum of the reaction of **3** with 2,6-lutidinium BAr^{F}_{4} at room temperature for one hour, indicating that free ligand is released.

*Reaction of (dppf)Ni^{I}(2,4,6-^{i}Pr$_3$C$_6$H$_2$) (**3**) with TEMPOH*

A stock solution of TEMPOH was prepared by dissolving 1.4 mg of TEMPOH in 200 µL of C_6D_6. A stock solution of COD was also prepared by adding 4 µL of COD to 10 µL of C_6D_6. To a J-Young tube containing a capillary of cobaltocene in C_6D_6 as well as a capillary of PPh_3 in C_6D_6 was added **3** (0.00316 mmol, 2.6 mg). 400 µL of C_6D_6 was added to the J-Young tube via micropipette, after which the tube was capped and agitated until **3** dissolved. ^{1}H and ^{31}P NMR spectra were immediately recorded in order to calibrate the internal standards. The tube was then quickly brought into a glovebox, after which 106.5 µL of TEMPOH stock solution (1.5 equiv., 0.00474 mmol) and 1 µL of COD stock solution (1.5 equiv., 0.00474 mmol) were added via micropipette. The tube was capped, inverted to mix, and then ^{1}H and ^{31}P NMR spectra were taken intermittently with agitation of the tube before each time point. The following parameters were used for ^{1}H NMR spectroscopy: nt=256 scans, d1=0.5 s, at=1.0 s, sweep width (-75, 75 ppm). Analysis using EPR spectroscopy was conducted by removing a 35 µL aliquot of the solution in the J-Young tube after one hour of reaction time and adding the aliquot to an EPR tube containing 165 µL of toluene. A room temperature, X-Band EPR spectrum was recorded in order to establish that TEMPO radical formed in the reaction.

^{1}H NMR spectra of the reaction as a function of time (Figure S19A) indicate that 68% of starting the nickel(I) aryl species disappears after 24 hours, with full conversion achieved after 36 hours. The final nickel product is **8**, obtained in 61% spectroscopic yield after 24 hours and 100% spectroscopic yield after 36 hours. 1,3,5-triisopropylbenzene is formed as an organic product in this reaction, reaching a 55% yield after 24 hours and a 94% yield at full consumption of the nickel(I) aryl starting material. ^{31}P{^{1}H} NMR spectra of the reaction as function of time clearly shows an increase in a singlet at 33.7 ppm, corresponding to **8** (Figure S19B).[11] The product of hydrogen atom donation from TEMPOH was detected using EPR spectroscopy; after one hour of reaction, a signal corresponding to TEMPO radical is apparent in the room temperature X-band EPR spectrum (Figure S19C).[12]

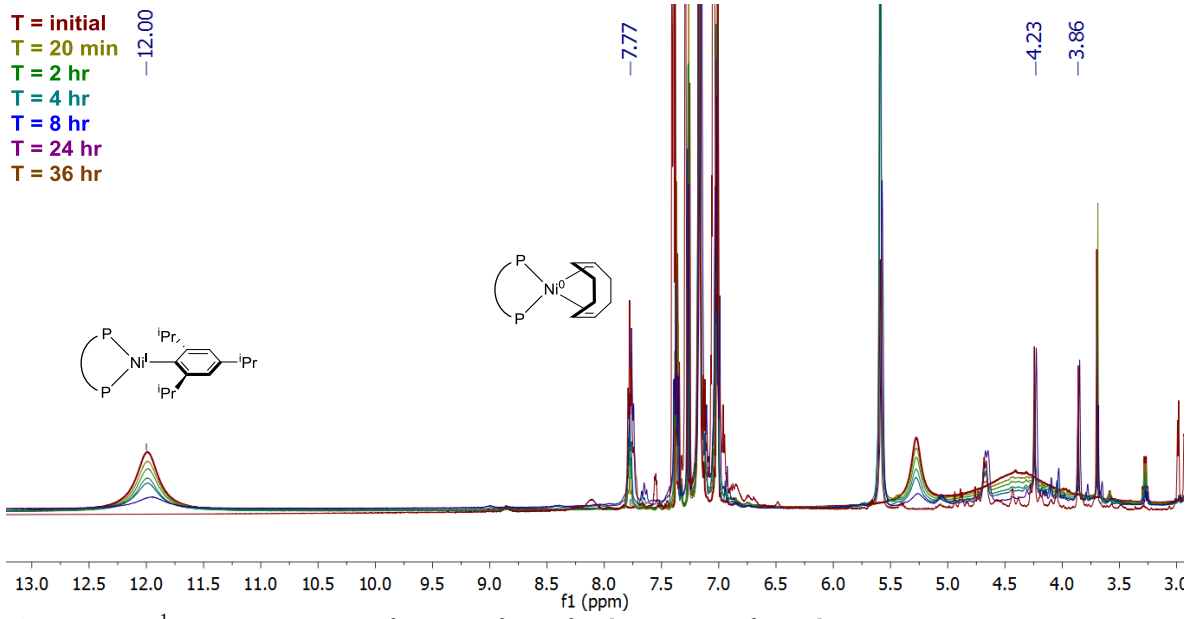

Figure S19A. ^{1}H NMR spectra as a function of time for the reaction of **3** with TEMPOH.

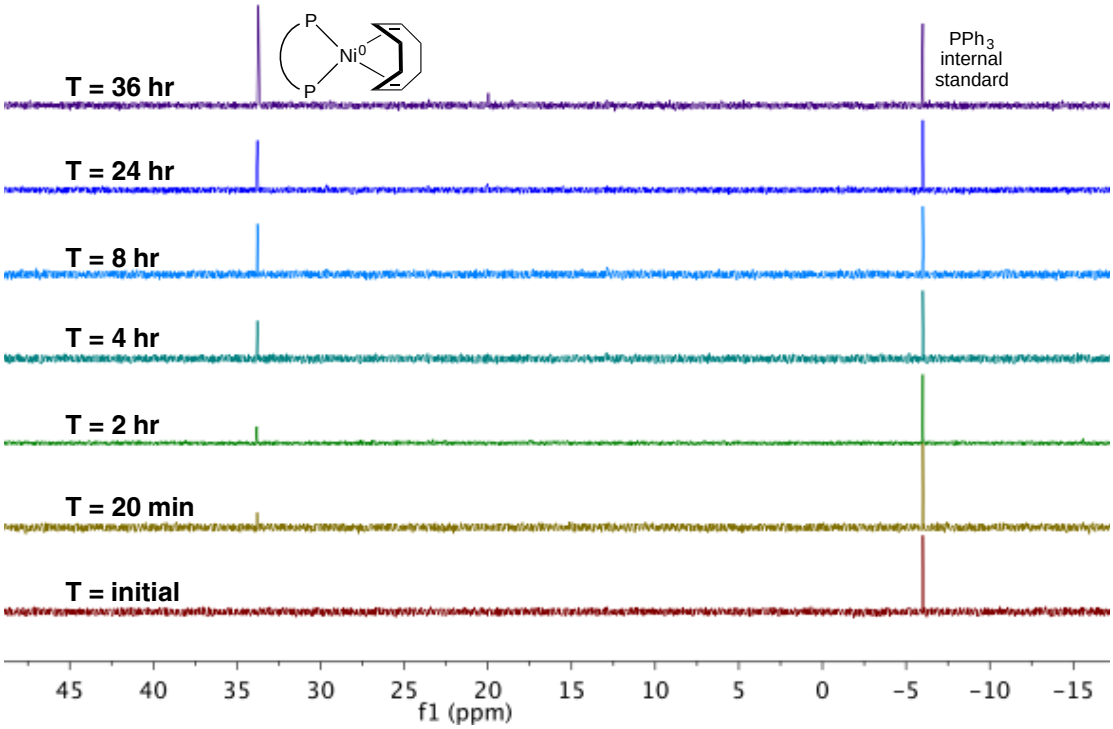

Figure S19B. ^{31}P{^{1}H} NMR spectra showing the formation of (dppf)Ni^{0}(COD) **(8)** as a function of time in the reaction of **3** with TEMPOH.

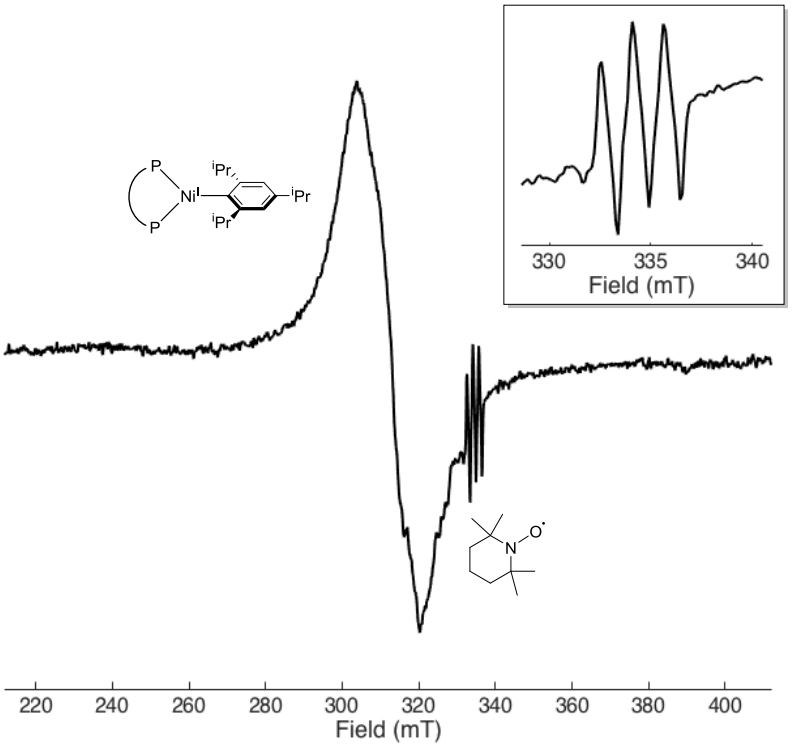

Figure S19C. Room temperature, X-band EPR spectrum from reaction of **3** with TEMPOH in the presence of COD for one hour. Inset: The triplet at ~335 mT is consistent with that of TEMPO radical, indicating that a hydrogen atom has been donated from TEMPOH. MW Frequency: 9.37 GHz, MW Power: 0.2 mW. Spectrum is the sum of 12 scans.

*Reaction of (dppf)Ni^{I}(2,4,6-^{i}Pr$_3$C$_6$H$_2$) (**3**) with Electrophile (1-Chloronaphthalene)*

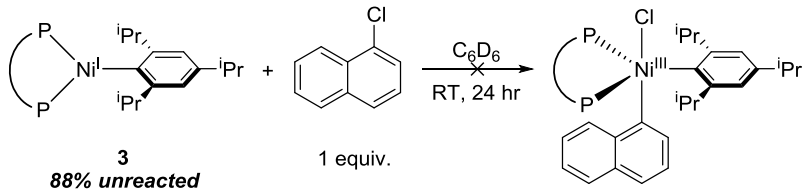

3
88% unreacted

1 equiv.

To a J-Young tube containing a capillary of cobaltocene in C_6D_6 as well as a capillary of PPh_3 in C_6D_6 was added **3** (0.00316 mmol, 2.6 mg). A stock solution containing 4 µL of 1-chloronaphthalene in 100 µL of C_6D_6 was prepared. The contents of the J-Young tube were dissolved in 500 µL of C_6D_6, after which 10 µL (1 equiv., 0.00316 mmol) of the 1-chloronaphthalene stock solution was added via micropipette. The tube was capped and agitated, after which ^{1}H and ^{31}P NMR spectra were recorded, with the following parameters used for ^{1}H NMR spectroscopy: nt=256 scans, d1=0.5 s, at=1.0 s, sweep width (-75, 75 ppm). Spectra were taken intermittently, with agitation of the tube prior to each time point. There was no discernible reaction between **3** and 1-chloronaphthalene, as monitored by ^{1}H and ^{31}P NMR spectroscopy (Figure S20A & S20B). However slow degradation of **3** was observed; over 24 hours, 12% of the nickel(I) aryl species is consumed. This rate of decomposition is consistent with the solution instability of **3** in C_6D_6 and is inconsistent with any reactivity between **3** and 1-chloronaphthalene.

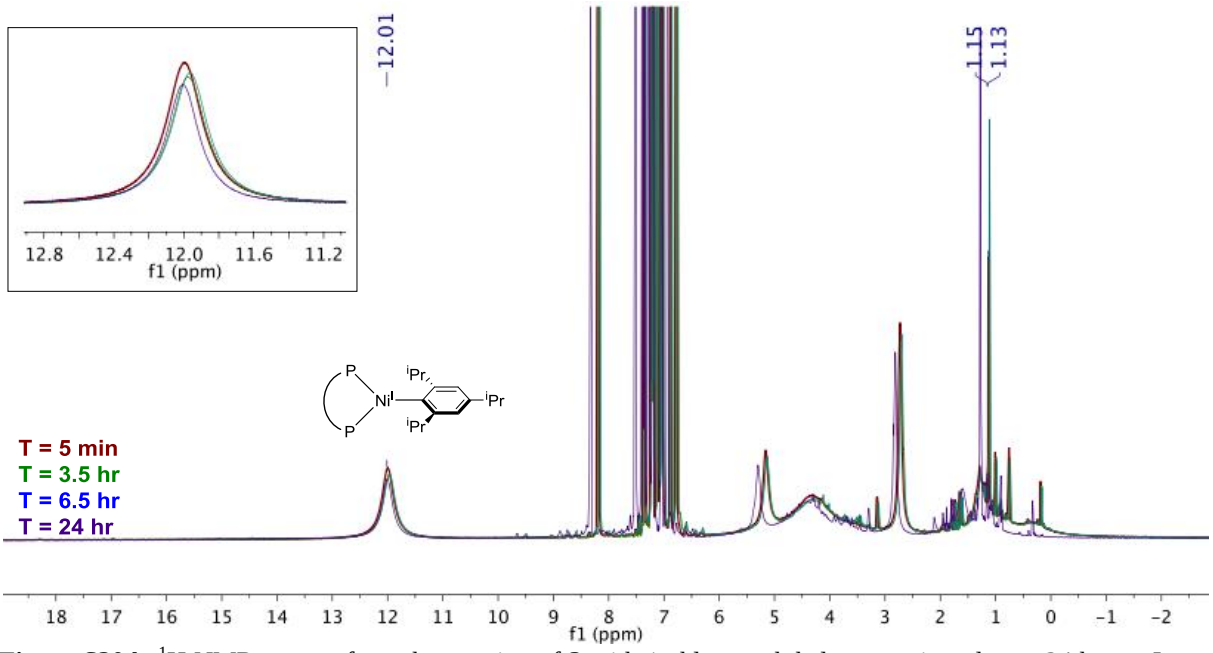

Figure S20A. ^{1}H NMR spectra from the reaction of **3** with 1-chloronaphthalene monitored over 24 hours. Inset: decrease in the phenyl proton signal of **3** over 24 hours.

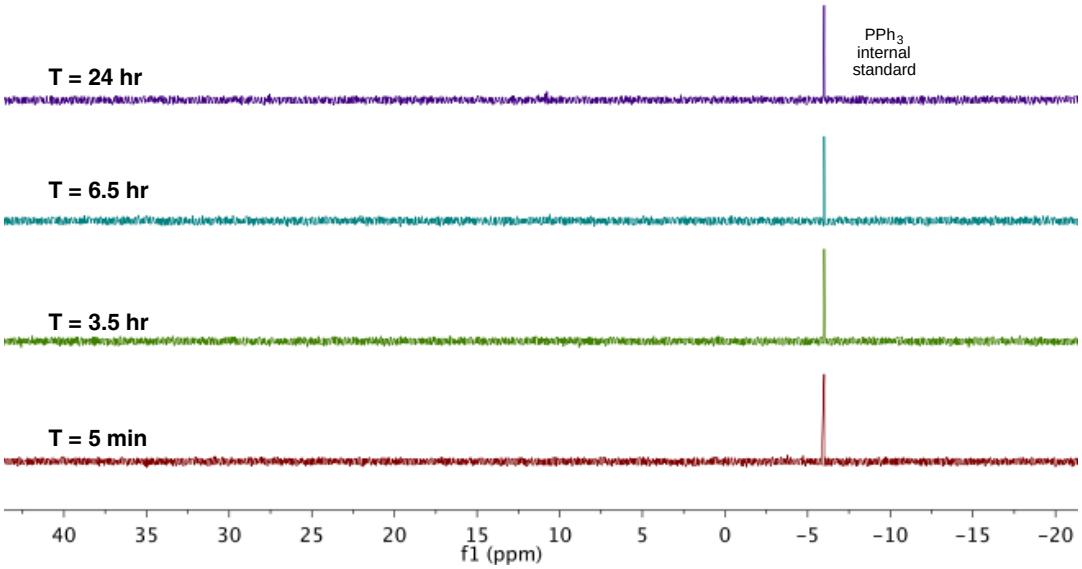

Figure S20B. ^{31}P{^{1}H} NMR spectra from the reaction of **3** with 1-chloronaphthalene monitored over 24 hours.

*Reaction of (dppf)Ni^{I}(2,4,6-mesityl) (**6**) and (dppf)Ni^{I}(2,6-xylyl) (**5**) with Electrophile (1-Chloronaphthalene)*

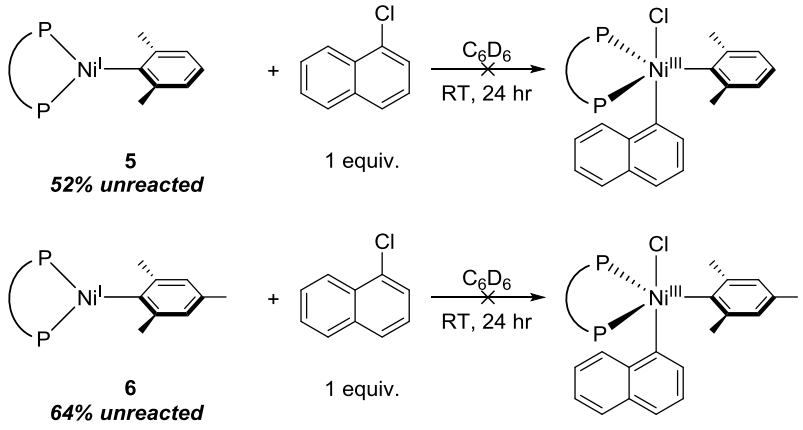

To a J-Young tube containing a capillary of cobaltocene in C_6D_6 as well as a capillary of PPh_3 in C_6D_6 was added **1** (0.00316 mmol, 2.0 mg). 500 µL of C_6D_6 was added to the tube via micropipette, and the tube was agitated until the contents dissolved. The appropriate arylmagnesium bromide (1.5 equiv., 0.00474 mmol) was added via micropipette, and the tube was capped tightly and agitated by inversion twice. ^{1}H and ^{31}P NMR spectra were immediately recorded, with the following parameters used for ^{1}H NMR spectroscopy: nt=256 scans, d1=0.5 s, at=1.0 s, sweep width (-75, 75 ppm). A stock solution containing 4 µL of 1-chloronaphthalene in 100 µL of C_6D_6 was prepared. After the initial set of spectra were recorded, the tubes were pumped into the glove box, after which 10 µL (1 equiv., 0.00316 mmol) of the 1-chloronaphthalene stock solution was added via micropipette. The tube was capped and agitated, after which ^{1}H and ^{31}P NMR spectra were recorded. Spectra were taken intermittently, with agitation of the tube prior to each time point.

In both cases the addition of 1-chloronaphthalene did not result in an observable oxidative addition product to the nickel(I) aryl species by ^{1}H NMR spectroscopy, and the rate of decay of the *in situ* formed nickel(I) aryl species was consistent with the of the rate of decay determined in Figure S2A (Figure S21A and S22A). By ^{31}P NMR spectroscopy, an identical set of new doublets was formed in both cases (Figure S21B and S22B). It is proposed that this species is the result of oxidative addition of 1-chloronaphthalene to (dppf)Ni^{0}, (dppf)Ni^{II}(1-naphthyl)(Cl), which is formed from the decay of the nickel(I) aryl species. These results suggest that the nickel(I) aryl species themselves do not react with 1-chloronaphthalene.

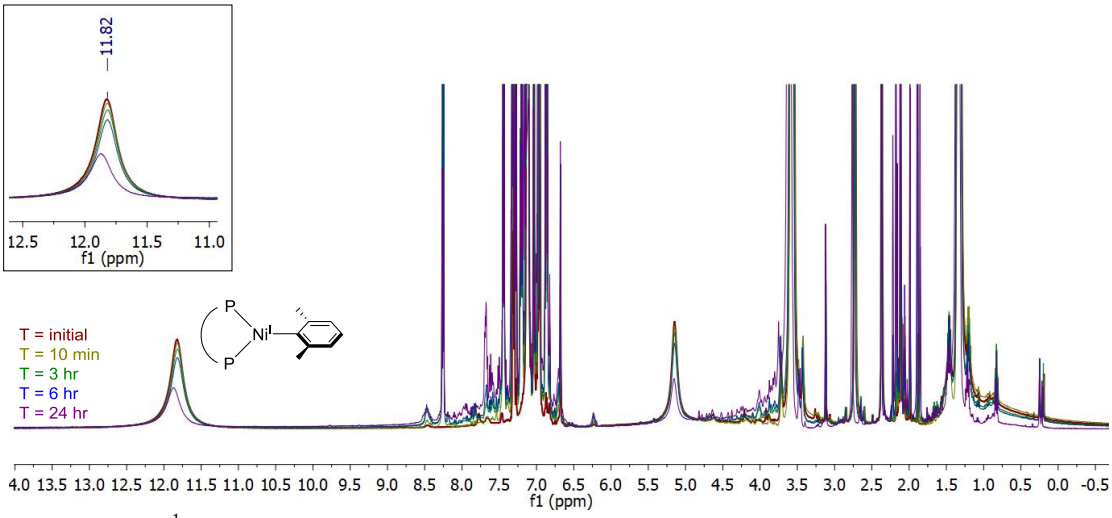

Figure S21A. ^{1}H NMR spectra from the reaction of *in situ* formed **5** with 1-chloronaphthalene monitored over 24 hours. Inset: decrease in the phenyl proton signal of **5** over 24 hours.

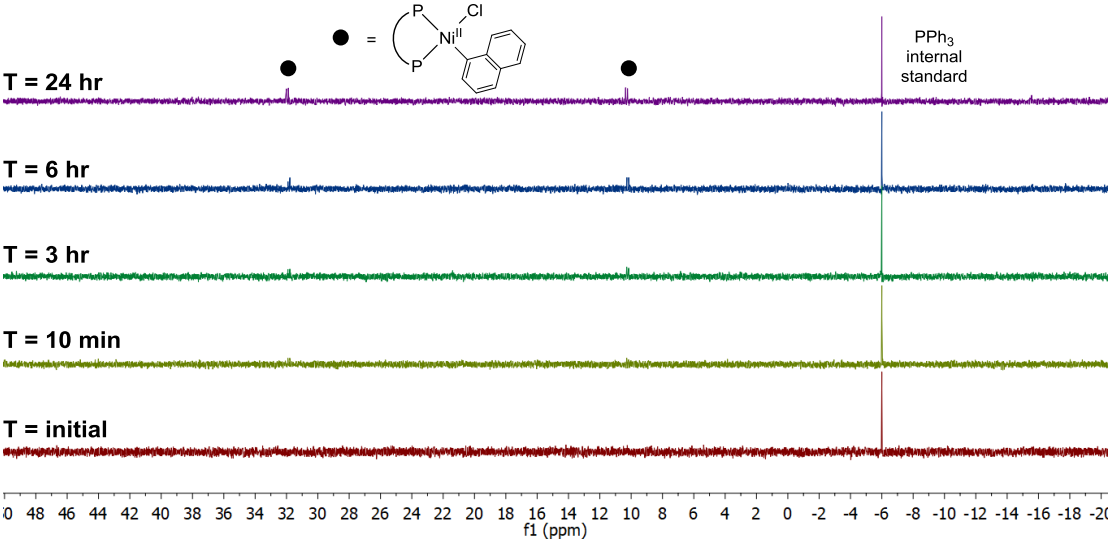

Figure S21B. ^{31}P{^{1}H} NMR spectra from the reaction of *in situ* formed **5** with 1-chloronaphthalene monitored over 24 hours.

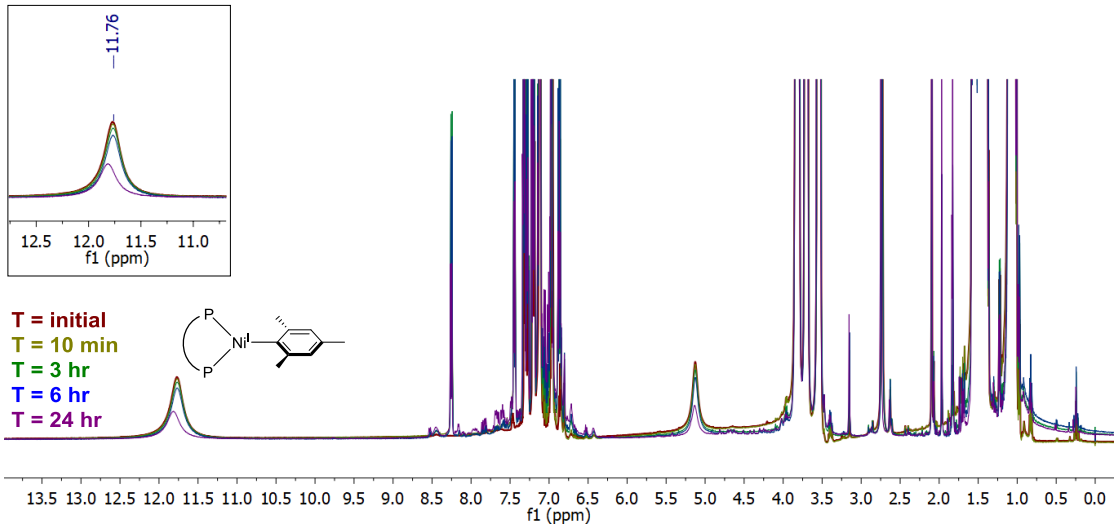

Figure S22A. ^{1}H NMR spectra from the reaction of *in situ* formed **6** with 1-chloronaphthalene monitored over 24 hours. Inset: decrease in the phenyl proton signal of **6** over 24 hours.

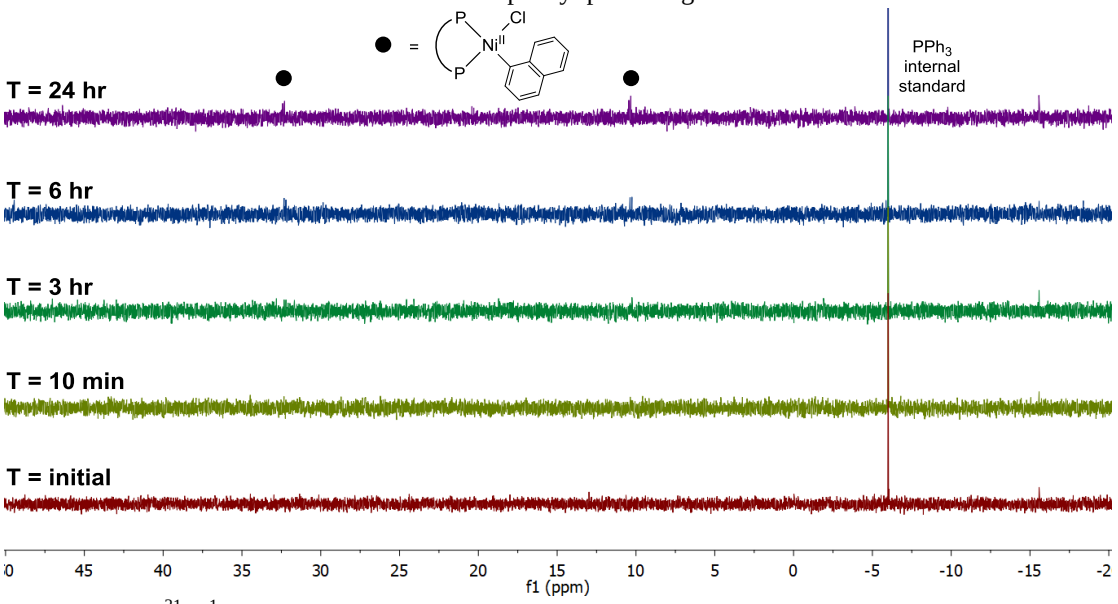

Figure S22B. ^{31}P{^{1}H} NMR spectra from the reaction of *in situ* formed **6** with 1-chloronaphthalene monitored over 24 hours.

*Disproportionation of (dppf)Ni^{I}(2,4,6-^{i}Pr$_3$C$_6$H$_2$) (**3**) and (dppf)Ni^{I}Br (**2**)*

To a J-Young tube containing a capillary of cobaltocene in C_6D_6 as well as a capillary of PPh_3 in C_6D_6 was added **3** (0.00316 mmol, 2.6 mg) and **2** (0.00316 mmol, 2.2 mg). A stock solution containing 4 µL of COD in 100 µL of C_6D_6 was prepared. 10 µL (1 equiv., 0.00316 mmol) of the COD stock solution was added to the J-Young tube, after which the contents were dissolved in 500 µL of C_6D_6. The tube was capped and left at room temperature for 30 minutes with occasional agitation by inversion. After 30 minutes, ^{1}H and ^{31}P NMR spectra were recorded, with the following parameters used for ^{1}H NMR spectroscopy: nt=256 scans, d1=0.5 s, at=1.0 s, sweep width (-75, 75 ppm). At this time, all starting material was consumed and no further timepoints were taken. The ^{31}P{^{1}H} NMR spectra indicates conversion to the disproportionation products (dppf)Ni^{II}(2,4,6-^{i}Pr$_3$C$_6$H$_2$)(Br) (**9**) and (dppf)Ni^{0}(COD) (**8**) in the 1:1 ratio expected for the binuclear event (Figure S23).

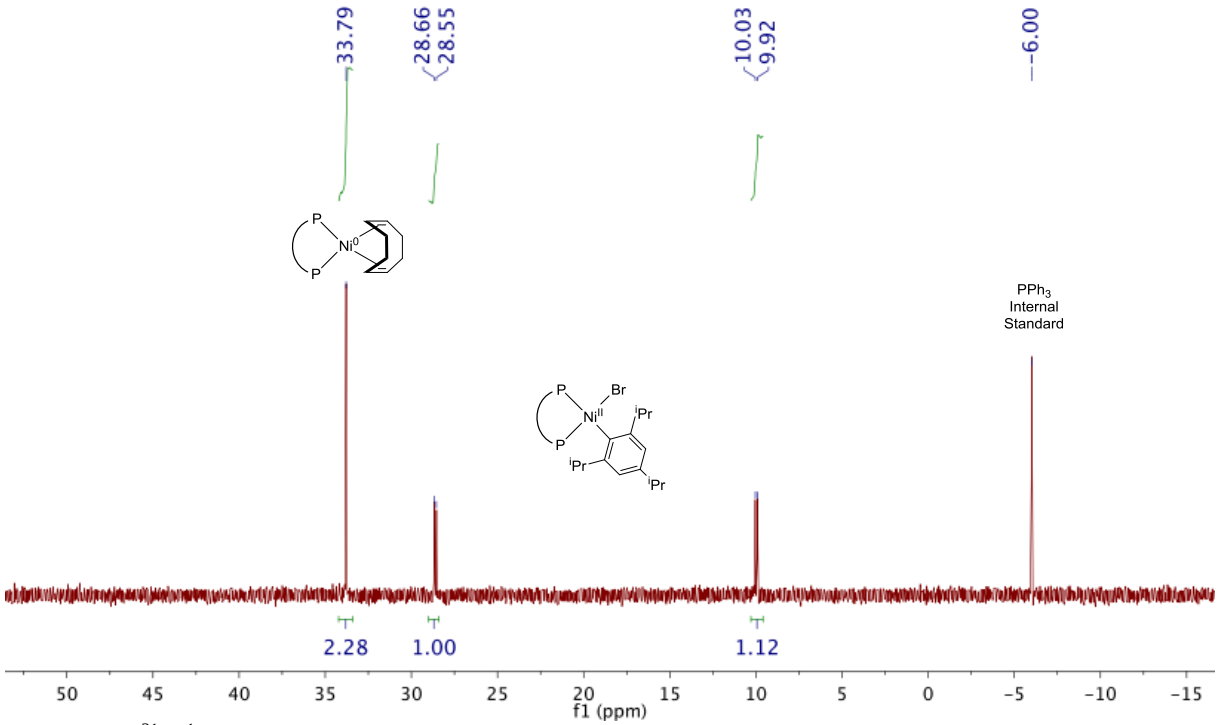

Figure S23. ^{31}P{^{1}H} NMR spectrum showing the formation of **9** and **8** in a 1:1 ratio from the disproportionation of **3** and **2** in the presence of COD after 30 minutes at room temperature.

*Comproportionation of (dppf)Ni^{II}(2,4,6-^{i}Pr$_3$C$_6$H$_2$)(Br) (**9**) with (dppf)Ni^{0}(C$_2$H$_4$) (**10**)*

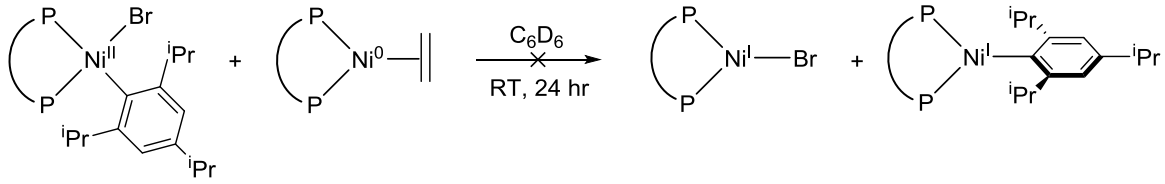

9 1 equiv. | **10** 1 equiv. | **2** + **3** ***97% retention of Ni(II) and Ni(0)***

To a J-Young tube containing a capillary of cobaltocene in C_6D_6 as well as a capillary of PPh_3 in C_6D_6 was added **9** (0.00418 mmol, 3.7 mg) and (dppf)Ni^{0}(C_2H_4) (**10**) (0.00418 mmol, 2.0 mg). 500 µL of C_6D_6 was added, and the tube was sealed and sonicated for ten minutes until dissolution of all components. ^{1}H and ^{31}P NMR spectra were taken, with the following parameters used for ^{1}H NMR spectroscopy: nt=256 scans, d1=0.5 s, at=1.0 s, sweep width (-75, 75 ppm). The tube was then returned to the sonicator and sonicated for another hour, ensuring that the water bath stayed at room temperature. Another set of spectra were obtained. The tube was then left without sonication for 23 hours, after which a final time point was recorded.

The ^{1}H NMR spectra indicates that, after 24 hours at room temperature, a small amount (~3%) of **2** is formed (as evidenced by the appearance of a new peak at ~12.5 ppm, Figure S24A), but there is no evidence for a nickel(I) aryl species. Additionally, when **9** is left for 24 hours at room temperature in C_6D_6 a small amount (~3%) of **2** is formed (Figure S25), suggesting that decomposition of the starting material is responsible for this product. The ^{31}P{^{1}H} NMR spectrum shows essentially no consumption of starting materials or formation of new products (Figure 24B). Overall, this model reaction indicates that comproportionation is not occurring.

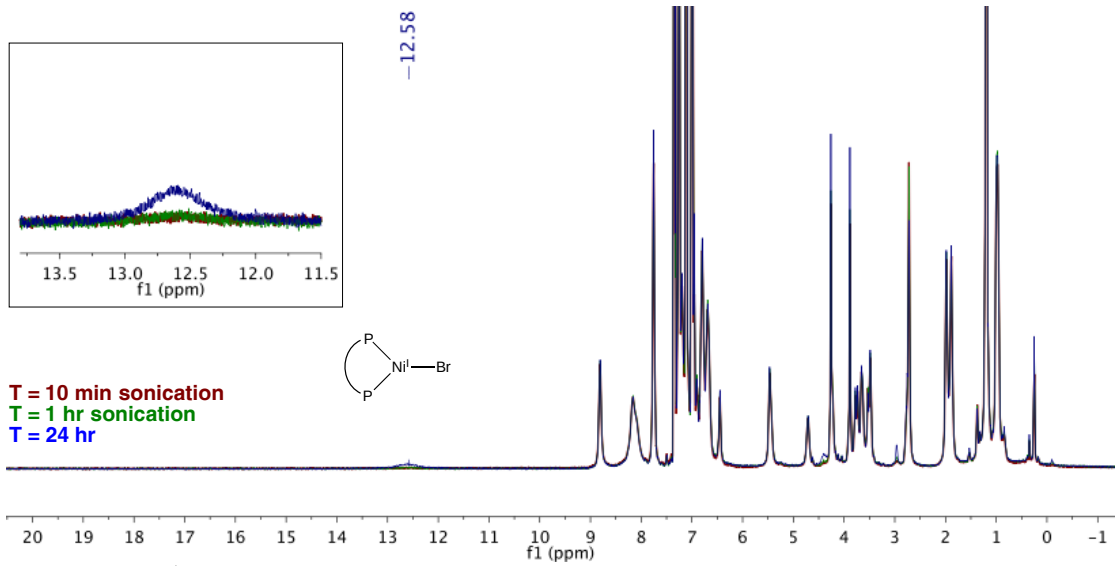

Figure S24A. ^{1}H NMR spectrum indicating no formation of comproportionation products after 24 hours for the reaction of **9** with **10**. Inset: Formation of ~3% **2** occurs after 24 hours.

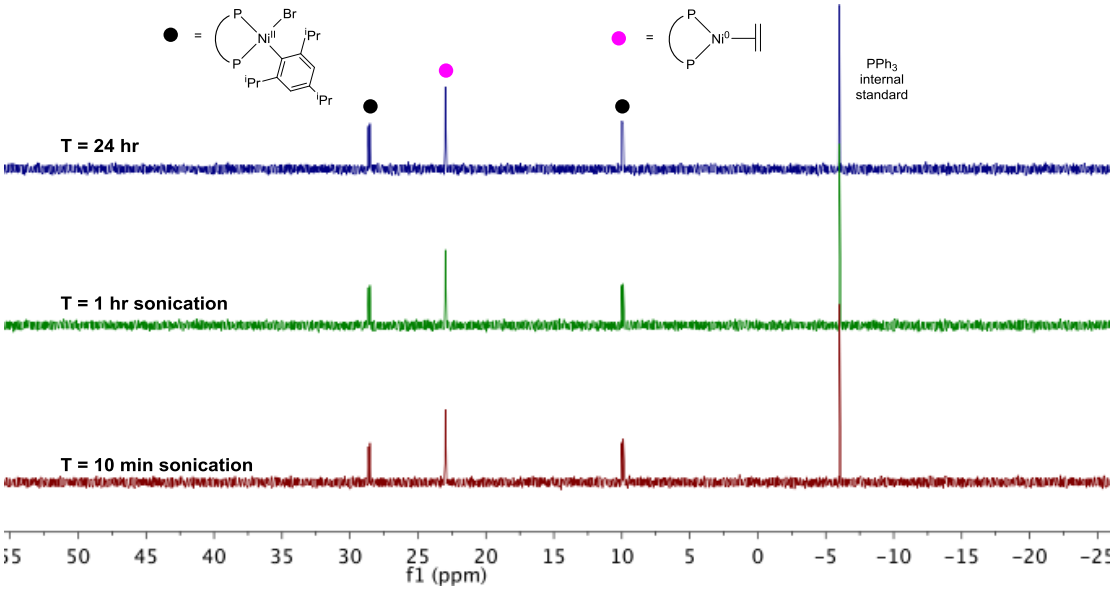

Figure S24B. ^{31}P{^{1}H} NMR spectra indicating essentially no consumption of starting material or formation of new products after 24 hours for the reaction of **9** with **10**.

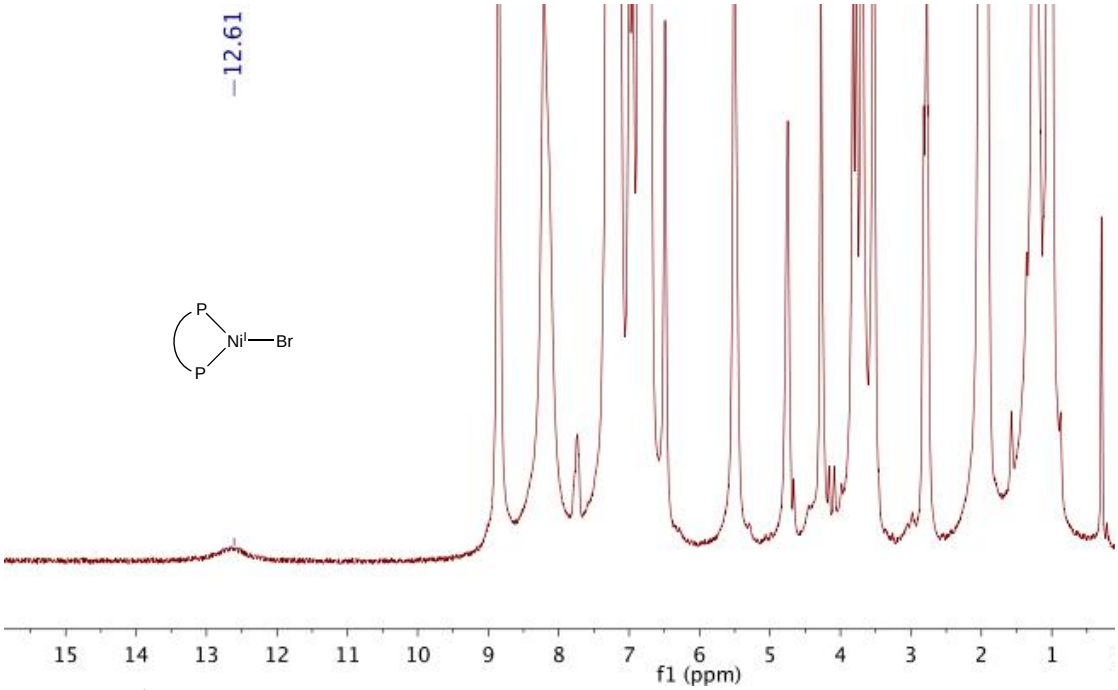

Figure S25. ^{1}H NMR spectrum of **9** in C_6D_6 for 24 hours, indicating the formation of a small amount of **2**.

SVIII. Catalytic Reactions

General Procedure for Pre-Mixing of a Nickel(I) Halide Precatalyst with Additive

A stock solution containing naphthalen-1-yl sulfamate (0.266 mmol) and naphthalene (0.133 mmol) in 2 mL of toluene was prepared. 4-methoxyphenylboronic acid (50.0 mg, 0.333 mmol) and K_3PO_4 (127.2 mg, 0.599 mmol) were weighed into a 1-dram vial containing a stir bar. 1 mL of the electrophile stock solution was added via micropipette to the vial. Another stock solution containing **1** (2.5 mol%, 0.00665 mmol, 4.4 mg) in 200 µL of toluene was prepared. The appropriate Grignard reagent (1.5 equiv.) was added to the nickel solution via micropipette, after which the solution was agitated for a minute before 100 µL was added to the reaction vial. The vial was tightly capped and removed from the glovebox. The vial was then placed in an aluminum heating block with a thermocouple at room temperature and stirred for 4 hours. The reactions were quenched by exposure to air, after which 100-200 µL of the reaction mixture was added to a ~5 cm plug of silica and eluted with ethyl acetate. The yield of cross-coupled product was determined by gas chromatography, referenced to the naphthalene internal standard. All reactions were performed in duplicate and the reported yields are the average of two runs. Because the pre-mixing of **1** and phenylmagnesium bromide appeared to degrade most of the active nickel at room temperature, the *in situ* generation of **7** was repeated at low temperature. The procedure above was repeated, except the solution of **1** was frozen. The solution was then brought up to slightly above the freezing temperature, after which phenylmagnesium bromide was added. The mixture was swirled to mix, after which it was immediately transferred to the reaction vial, and the reaction was performed and worked up as normal. The low temperature preparation of **7** gave a 70% yield of cross-coupled product.

Procedure for the Comparative Selectivity of Nickel(I) Aryl Precatalysts

A stock solution containing 4-trifluoromethylphenyl sulfamate (71.6 mg, 0.266 mmol), 4-methoxyphenyl sulfamate (61.6 mg, 0.266 mmol), and naphthalene (16.8 mg, 0.133 mmol was prepared in 2 mL toluene. In the case of **3**, the precatalyst (2.5 mol%, 0.00665 mmol, 5.4 mg) was included in this stock solution. For the nickel(I) aryl species generated *in situ*, **1** (2.5 mol %, 4.4 mg, 0.00665 mmol) was added to a separate vial and dissolved in 200 µL of toluene, after which the appropriate arylmagnesium bromide Grignard reagent (0.00665 mmol, 2.5 mol %) was added via micropipette. To a 1-dram vial containing a stir bar was added 4-methoxyphenylboronic acid (20.2 mg, 0.133 mmol) and K_3PO_4 (127.2 mg, 0.599 mmol). 1 mL of stock solution was added to the vial via micropipette, and 100 µL of *in* situ generated nickel(I) aryl stock solution was added, if applicable. The vial was capped tightly, removed from the glovebox, and placed in an aluminum heating block. The reaction mixture was stirred at 80 °C for 24 hours, after which the reactions were quenched by exposure to air. 50-100 µL of the reaction mixture was eluted through a ~5 cm plug of silica with ethyl acetate. Yields were determined by gas chromatography, referenced to the internal standard. The amount of aryl product of interest was quantified by the ratio of peak area of the peak of interest to the peak area of internal standard. All reactions were performed in duplicate and the yields are the average of two runs.

Comparison of the ratio of product formed in the reaction catalyzed by **3**, **6** and **5** indicates that, within error, a similar ratio is formed to that of the closed-shell precatalysts **11** and (dppf)Ni^{II}(*o*-tolyl)(Cl), **12** (Table S2).[8] This suggests that, regardless of the initial oxidation state, the precatalysts are forming the same catalytic intermediates. Paired with the data that nickel(I) aryl species degrade to zerovalent nickel species under catalytic conditions, this implies that nickel(0) may be the true catalytically relevant oxidation state when nickel(I) aryl precatalysts are employed in Suzuki-Miyaura reactions.

Table S2. Selectivity ratios for the comparative product formation experiment using dppf-ligated precatalysts in a range of oxidation states.

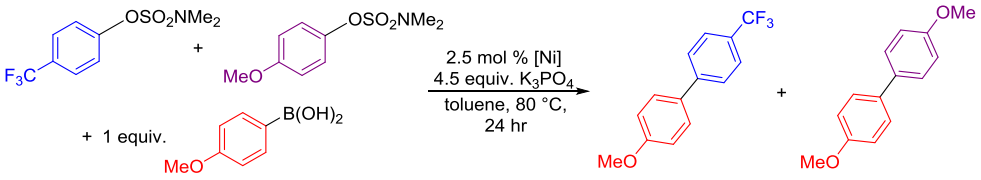

Entry	[Ni]	EWG/EDG product ratio
1	**11**	1.67 ± 0.11[12]
2	**1**	1.66 ± 0.11[12]
3	**1** + 2,6-xylylMgBr	1.99 ± 0.26
4	**1** + 2,4,6-mesitylMgBr	2.09 ± 0.18
5	**3**	1.63 ± 0.19
6	**12**	1.86 ± 0.04[12]

Reaction conditions: 0.133 mmol 4-trifluoromethylphenyl dimethylsulfamate, 0.133 mmol 4-methoxyphenyl dimethylsulfamate 0.133 mmol 4-methoxyphenylboronic acid, 0.599 mmol K_3PO_4, 0.0665 mmol naphthalene (internal standard), 2.5 mol % precatalyst and 1 mL toluene. Yields are the average of two runs and were determined by GC.

SIX. Discussion on the Role of Nickel(I) Aryl Species in Suzuki-Miyaura Reactions

The Role of Ni(I) Aryl Species in Suzuki-Miyaura Reactions Catalyzed by Nickel(0) and Nickel(II) Precatalysts

We have previously demonstrated that a problem in Suzuki-Miyaura reactions using the state-of-the-art (dppf)Ni^{II}(*o*-tolyl)(X) (X = Cl, **12** or Br, **13**) as a precatalyst is a lack of selectivity during activation.[13] Activation of **12** or **13** to the nickel(0) active species is proposed to occur via transmetalation with the arylboronic acid to generate a species of the form (dppf)Ni^{II}(*o*-tolyl)(Ar), which subsequently reductively eliminates a biaryl product to form nickel(0). However, as a result of a competing comproportionation reaction between unreacted (dppf)Ni^{II}(*o*-tolyl)(X) and the active nickel(0) species, (dppf)Ni^{I}X and an intermediate that we postulated to be a nickel(I) aryl species form (Scheme 1A). Further, if transmetalation is slow, comproportionation can also occur during oxidative addition to generate a nickel(I) aryl species and a nickel(I) halide species (Scheme 1B). We surmised that the lack of selectivity in the activation and oxidative addition processes reduces the total amount of nickel that is in an active form initially and decreases catalytic activity through the formation of off-cycle species.

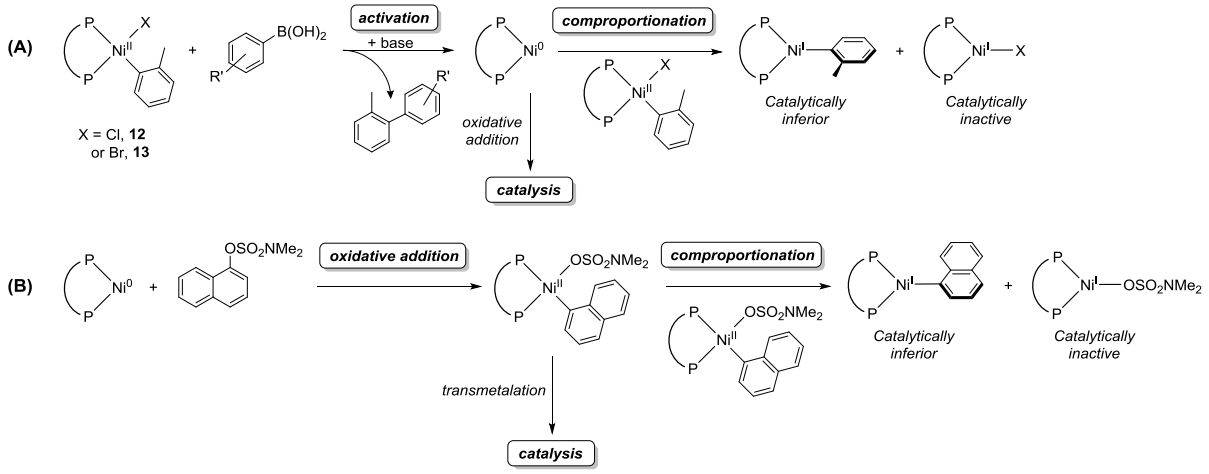

Scheme S1. Proposed mechanism of comproportionation during **(A)** activation and **(B)** oxidative addition for a state-of-the-art nickel(II) precatalyst.

Based on our experimental evidence on the catalytic activity of nickel(I) aryl species in the Suzuki-Miyaura coupling of naphthalen-1-yl sulfamate and our previous data on the performance of nickel(II) and nickel(0) precatalysts, it is evident that, in most cases, the nickel(I) aryl species have inferior catalytic activity to that of nickel(0) and nickel(II) precatalysts (Table S3). The inferior catalytic activity of the nickel(I) aryl species is consistent with the mechanistic proposal

that nickel(I) aryl species are off-cycle, and their formation is detrimental to catalysis employing closed-shell nickel species. Additional support for this notion comes from our experimental data from the comparative selectivity experiment, in which the nickel(I) aryl species generate the same product ratio as their nickel(0) counterpart, implying that the on-cycle intermediates are similar. Paired with the discovery that nickel(I) aryl species readily degrade to zerovalent nickel species, we propose that the true catalytically active oxidation state is nickel(0), and formation of nickel(I) aryl species delays formation of nickel(0), reducing the efficiency of productive catalysis.

Table S3. Comparison of Ni(I) precatalysts for the Suzuki-Miyaura reaction of naphthalen-1-yl sulfamate and 4-methoxyphenylboronic acid.

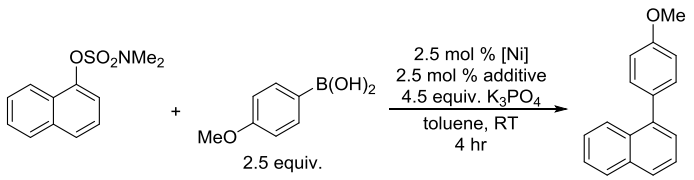

	Entry	[Ni]	Additive	Yield
Ni(I) precatalysts	1	**1**	none	<1%
	2	**1**	(Ph)MgBr	70%
	3	**1**	(*o*-tolyl)MgBr	>99%
	4	**1**	(2,6-xylyl)MgBr	79%
	5	**1**	(2,4,6-mesityl)MgBr	79%
	6	**1**	(2,4,6-$^{i}Pr_3C_6H_2$)MgBr	19%
	7	**3**	none	10%
Ni(0)/(II) precatalysts[13]	8	**11**	none	>99%
	9	**12**	none	>99%
	10	**13**	none	>99%

Reaction conditions: 0.133 mmol naphthalene-1-yl dimethylsulfamate, 0.333 mmol 4-methoxyphenylboronic acid, 0.599 mmol K_3PO_4, 0.0665 mmol naphthalene (internal standard), 2.5 mol % precatalyst and 2.5 mol % additive, and 1 mL toluene. Ni precatalyst was premixed with additive prior to addition of other reagents (see SI). Yields are the average of two runs and were determined by GC. Data for entries 8-10 taken from ref. 13.

The Role of Ni(I) Aryl Species in Suzuki-Miyaura Reactions Catalyzed by Nickel(I) Halide Precatalysts

When using nickel(I) halide precatalysts we propose that nickel(I) aryl species are intermediates in precatalyst activation to a nickel(0) active species. Evidence for this comes from the reaction of nickel(I) halide species **1** and **2** with boronic acid and base mixtures to generate nickel(I) aryl species. Additionally, we have determined that the catalytic efficiency of the nickel(I) aryl species is inversely correlated to the stability of the species (Table S3), with stability essentially defining the rate at which zerovalent nickel species are formed from the decomposition processes. With these two pieces of data, we propose that nickel(I) halide species, when used as precatalysts in the Suzuki-Miyaura reaction, activate by transmetallation to generate transiently stable nickel(I) aryl intermediates, which then degrade to produce zerovalent nickel species that are the true catalytically active intermediates (Scheme 2). Here, rapid formation of nickel(I) aryl species is *preferred*, as its subsequent degradation to nickel(0) results in more efficient catalysis. In contrast, when using nickel(0) and nickel(II) precatalysts the formation of nickel(I) aryl species via comproportionation (as described above) is *detrimental* to catalysis.

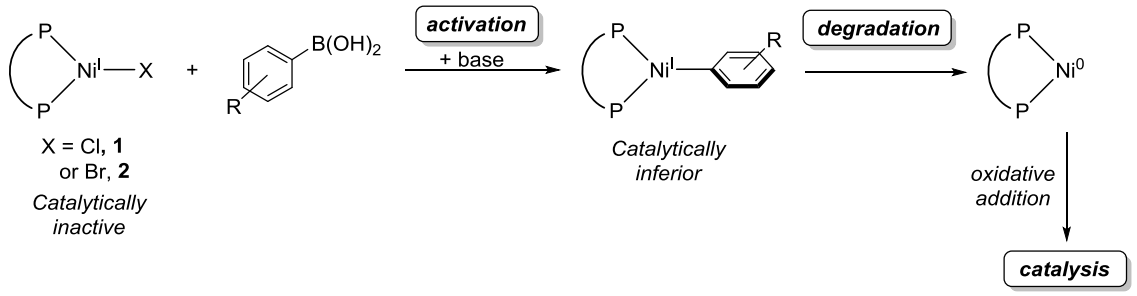

Scheme S2. Proposed mechanism of activation of nickel(I) halide precatalysts in Suzuki-Miyaura reactions, indicating the intermediacy of nickel(I) aryl species in forming catalytically active nickel(0) species.

SX. Crystallographic Data

*Crystallographic Information for (dppf)Ni^{I}(2,6-xylyl) (**5**) (CCDC: 1815574)*

Single crystals of **5** were grown from a concentrated toluene solution layered with pentane at -35 °C. Low-temperature diffraction data (ω-scans) were collected on a Rigaku SCX Mini diffractometer coupled to a Rigaku Mercury275R CCD with Mo Kα radiation (λ = 0.71073 Å) for the structure of **5**. The diffraction images were processed and scaled using Rigaku Oxford Diffraction software.[14] The structure was solved with SHELXT and was refined against F^2 on all data by full-matrix least squares with SHELXL.[15] All non-hydrogen atoms were refined anisotropically. Hydrogen atoms were included in the model at geometrically calculated positions and refined using a riding model. The isotropic displacement parameters of all hydrogen atoms were fixed to 1.2 times the U value of the atoms to which they are linked (1.5 times for methyl groups). The m-xylene group is equally disordered over two positions with respect to the crystallographic 2-fold axis. The special position constraints were suppressed. All chemically identical C-C bonds were refined with similarity restraints. The group was expected to behave as a rigid body and restrained to reflect this assertion. All disordered hydrogens were geometrically generated as riding atoms on their disordered carbons. After repeated attempts to model evidence of disorder in the toluene solvent, distance restraints of 1.395(2) Å were applied to all aryl C-C bonds in the toluene model to resolve the chemically unreasonable values that resulted from a free refinement. The full details of the X-ray structure determination are included in the .cif.

*X-ray Structure of **5***

Table S4. Crystal data and structure refinement for **5**.

Empirical formula	$C_{56}H_{53}FeNiP_2$	
Formula weight	902.48	
Temperature	93(2) K	
Wavelength	0.71073 Å	
Crystal system	Monoclinic	
Space group	I2/a	
Unit cell dimensions	a = 14.0344(9) Å	a= 90°.
	b = 13.3580(9) Å	β= 95.985(7)°.
	c = 23.5713(19) Å	γ = 90°.
Volume	4394.9(5) Å^3	
Z	4	
Density (calculated)	1.364 Mg/m^3	
Absorption coefficient	0.870 mm^{-1}	

F(000)	1892
Crystal size	0.300 x 0.050 x 0.050 mm^3
Crystal color and habit	Orange Plate
Theta range for data collection	2.635 to 26.425°.
Index ranges	-17<=h<=17, -16<=k<=16, -29<=l<=29
Reflections collected	28371
Independent reflections	4514 [R(int) = 0.0764]
Observed reflections (I > 2sigma(I))	3209
Completeness to theta = 25.242°	99.9 %
Absorption correction	Semi-empirical from equivalents
Max. and min. transmission	1.00000 and 0.84705
Data / restraints / parameters	4514 / 76 / 311
Goodness-of-fit on F^2	1.026
Final R indices [I>2sigma(I)]	R1 = 0.0475, wR2 = 0.1098
R indices (all data)	R1 = 0.0778, wR2 = 0.1246
Largest diff. peak and hole	0.641 and -0.486 e.$Å^{-3}$

Table S5. Atomic coordinates (x 10^4) and equivalent isotropic displacement parameters ($Å^2$ x 10^3) for **5**. U(eq) is defined as one third of the trace of the orthogonalized U^{ij} tensor.

	x	**y**	**z**	**U(eq)**
Ni(1)	7500	2582(1)	5000	26(1)
Fe(1)	7500	5806(1)	5000	22(1)
P(1)	7063(1)	3595(1)	5656(1)	24(1)
C(1)	7675(6)	1131(5)	5001(8)	32(2)
C(2)	8565(8)	681(6)	5202(4)	36(2)
C(3)	8652(7)	-359(6)	5225(4)	54(2)
C(4)	7838(7)	-962(6)	5072(5)	51(2)
C(5)	6956(9)	-564(6)	4878(5)	55(3)
C(6)	6893(7)	487(6)	4843(4)	38(2)
C(7)	9426(7)	1333(7)	5388(4)	46(2)
C(8)	5944(8)	911(7)	4620(5)	46(2)
C(9)	6826(2)	4915(2)	5535(1)	23(1)
C(10)	7245(2)	5757(2)	5841(1)	27(1)
C(11)	6853(2)	6648(2)	5589(1)	29(1)
C(12)	6178(2)	6375(2)	5122(1)	28(1)
C(13)	6154(2)	5315(2)	5082(1)	24(1)
C(14)	8035(2)	3598(2)	6241(1)	28(1)
C(15)	8974(2)	3511(3)	6107(2)	32(1)
C(16)	9732(2)	3487(3)	6536(2)	36(1)
C(17)	9562(3)	3542(3)	7099(2)	45(1)
C(18)	8635(3)	3621(3)	7240(2)	48(1)
C(19)	7875(3)	3651(3)	6813(2)	40(1)
C(20)	6019(2)	3215(2)	6011(1)	25(1)
C(21)	5807(3)	2200(3)	6044(1)	32(1)
C(22)	5019(3)	1888(3)	6304(2)	40(1)
C(23)	4442(3)	2571(3)	6536(2)	39(1)

C(24)	4653(2)	3577(3)	6520(1)	34(1)
C(25)	5439(2)	3902(3)	6249(1)	29(1)
C(26)	6874(3)	4982(3)	8036(2)	59(1)
C(27)	7565(3)	5092(4)	8498(2)	79(2)
C(28)	8306(3)	5775(4)	8472(2)	95(2)
C(29)	8372(4)	6365(4)	7991(2)	91(2)
C(30)	7700(3)	6239(3)	7520(2)	72(1)
C(31)	6949(3)	5576(3)	7561(2)	60(1)
C(32)	6075(5)	4240(5)	8027(3)	103(2)

Table S6. Bond lengths [Å] and angles [°] for **5**.

Ni(1)-C(1)	1.954(6)
Ni(1)-P(1)	2.1900(9)
Ni(1)-P(1)#1	2.1900(9)
Fe(1)-C(13)	2.028(3)
Fe(1)-C(13)#1	2.028(3)
Fe(1)-C(9)	2.038(3)
Fe(1)-C(9)#1	2.038(3)
Fe(1)-C(10)#1	2.052(3)
Fe(1)-C(10)	2.052(3)
Fe(1)-C(12)	2.053(3)
Fe(1)-C(12)#1	2.053(3)
Fe(1)-C(11)#1	2.069(3)
Fe(1)-C(11)	2.069(3)
P(1)-C(9)	1.811(3)
P(1)-C(20)	1.833(3)
P(1)-C(14)	1.835(3)
C(1)-C(6)	1.413(10)
C(1)-C(2)	1.423(10)
C(2)-C(3)	1.395(10)
C(2)-C(7)	1.518(12)
C(3)-C(4)	1.413(11)
C(4)-C(5)	1.382(10)
C(5)-C(6)	1.409(10)
C(6)-C(8)	1.492(12)
C(9)-C(10)	1.429(4)
C(9)-C(13)	1.450(4)
C(10)-C(11)	1.416(5)
C(11)-C(12)	1.423(5)
C(12)-C(13)	1.420(4)
C(14)-C(19)	1.390(5)
C(14)-C(15)	1.392(5)
C(15)-C(16)	1.389(5)
C(16)-C(17)	1.375(5)
C(17)-C(18)	1.380(5)
C(18)-C(19)	1.390(5)

C(20)-C(25)	1.383(4)
C(20)-C(21)	1.392(5)
C(21)-C(22)	1.384(5)
C(22)-C(23)	1.371(5)
C(23)-C(24)	1.377(5)
C(24)-C(25)	1.399(5)
C(26)-C(31)	1.386(2)
C(26)-C(27)	1.388(2)
C(26)-C(32)	1.494(7)
C(27)-C(28)	1.390(2)
C(28)-C(29)	1.391(2)
C(29)-C(30)	1.390(2)
C(30)-C(31)	1.388(2)

C(1)-Ni(1)-P(1)	131.0(5)
C(1)-Ni(1)-P(1)#1	124.7(5)
P(1)-Ni(1)-P(1)#1	103.69(5)
C(13)-Fe(1)-C(13)#1	142.20(18)
C(13)-Fe(1)-C(9)	41.80(12)
C(13)#1-Fe(1)-C(9)	111.52(13)
C(13)-Fe(1)-C(9)#1	111.52(13)
C(13)#1-Fe(1)-C(9)#1	41.80(12)
C(9)-Fe(1)-C(9)#1	108.47(17)
C(13)-Fe(1)-C(10)#1	109.84(13)
C(13)#1-Fe(1)-C(10)#1	68.87(12)
C(9)-Fe(1)-C(10)#1	135.87(13)
C(9)#1-Fe(1)-C(10)#1	40.91(12)
C(13)-Fe(1)-C(10)	68.87(12)
C(13)#1-Fe(1)-C(10)	109.84(13)
C(9)-Fe(1)-C(10)	40.91(12)
C(9)#1-Fe(1)-C(10)	135.87(13)
C(10)#1-Fe(1)-C(10)	176.27(18)
C(13)-Fe(1)-C(12)	40.71(12)
C(13)#1-Fe(1)-C(12)	176.10(13)
C(9)-Fe(1)-C(12)	69.18(12)
C(9)#1-Fe(1)-C(12)	141.99(13)
C(10)#1-Fe(1)-C(12)	113.50(13)
C(10)-Fe(1)-C(12)	68.00(13)
C(13)-Fe(1)-C(12)#1	176.10(13)
C(13)#1-Fe(1)-C(12)#1	40.71(12)
C(9)-Fe(1)-C(12)#1	141.99(13)
C(9)#1-Fe(1)-C(12)#1	69.18(12)
C(10)#1-Fe(1)-C(12)#1	67.99(13)
C(10)-Fe(1)-C(12)#1	113.50(13)
C(12)-Fe(1)-C(12)#1	136.57(18)
C(13)-Fe(1)-C(11)#1	135.91(13)

C(13)#1-Fe(1)-C(11)#1	68.52(13)
C(9)-Fe(1)-C(11)#1	176.02(13)
C(9)#1-Fe(1)-C(11)#1	68.75(12)
C(10)#1-Fe(1)-C(11)#1	40.19(13)
C(10)-Fe(1)-C(11)#1	143.05(13)
C(12)-Fe(1)-C(11)#1	111.07(13)
C(12)#1-Fe(1)-C(11)#1	40.40(13)
C(13)-Fe(1)-C(11)	68.52(13)
C(13)#1-Fe(1)-C(11)	135.91(13)
C(9)-Fe(1)-C(11)	68.76(12)
C(9)#1-Fe(1)-C(11)	176.02(13)
C(10)#1-Fe(1)-C(11)	143.05(13)
C(10)-Fe(1)-C(11)	40.20(13)
C(12)-Fe(1)-C(11)	40.40(13)
C(12)#1-Fe(1)-C(11)	111.07(13)
C(11)#1-Fe(1)-C(11)	114.17(18)
C(9)-P(1)-C(20)	101.46(14)
C(9)-P(1)-C(14)	103.09(14)
C(20)-P(1)-C(14)	102.93(14)
C(9)-P(1)-Ni(1)	123.41(10)
C(20)-P(1)-Ni(1)	116.58(11)
C(14)-P(1)-Ni(1)	106.92(11)
C(6)-C(1)-C(2)	117.5(9)
C(6)-C(1)-Ni(1)	120.6(7)
C(2)-C(1)-Ni(1)	121.7(7)
C(3)-C(2)-C(1)	120.3(9)
C(3)-C(2)-C(7)	119.8(8)
C(1)-C(2)-C(7)	119.9(7)
C(2)-C(3)-C(4)	119.5(9)
C(5)-C(4)-C(3)	122.5(8)
C(4)-C(5)-C(6)	116.8(9)
C(5)-C(6)-C(1)	123.3(9)
C(5)-C(6)-C(8)	116.6(8)
C(1)-C(6)-C(8)	120.2(8)
C(10)-C(9)-C(13)	106.5(3)
C(10)-C(9)-P(1)	128.8(2)
C(13)-C(9)-P(1)	124.7(2)
C(10)-C(9)-Fe(1)	70.06(17)
C(13)-C(9)-Fe(1)	68.71(17)
P(1)-C(9)-Fe(1)	125.22(16)
C(11)-C(10)-C(9)	109.2(3)
C(11)-C(10)-Fe(1)	70.54(18)
C(9)-C(10)-Fe(1)	69.03(17)
C(10)-C(11)-C(12)	107.9(3)
C(10)-C(11)-Fe(1)	69.27(18)
C(12)-C(11)-Fe(1)	69.22(17)

C(13)-C(12)-C(11)	108.4(3)
C(13)-C(12)-Fe(1)	68.67(17)
C(11)-C(12)-Fe(1)	70.38(17)
C(12)-C(13)-C(9)	108.1(3)
C(12)-C(13)-Fe(1)	70.62(18)
C(9)-C(13)-Fe(1)	69.50(16)
C(19)-C(14)-C(15)	118.5(3)
C(19)-C(14)-P(1)	123.1(3)
C(15)-C(14)-P(1)	118.4(2)
C(16)-C(15)-C(14)	120.5(3)
C(17)-C(16)-C(15)	120.3(3)
C(16)-C(17)-C(18)	120.1(3)
C(17)-C(18)-C(19)	119.8(4)
C(14)-C(19)-C(18)	120.8(3)
C(25)-C(20)-C(21)	119.0(3)
C(25)-C(20)-P(1)	122.3(2)
C(21)-C(20)-P(1)	118.7(2)
C(22)-C(21)-C(20)	120.2(3)
C(23)-C(22)-C(21)	120.6(3)
C(22)-C(23)-C(24)	120.0(3)
C(23)-C(24)-C(25)	119.9(3)
C(20)-C(25)-C(24)	120.3(3)
C(31)-C(26)-C(27)	117.9(4)
C(31)-C(26)-C(32)	119.2(4)
C(27)-C(26)-C(32)	122.9(5)
C(26)-C(27)-C(28)	119.9(5)
C(27)-C(28)-C(29)	121.6(5)
C(30)-C(29)-C(28)	118.9(5)
C(31)-C(30)-C(29)	118.7(5)
C(26)-C(31)-C(30)	122.9(4)

Symmetry transformations used to generate equivalent atoms:
#1 -x+3/2,y,-z+1

Table S7. Anisotropic displacement parameters ($Å^2 x\ 10^3$) for **5**. The anisotropic displacement factor exponent takes the form: $-2\pi^2[\ h^2\ a^{*2}U^{11} + ... + 2\ h\ k\ a^*\ b^*\ U^{12}]$

	U^{11}	**U^{22}**	**U^{33}**	**U^{23}**	**U^{13}**	**U^{12}**
Ni(1)	24(1)	19(1)	35(1)	0	2(1)	0
Fe(1)	20(1)	19(1)	26(1)	0	2(1)	0
P(1)	21(1)	23(1)	26(1)	3(1)	0(1)	-1(1)
C(1)	47(6)	24(2)	26(3)	-1(4)	9(5)	2(3)
C(2)	51(6)	30(4)	30(5)	3(3)	11(5)	8(3)
C(3)	84(6)	31(4)	50(5)	6(3)	23(5)	14(4)
C(4)	98(6)	22(4)	37(5)	-2(4)	31(5)	-1(3)
C(5)	96(6)	24(4)	48(6)	-1(4)	23(5)	0(4)
C(6)	55(6)	23(4)	37(4)	-1(3)	7(4)	-7(3)

C(7)	48(5)	41(5)	48(5)	7(4)	-5(4)	11(4)
C(8)	54(6)	26(5)	58(6)	-1(4)	1(5)	-17(4)
C(9)	23(2)	22(2)	24(2)	-2(1)	7(1)	-3(1)
C(10)	26(2)	30(2)	26(2)	-3(1)	5(1)	-4(1)
C(11)	36(2)	21(2)	32(2)	-6(1)	13(2)	0(1)
C(12)	24(2)	23(2)	36(2)	4(1)	8(1)	5(1)
C(13)	19(1)	27(2)	26(2)	0(1)	4(1)	-1(1)
C(14)	26(2)	26(2)	30(2)	3(1)	-5(1)	1(1)
C(15)	32(2)	32(2)	32(2)	8(2)	1(1)	-2(2)
C(16)	25(2)	37(2)	44(2)	8(2)	-5(2)	1(2)
C(17)	33(2)	53(2)	44(2)	4(2)	-14(2)	4(2)
C(18)	43(2)	69(3)	30(2)	-4(2)	-10(2)	10(2)
C(19)	32(2)	51(2)	36(2)	-1(2)	0(2)	7(2)
C(20)	25(2)	31(2)	18(2)	4(1)	-2(1)	-1(1)
C(21)	42(2)	30(2)	26(2)	2(1)	8(2)	-1(2)
C(22)	49(2)	37(2)	35(2)	7(2)	10(2)	-12(2)
C(23)	33(2)	55(2)	30(2)	12(2)	7(2)	-6(2)
C(24)	27(2)	47(2)	28(2)	5(2)	5(1)	7(2)
C(25)	26(2)	33(2)	28(2)	2(1)	1(1)	1(1)
C(26)	59(3)	61(3)	60(3)	-4(2)	18(2)	12(2)
C(27)	90(4)	95(4)	52(3)	0(3)	11(3)	28(4)
C(28)	50(3)	165(7)	67(4)	-52(4)	-7(3)	15(4)
C(29)	79(4)	91(5)	107(5)	-42(4)	36(4)	-27(3)
C(30)	86(4)	56(3)	76(4)	-13(3)	21(3)	-1(3)
C(31)	43(2)	61(3)	75(3)	10(2)	0(2)	8(2)
C(32)	105(5)	86(5)	126(6)	-11(4)	51(4)	-28(4)

Table S8. Torsion angles [°] for **5**.

C(6)-C(1)-C(2)-C(3)	1.5(19)
Ni(1)-C(1)-C(2)-C(3)	176.6(9)
C(6)-C(1)-C(2)-C(7)	-178.8(10)
Ni(1)-C(1)-C(2)-C(7)	-3.7(17)
C(1)-C(2)-C(3)-C(4)	-2.9(15)
C(7)-C(2)-C(3)-C(4)	177.4(9)
C(2)-C(3)-C(4)-C(5)	2.6(15)
C(3)-C(4)-C(5)-C(6)	-0.9(14)
C(4)-C(5)-C(6)-C(1)	-0.6(16)
C(4)-C(5)-C(6)-C(8)	178.6(8)
C(2)-C(1)-C(6)-C(5)	0(2)
Ni(1)-C(1)-C(6)-C(5)	-174.9(11)
C(2)-C(1)-C(6)-C(8)	-179.0(11)
Ni(1)-C(1)-C(6)-C(8)	5.9(16)
C(20)-P(1)-C(9)-C(10)	102.8(3)
C(14)-P(1)-C(9)-C(10)	-3.5(3)
Ni(1)-P(1)-C(9)-C(10)	-124.3(3)
C(20)-P(1)-C(9)-C(13)	-78.3(3)

C(14)-P(1)-C(9)-C(13)	175.3(3)
Ni(1)-P(1)-C(9)-C(13)	54.6(3)
C(20)-P(1)-C(9)-Fe(1)	-165.34(18)
C(14)-P(1)-C(9)-Fe(1)	88.3(2)
Ni(1)-P(1)-C(9)-Fe(1)	-32.4(2)
C(13)-C(9)-C(10)-C(11)	-0.1(3)
P(1)-C(9)-C(10)-C(11)	179.0(2)
Fe(1)-C(9)-C(10)-C(11)	59.3(2)
C(13)-C(9)-C(10)-Fe(1)	-59.3(2)
P(1)-C(9)-C(10)-Fe(1)	119.7(3)
C(9)-C(10)-C(11)-C(12)	0.3(3)
Fe(1)-C(10)-C(11)-C(12)	58.6(2)
C(9)-C(10)-C(11)-Fe(1)	-58.3(2)
C(10)-C(11)-C(12)-C(13)	-0.4(3)
Fe(1)-C(11)-C(12)-C(13)	58.3(2)
C(10)-C(11)-C(12)-Fe(1)	-58.6(2)
C(11)-C(12)-C(13)-C(9)	0.3(3)
Fe(1)-C(12)-C(13)-C(9)	59.7(2)
C(11)-C(12)-C(13)-Fe(1)	-59.3(2)
C(10)-C(9)-C(13)-C(12)	-0.1(3)
P(1)-C(9)-C(13)-C(12)	-179.2(2)
Fe(1)-C(9)-C(13)-C(12)	-60.4(2)
C(10)-C(9)-C(13)-Fe(1)	60.2(2)
P(1)-C(9)-C(13)-Fe(1)	-118.9(2)
C(9)-P(1)-C(14)-C(19)	85.4(3)
C(20)-P(1)-C(14)-C(19)	-19.9(3)
Ni(1)-P(1)-C(14)-C(19)	-143.2(3)
C(9)-P(1)-C(14)-C(15)	-96.7(3)
C(20)-P(1)-C(14)-C(15)	158.0(3)
Ni(1)-P(1)-C(14)-C(15)	34.7(3)
C(19)-C(14)-C(15)-C(16)	-0.5(5)
P(1)-C(14)-C(15)-C(16)	-178.5(3)
C(14)-C(15)-C(16)-C(17)	0.4(5)
C(15)-C(16)-C(17)-C(18)	0.1(6)
C(16)-C(17)-C(18)-C(19)	-0.4(6)
C(15)-C(14)-C(19)-C(18)	0.2(6)
P(1)-C(14)-C(19)-C(18)	178.1(3)
C(17)-C(18)-C(19)-C(14)	0.2(6)
C(9)-P(1)-C(20)-C(25)	-16.6(3)
C(14)-P(1)-C(20)-C(25)	89.9(3)
Ni(1)-P(1)-C(20)-C(25)	-153.5(2)
C(9)-P(1)-C(20)-C(21)	163.5(2)
C(14)-P(1)-C(20)-C(21)	-90.0(3)
Ni(1)-P(1)-C(20)-C(21)	26.7(3)
C(25)-C(20)-C(21)-C(22)	0.8(5)
P(1)-C(20)-C(21)-C(22)	-179.4(3)

C(20)-C(21)-C(22)-C(23)	-0.4(5)
C(21)-C(22)-C(23)-C(24)	-1.1(5)
C(22)-C(23)-C(24)-C(25)	2.2(5)
C(21)-C(20)-C(25)-C(24)	0.3(5)
P(1)-C(20)-C(25)-C(24)	-179.5(2)
C(23)-C(24)-C(25)-C(20)	-1.8(5)
C(31)-C(26)-C(27)-C(28)	-0.5(7)
C(32)-C(26)-C(27)-C(28)	178.0(5)
C(26)-C(27)-C(28)-C(29)	0.5(8)
C(27)-C(28)-C(29)-C(30)	-2.4(8)
C(28)-C(29)-C(30)-C(31)	4.3(8)
C(27)-C(26)-C(31)-C(30)	2.6(7)
C(32)-C(26)-C(31)-C(30)	-175.9(5)
C(29)-C(30)-C(31)-C(26)	-4.5(8)

*Crystallographic Information for (dppf)Ni^{I}(2,4,6-mesityl) (**6**) (CCDC: 1815575)*

Single crystals of **6** were obtained from a reaction mixture of **1** and mesitylmagnesium bromide (1.5 equiv.) in a 2:1 mixture of pentane:d_8-toluene at room-temperature under vacuum. Low-temperature diffraction data (ω-scans) were collected on a Rigaku MicroMax-007HF diffractometer coupled to a Saturn994+ CCD detector with Cu Kα (λ = 1.54178 Å) for the structure of **6**. The diffraction images were processed and scaled using Rigaku Oxford Diffraction software.[14] The structure was solved with SHELXT and was refined against F^2 on all data by full-matrix least squares with SHELXL.[15] All non-hydrogen atoms were refined anisotropically. One low angle reflection was obscured by instrument artifacts and omitted from the refinement. Hydrogen atoms were included in the model at geometrically calculated positions and refined using a riding model. The isotropic displacement parameters of all hydrogen atoms were fixed to 1.2 times the U value of the atoms to which they are linked (1.5 times for methyl groups). The program SQUEEZE was used to compensate for the contribution of disordered solvents contained in voids within the crystal lattice from the diffraction intensities. This procedure was applied to the data file and the submitted model is based on the solvent removed data. Based on the total electron density found in the voids (295.9 e/A^3), it is likely that ~7 pentane molecules, ~6 toluene molecules, or some combination of these molecules are present in the unit cell. See "_platon_squeeze_details" in the .cif for more information. The full details of the X-ray structure determination are included in the .cif.

*X-ray Structure of **6***

Table S9. Crystal data and structure refinement for **6**.

Empirical formula	$C_{43}H_{39}FeNiP_2$	
Formula weight	732.24	
Temperature	93(2) K	
Wavelength	1.54184 Å	
Crystal system	Monoclinic	
Space group	C2/c	
Unit cell dimensions	a = 23.2567(4) Å	α= 90°.
	b = 16.9768(2) Å	β= 106.649(2)°.
	c = 21.0881(5) Å	γ = 90°.
Volume	7977.0(3) Å^3	
Z	8	
Density (calculated)	1.219 Mg/m^3	
Absorption coefficient	4.454 mm^{-1}	

F(000)	3048
Crystal size	0.050 x 0.050 x 0.020 mm^3
Theta range for data collection	3.273 to 66.811°.
Index ranges	-27<=h<=27, -20<=k<=20, -24<=l<=25
Reflections collected	139590
Independent reflections	7071 [R(int) = 0.1172]
Completeness to theta = 66.811°	99.7 %
Absorption correction	Semi-empirical from equivalents
Max. and min. transmission	1.00000 and 0.61342
Refinement method	Full-matrix least-squares on F^2
Data / restraints / parameters	7071 / 0 / 427
Goodness-of-fit on F^2	1.035
Final R indices [I>2sigma(I)]	R1 = 0.0348, wR2 = 0.0909
R indices (all data)	R1 = 0.0404, wR2 = 0.0951
Largest diff. peak and hole	0.310 and -0.392 e.$Å^{-3}$

Table S10. Atomic coordinates (x 10^4) and equivalent isotropic displacement parameters ($Å^2$ x 10^3) for **6**. U(eq) is defined as one third of the trace of the orthogonalized U^{ij} tensor.

	x	**y**	**z**	**U(eq)**
Ni(1)	3246(1)	6281(1)	3456(1)	27(1)
Fe(1)	3786(1)	6155(1)	5568(1)	24(1)
P(1)	3605(1)	7231(1)	4156(1)	26(1)
P(2)	3370(1)	5220(1)	4075(1)	25(1)
C(1)	2927(1)	6553(1)	2524(1)	31(1)
C(2)	3276(1)	6544(1)	2070(1)	33(1)
C(3)	3008(1)	6615(1)	1393(1)	40(1)
C(4)	2396(1)	6722(1)	1132(1)	41(1)
C(5)	2049(1)	6770(1)	1570(1)	40(1)
C(6)	2303(1)	6681(1)	2248(1)	37(1)
C(7)	3951(1)	6481(2)	2333(1)	42(1)
C(8)	2105(2)	6791(2)	396(1)	57(1)
C(9)	1900(1)	6708(2)	2697(1)	54(1)
C(10)	3601(1)	7161(1)	5011(1)	26(1)
C(11)	4084(1)	7296(1)	5602(1)	30(1)
C(12)	3877(1)	7142(1)	6160(1)	30(1)
C(13)	3264(1)	6912(1)	5927(1)	30(1)
C(14)	3092(1)	6919(1)	5227(1)	27(1)
C(15)	3732(1)	5198(1)	4958(1)	24(1)
C(16)	4348(1)	5411(1)	5271(1)	27(1)
C(17)	4455(1)	5355(1)	5969(1)	31(1)
C(18)	3912(1)	5117(1)	6095(1)	30(1)
C(19)	3469(1)	5016(1)	5479(1)	28(1)
C(20)	4407(1)	7368(1)	4236(1)	32(1)
C(21)	4726(1)	6734(1)	4087(1)	30(1)
C(22)	5329(1)	6808(1)	4124(1)	35(1)
C(23)	5620(1)	7509(2)	4312(2)	50(1)

C(24)	5311(1)	8142(2)	4472(2)	63(1)
C(25)	4708(1)	8072(1)	4429(2)	50(1)
C(26)	3290(1)	8218(1)	3932(1)	28(1)
C(27)	3259(1)	8783(1)	4402(1)	30(1)
C(28)	3002(1)	9515(1)	4198(1)	33(1)
C(29)	2773(1)	9690(1)	3531(1)	35(1)
C(30)	2809(1)	9132(1)	3067(1)	37(1)
C(31)	3063(1)	8398(1)	3261(1)	33(1)
C(32)	3759(1)	4431(1)	3774(1)	28(1)
C(33)	3753(1)	4444(1)	3111(1)	34(1)
C(34)	4022(1)	3840(1)	2857(1)	42(1)
C(35)	4296(1)	3224(1)	3258(1)	42(1)
C(36)	4300(1)	3202(1)	3914(1)	37(1)
C(37)	4033(1)	3805(1)	4174(1)	32(1)
C(38)	2629(1)	4788(1)	3992(1)	28(1)
C(39)	2177(1)	5286(1)	4064(1)	40(1)
C(40)	1594(1)	5010(2)	3954(1)	51(1)
C(41)	1456(1)	4243(2)	3754(1)	45(1)
C(42)	1897(1)	3744(1)	3677(1)	41(1)
C(43)	2481(1)	4011(1)	3798(1)	34(1)

Table S11. Bond lengths [Å] and angles [°] for **6**.

Ni(1)-C(1)	1.948(2)
Ni(1)-P(1)	2.1843(6)
Ni(1)-P(2)	2.1941(6)
Fe(1)-C(14)	2.034(2)
Fe(1)-C(16)	2.041(2)
Fe(1)-C(10)	2.047(2)
Fe(1)-C(15)	2.0527(19)
Fe(1)-C(11)	2.054(2)
Fe(1)-C(13)	2.056(2)
Fe(1)-C(17)	2.056(2)
Fe(1)-C(19)	2.058(2)
Fe(1)-C(18)	2.059(2)
Fe(1)-C(12)	2.065(2)
P(1)-C(10)	1.809(2)
P(1)-C(26)	1.835(2)
P(1)-C(20)	1.839(2)
P(2)-C(15)	1.811(2)
P(2)-C(32)	1.828(2)
P(2)-C(38)	1.835(2)
C(1)-C(6)	1.417(3)
C(1)-C(2)	1.421(3)
C(2)-C(3)	1.390(3)
C(2)-C(7)	1.511(3)
C(3)-C(4)	1.383(4)

C(4)-C(5)	1.393(4)
C(4)-C(8)	1.509(3)
C(5)-C(6)	1.390(3)
C(6)-C(9)	1.514(3)
C(10)-C(11)	1.438(3)
C(10)-C(14)	1.443(3)
C(11)-C(12)	1.418(3)
C(12)-C(13)	1.423(3)
C(13)-C(14)	1.416(3)
C(15)-C(19)	1.436(3)
C(15)-C(16)	1.441(3)
C(16)-C(17)	1.423(3)
C(17)-C(18)	1.422(3)
C(18)-C(19)	1.418(3)
C(20)-C(25)	1.387(3)
C(20)-C(21)	1.393(3)
C(21)-C(22)	1.388(3)
C(22)-C(23)	1.370(3)
C(23)-C(24)	1.385(4)
C(24)-C(25)	1.385(3)
C(26)-C(31)	1.395(3)
C(26)-C(27)	1.396(3)
C(27)-C(28)	1.392(3)
C(28)-C(29)	1.386(3)
C(29)-C(30)	1.381(3)
C(30)-C(31)	1.389(3)
C(32)-C(37)	1.392(3)
C(32)-C(33)	1.394(3)
C(33)-C(34)	1.387(3)
C(34)-C(35)	1.382(4)
C(35)-C(36)	1.383(4)
C(36)-C(37)	1.389(3)
C(38)-C(39)	1.391(3)
C(38)-C(43)	1.395(3)
C(39)-C(40)	1.390(3)
C(40)-C(41)	1.379(4)
C(41)-C(42)	1.376(4)
C(42)-C(43)	1.385(3)

C(1)-Ni(1)-P(1)	117.95(6)
C(1)-Ni(1)-P(2)	137.90(6)
P(1)-Ni(1)-P(2)	104.16(2)
C(14)-Fe(1)-C(16)	143.03(9)
C(14)-Fe(1)-C(10)	41.41(8)
C(16)-Fe(1)-C(10)	112.79(8)
C(14)-Fe(1)-C(15)	112.55(8)

C(16)-Fe(1)-C(15)	41.23(8)
C(10)-Fe(1)-C(15)	109.57(8)
C(14)-Fe(1)-C(11)	68.64(8)
C(16)-Fe(1)-C(11)	110.73(8)
C(10)-Fe(1)-C(11)	41.04(8)
C(15)-Fe(1)-C(11)	136.66(9)
C(14)-Fe(1)-C(13)	40.51(8)
C(16)-Fe(1)-C(13)	176.06(9)
C(10)-Fe(1)-C(13)	68.95(8)
C(15)-Fe(1)-C(13)	142.15(8)
C(11)-Fe(1)-C(13)	68.05(8)
C(14)-Fe(1)-C(17)	175.50(9)
C(16)-Fe(1)-C(17)	40.65(8)
C(10)-Fe(1)-C(17)	142.75(8)
C(15)-Fe(1)-C(17)	68.81(8)
C(11)-Fe(1)-C(17)	113.56(8)
C(13)-Fe(1)-C(17)	135.94(9)
C(14)-Fe(1)-C(19)	109.94(8)
C(16)-Fe(1)-C(19)	68.59(8)
C(10)-Fe(1)-C(19)	136.10(8)
C(15)-Fe(1)-C(19)	40.89(8)
C(11)-Fe(1)-C(19)	176.88(9)
C(13)-Fe(1)-C(19)	112.84(8)
C(17)-Fe(1)-C(19)	68.07(8)
C(14)-Fe(1)-C(18)	135.52(8)
C(16)-Fe(1)-C(18)	68.36(8)
C(10)-Fe(1)-C(18)	176.05(8)
C(15)-Fe(1)-C(18)	68.61(8)
C(11)-Fe(1)-C(18)	142.59(9)
C(13)-Fe(1)-C(18)	110.15(9)
C(17)-Fe(1)-C(18)	40.44(8)
C(19)-Fe(1)-C(18)	40.31(8)
C(14)-Fe(1)-C(12)	68.24(8)
C(16)-Fe(1)-C(12)	136.35(8)
C(10)-Fe(1)-C(12)	68.76(9)
C(15)-Fe(1)-C(12)	176.72(8)
C(11)-Fe(1)-C(12)	40.29(9)
C(13)-Fe(1)-C(12)	40.39(8)
C(17)-Fe(1)-C(12)	110.65(9)
C(19)-Fe(1)-C(12)	142.21(8)
C(18)-Fe(1)-C(12)	113.24(9)
C(10)-P(1)-C(26)	101.63(9)
C(10)-P(1)-C(20)	102.29(10)
C(26)-P(1)-C(20)	103.20(9)
C(10)-P(1)-Ni(1)	120.93(7)
C(26)-P(1)-Ni(1)	116.88(7)

C(20)-P(1)-Ni(1)	109.66(7)
C(15)-P(2)-C(32)	102.19(9)
C(15)-P(2)-C(38)	103.76(9)
C(32)-P(2)-C(38)	102.57(9)
C(15)-P(2)-Ni(1)	124.85(6)
C(32)-P(2)-Ni(1)	112.94(7)
C(38)-P(2)-Ni(1)	108.11(7)
C(6)-C(1)-C(2)	116.1(2)
C(6)-C(1)-Ni(1)	119.95(16)
C(2)-C(1)-Ni(1)	123.55(17)
C(3)-C(2)-C(1)	121.1(2)
C(3)-C(2)-C(7)	119.8(2)
C(1)-C(2)-C(7)	119.1(2)
C(4)-C(3)-C(2)	121.9(2)
C(3)-C(4)-C(5)	118.0(2)
C(3)-C(4)-C(8)	121.8(2)
C(5)-C(4)-C(8)	120.2(2)
C(6)-C(5)-C(4)	121.3(2)
C(5)-C(6)-C(1)	121.6(2)
C(5)-C(6)-C(9)	118.8(2)
C(1)-C(6)-C(9)	119.6(2)
C(11)-C(10)-C(14)	106.28(18)
C(11)-C(10)-P(1)	128.83(15)
C(14)-C(10)-P(1)	124.86(16)
C(11)-C(10)-Fe(1)	69.71(11)
C(14)-C(10)-Fe(1)	68.80(11)
P(1)-C(10)-Fe(1)	124.53(10)
C(12)-C(11)-C(10)	108.79(18)
C(12)-C(11)-Fe(1)	70.27(12)
C(10)-C(11)-Fe(1)	69.25(11)
C(11)-C(12)-C(13)	108.09(19)
C(11)-C(12)-Fe(1)	69.44(12)
C(13)-C(12)-Fe(1)	69.49(12)
C(14)-C(13)-C(12)	108.18(18)
C(14)-C(13)-Fe(1)	68.90(11)
C(12)-C(13)-Fe(1)	70.12(12)
C(13)-C(14)-C(10)	108.67(18)
C(13)-C(14)-Fe(1)	70.59(12)
C(10)-C(14)-Fe(1)	69.79(11)
C(19)-C(15)-C(16)	106.78(18)
C(19)-C(15)-P(2)	128.04(15)
C(16)-C(15)-P(2)	125.09(15)
C(19)-C(15)-Fe(1)	69.74(11)
C(16)-C(15)-Fe(1)	68.97(11)
P(2)-C(15)-Fe(1)	123.71(10)
C(17)-C(16)-C(15)	108.28(18)

C(17)-C(16)-Fe(1)	70.24(11)
C(15)-C(16)-Fe(1)	69.81(11)
C(18)-C(17)-C(16)	108.08(18)
C(18)-C(17)-Fe(1)	69.87(12)
C(16)-C(17)-Fe(1)	69.11(11)
C(19)-C(18)-C(17)	108.31(19)
C(19)-C(18)-Fe(1)	69.81(11)
C(17)-C(18)-Fe(1)	69.69(12)
C(18)-C(19)-C(15)	108.54(18)
C(18)-C(19)-Fe(1)	69.88(12)
C(15)-C(19)-Fe(1)	69.37(11)
C(25)-C(20)-C(21)	118.39(19)
C(25)-C(20)-P(1)	123.32(16)
C(21)-C(20)-P(1)	118.29(16)
C(22)-C(21)-C(20)	120.8(2)
C(23)-C(22)-C(21)	120.1(2)
C(22)-C(23)-C(24)	119.8(2)
C(25)-C(24)-C(23)	120.2(2)
C(24)-C(25)-C(20)	120.7(2)
C(31)-C(26)-C(27)	119.12(19)
C(31)-C(26)-P(1)	117.98(16)
C(27)-C(26)-P(1)	122.89(17)
C(28)-C(27)-C(26)	120.0(2)
C(29)-C(28)-C(27)	120.7(2)
C(30)-C(29)-C(28)	119.3(2)
C(29)-C(30)-C(31)	120.8(2)
C(30)-C(31)-C(26)	120.1(2)
C(37)-C(32)-C(33)	119.34(19)
C(37)-C(32)-P(2)	122.38(17)
C(33)-C(32)-P(2)	118.21(16)
C(34)-C(33)-C(32)	120.1(2)
C(35)-C(34)-C(33)	120.2(2)
C(34)-C(35)-C(36)	120.2(2)
C(35)-C(36)-C(37)	120.0(2)
C(36)-C(37)-C(32)	120.2(2)
C(39)-C(38)-C(43)	118.5(2)
C(39)-C(38)-P(2)	117.71(16)
C(43)-C(38)-P(2)	123.51(16)
C(40)-C(39)-C(38)	120.6(2)
C(41)-C(40)-C(39)	120.1(2)
C(42)-C(41)-C(40)	120.0(2)
C(41)-C(42)-C(43)	120.2(2)
C(42)-C(43)-C(38)	120.6(2)

Table S12. Anisotropic displacement parameters ($Å^2 x\ 10^3$) for **6**. The anisotropic displacement factor exponent takes the form: $-2\pi^2[\ h^2\ a^{*2}U^{11} + ... + 2\ h\ k\ a^*\ b^*\ U^{12}]$

	U^{11}	U^{22}	U^{33}	U^{23}	U^{13}	U^{12}
Ni(1)	30(1)	24(1)	28(1)	2(1)	11(1)	3(1)
Fe(1)	26(1)	20(1)	28(1)	0(1)	9(1)	1(1)
P(1)	27(1)	21(1)	34(1)	2(1)	14(1)	3(1)
P(2)	25(1)	22(1)	29(1)	0(1)	8(1)	1(1)
C(1)	42(1)	20(1)	32(1)	-1(1)	14(1)	2(1)
C(2)	48(1)	22(1)	32(1)	-3(1)	15(1)	-7(1)
C(3)	61(2)	30(1)	33(1)	-4(1)	20(1)	-14(1)
C(4)	66(2)	24(1)	29(1)	1(1)	8(1)	-7(1)
C(5)	51(1)	30(1)	35(1)	-1(1)	3(1)	10(1)
C(6)	47(1)	29(1)	33(1)	-2(1)	10(1)	11(1)
C(7)	49(1)	45(1)	38(1)	-9(1)	23(1)	-14(1)
C(8)	84(2)	49(2)	33(2)	4(1)	7(1)	-14(1)
C(9)	42(1)	78(2)	40(2)	-4(1)	11(1)	24(1)
C(10)	27(1)	18(1)	33(1)	1(1)	11(1)	2(1)
C(11)	27(1)	21(1)	40(1)	-1(1)	9(1)	1(1)
C(12)	40(1)	22(1)	29(1)	-4(1)	9(1)	1(1)
C(13)	38(1)	23(1)	33(1)	-2(1)	17(1)	4(1)
C(14)	26(1)	22(1)	36(1)	-1(1)	12(1)	3(1)
C(15)	27(1)	18(1)	29(1)	-1(1)	9(1)	2(1)
C(16)	27(1)	22(1)	33(1)	-1(1)	9(1)	4(1)
C(17)	31(1)	24(1)	34(1)	-2(1)	4(1)	5(1)
C(18)	40(1)	22(1)	28(1)	4(1)	11(1)	3(1)
C(19)	32(1)	20(1)	33(1)	1(1)	13(1)	1(1)
C(20)	30(1)	29(1)	40(1)	4(1)	16(1)	2(1)
C(21)	31(1)	28(1)	32(1)	4(1)	13(1)	4(1)
C(22)	34(1)	37(1)	40(1)	5(1)	19(1)	9(1)
C(23)	32(1)	44(1)	79(2)	2(1)	28(1)	0(1)
C(24)	42(2)	37(1)	120(3)	-10(2)	40(2)	-10(1)
C(25)	37(1)	29(1)	93(2)	-6(1)	32(1)	0(1)
C(26)	26(1)	23(1)	38(1)	3(1)	14(1)	2(1)
C(27)	32(1)	25(1)	36(1)	3(1)	15(1)	1(1)
C(28)	37(1)	24(1)	44(1)	0(1)	20(1)	2(1)
C(29)	36(1)	22(1)	49(2)	5(1)	15(1)	5(1)
C(30)	43(1)	30(1)	38(1)	7(1)	12(1)	6(1)
C(31)	39(1)	27(1)	35(1)	0(1)	14(1)	4(1)
C(32)	25(1)	25(1)	34(1)	-4(1)	9(1)	-1(1)
C(33)	38(1)	30(1)	34(1)	-5(1)	9(1)	-1(1)
C(34)	49(1)	37(1)	40(1)	-12(1)	15(1)	0(1)
C(35)	38(1)	33(1)	57(2)	-17(1)	16(1)	0(1)
C(36)	29(1)	27(1)	52(2)	-3(1)	8(1)	2(1)
C(37)	28(1)	29(1)	37(1)	-1(1)	8(1)	1(1)
C(38)	27(1)	31(1)	27(1)	2(1)	6(1)	-1(1)
C(39)	34(1)	39(1)	50(2)	-12(1)	15(1)	-2(1)

C(40)	29(1)	59(2)	67(2)	-14(1)	18(1)	1(1)
C(41)	31(1)	54(2)	49(2)	3(1)	10(1)	-11(1)
C(42)	39(1)	34(1)	45(2)	6(1)	6(1)	-10(1)
C(43)	34(1)	29(1)	38(1)	5(1)	8(1)	0(1)

Table S13. Torsion angles [°] for **6**.

C(6)-C(1)-C(2)-C(3)	-3.4(3)
Ni(1)-C(1)-C(2)-C(3)	169.24(16)
C(6)-C(1)-C(2)-C(7)	174.8(2)
Ni(1)-C(1)-C(2)-C(7)	-12.6(3)
C(1)-C(2)-C(3)-C(4)	2.1(3)
C(7)-C(2)-C(3)-C(4)	-176.1(2)
C(2)-C(3)-C(4)-C(5)	1.0(3)
C(2)-C(3)-C(4)-C(8)	-179.4(2)
C(3)-C(4)-C(5)-C(6)	-2.7(3)
C(8)-C(4)-C(5)-C(6)	177.7(2)
C(4)-C(5)-C(6)-C(1)	1.3(3)
C(4)-C(5)-C(6)-C(9)	-177.6(2)
C(2)-C(1)-C(6)-C(5)	1.8(3)
Ni(1)-C(1)-C(6)-C(5)	-171.15(17)
C(2)-C(1)-C(6)-C(9)	-179.3(2)
Ni(1)-C(1)-C(6)-C(9)	7.8(3)
C(26)-P(1)-C(10)-C(11)	-98.00(19)
C(20)-P(1)-C(10)-C(11)	8.5(2)
Ni(1)-P(1)-C(10)-C(11)	130.60(16)
C(26)-P(1)-C(10)-C(14)	84.43(18)
C(20)-P(1)-C(10)-C(14)	-169.11(17)
Ni(1)-P(1)-C(10)-C(14)	-46.97(19)
C(26)-P(1)-C(10)-Fe(1)	171.23(12)
C(20)-P(1)-C(10)-Fe(1)	-82.31(13)
Ni(1)-P(1)-C(10)-Fe(1)	39.83(14)
C(14)-C(10)-C(11)-C(12)	0.0(2)
P(1)-C(10)-C(11)-C(12)	-177.89(15)
Fe(1)-C(10)-C(11)-C(12)	-59.33(14)
C(14)-C(10)-C(11)-Fe(1)	59.36(13)
P(1)-C(10)-C(11)-Fe(1)	-118.56(16)
C(10)-C(11)-C(12)-C(13)	-0.2(2)
Fe(1)-C(11)-C(12)-C(13)	-58.92(14)
C(10)-C(11)-C(12)-Fe(1)	58.70(14)
C(11)-C(12)-C(13)-C(14)	0.3(2)
Fe(1)-C(12)-C(13)-C(14)	-58.56(14)
C(11)-C(12)-C(13)-Fe(1)	58.89(14)
C(12)-C(13)-C(14)-C(10)	-0.3(2)
Fe(1)-C(13)-C(14)-C(10)	-59.63(13)
C(12)-C(13)-C(14)-Fe(1)	59.32(14)
C(11)-C(10)-C(14)-C(13)	0.2(2)

P(1)-C(10)-C(14)-C(13)	178.20(14)
Fe(1)-C(10)-C(14)-C(13)	60.12(14)
C(11)-C(10)-C(14)-Fe(1)	-59.95(13)
P(1)-C(10)-C(14)-Fe(1)	118.08(15)
C(32)-P(2)-C(15)-C(19)	-116.06(18)
C(38)-P(2)-C(15)-C(19)	-9.66(19)
Ni(1)-P(2)-C(15)-C(19)	114.42(16)
C(32)-P(2)-C(15)-C(16)	67.68(18)
C(38)-P(2)-C(15)-C(16)	174.07(16)
Ni(1)-P(2)-C(15)-C(16)	-61.84(18)
C(32)-P(2)-C(15)-Fe(1)	154.32(11)
C(38)-P(2)-C(15)-Fe(1)	-99.29(13)
Ni(1)-P(2)-C(15)-Fe(1)	24.79(15)
C(19)-C(15)-C(16)-C(17)	0.2(2)
P(2)-C(15)-C(16)-C(17)	177.10(14)
Fe(1)-C(15)-C(16)-C(17)	59.95(14)
C(19)-C(15)-C(16)-Fe(1)	-59.77(13)
P(2)-C(15)-C(16)-Fe(1)	117.16(15)
C(15)-C(16)-C(17)-C(18)	-0.5(2)
Fe(1)-C(16)-C(17)-C(18)	59.19(14)
C(15)-C(16)-C(17)-Fe(1)	-59.68(13)
C(16)-C(17)-C(18)-C(19)	0.6(2)
Fe(1)-C(17)-C(18)-C(19)	59.33(14)
C(16)-C(17)-C(18)-Fe(1)	-58.72(14)
C(17)-C(18)-C(19)-C(15)	-0.5(2)
Fe(1)-C(18)-C(19)-C(15)	58.75(13)
C(17)-C(18)-C(19)-Fe(1)	-59.26(14)
C(16)-C(15)-C(19)-C(18)	0.2(2)
P(2)-C(15)-C(19)-C(18)	-176.61(14)
Fe(1)-C(15)-C(19)-C(18)	-59.07(14)
C(16)-C(15)-C(19)-Fe(1)	59.27(13)
P(2)-C(15)-C(19)-Fe(1)	-117.53(16)
C(10)-P(1)-C(20)-C(25)	-75.4(2)
C(26)-P(1)-C(20)-C(25)	29.8(2)
Ni(1)-P(1)-C(20)-C(25)	155.1(2)
C(10)-P(1)-C(20)-C(21)	105.36(18)
C(26)-P(1)-C(20)-C(21)	-149.40(18)
Ni(1)-P(1)-C(20)-C(21)	-24.2(2)
C(25)-C(20)-C(21)-C(22)	-0.6(3)
P(1)-C(20)-C(21)-C(22)	178.68(17)
C(20)-C(21)-C(22)-C(23)	0.2(4)
C(21)-C(22)-C(23)-C(24)	0.7(4)
C(22)-C(23)-C(24)-C(25)	-1.3(5)
C(23)-C(24)-C(25)-C(20)	0.9(5)
C(21)-C(20)-C(25)-C(24)	0.0(4)
P(1)-C(20)-C(25)-C(24)	-179.2(2)

C(10)-P(1)-C(26)-C(31)	-161.84(16)
C(20)-P(1)-C(26)-C(31)	92.41(18)
Ni(1)-P(1)-C(26)-C(31)	-28.00(18)
C(10)-P(1)-C(26)-C(27)	16.99(19)
C(20)-P(1)-C(26)-C(27)	-88.76(19)
Ni(1)-P(1)-C(26)-C(27)	150.83(15)
C(31)-C(26)-C(27)-C(28)	0.1(3)
P(1)-C(26)-C(27)-C(28)	-178.68(16)
C(26)-C(27)-C(28)-C(29)	0.5(3)
C(27)-C(28)-C(29)-C(30)	-1.0(3)
C(28)-C(29)-C(30)-C(31)	1.0(3)
C(29)-C(30)-C(31)-C(26)	-0.4(3)
C(27)-C(26)-C(31)-C(30)	-0.1(3)
P(1)-C(26)-C(31)-C(30)	178.73(17)
C(15)-P(2)-C(32)-C(37)	24.86(19)
C(38)-P(2)-C(32)-C(37)	-82.45(18)
Ni(1)-P(2)-C(32)-C(37)	161.43(15)
C(15)-P(2)-C(32)-C(33)	-158.13(16)
C(38)-P(2)-C(32)-C(33)	94.56(17)
Ni(1)-P(2)-C(32)-C(33)	-21.56(18)
C(37)-C(32)-C(33)-C(34)	-0.4(3)
P(2)-C(32)-C(33)-C(34)	-177.54(17)
C(32)-C(33)-C(34)-C(35)	0.1(3)
C(33)-C(34)-C(35)-C(36)	0.5(4)
C(34)-C(35)-C(36)-C(37)	-0.8(3)
C(35)-C(36)-C(37)-C(32)	0.5(3)
C(33)-C(32)-C(37)-C(36)	0.1(3)
P(2)-C(32)-C(37)-C(36)	177.10(16)
C(15)-P(2)-C(38)-C(39)	85.52(19)
C(32)-P(2)-C(38)-C(39)	-168.38(18)
Ni(1)-P(2)-C(38)-C(39)	-48.83(19)
C(15)-P(2)-C(38)-C(43)	-100.9(2)
C(32)-P(2)-C(38)-C(43)	5.2(2)
Ni(1)-P(2)-C(38)-C(43)	124.71(18)
C(43)-C(38)-C(39)-C(40)	1.0(4)
P(2)-C(38)-C(39)-C(40)	174.8(2)
C(38)-C(39)-C(40)-C(41)	-1.9(4)
C(39)-C(40)-C(41)-C(42)	1.4(4)
C(40)-C(41)-C(42)-C(43)	-0.2(4)
C(41)-C(42)-C(43)-C(38)	-0.7(4)
C(39)-C(38)-C(43)-C(42)	0.3(3)
P(2)-C(38)-C(43)-C(42)	-173.17(18)

*Crystallographic Information for (dppf)Ni^{I}(2,4,6-^{i}Pr$_3$C$_6$H$_2$) (**3**) (CCDC: 1815576)*

Crystals of **3** were obtained from a concentrated solution in diethyl ether at -35 °C. Low-temperature diffraction data (ω-scans) were collected on a Rigaku MicroMax-007HF diffractometer coupled to a Saturn994+ CCD detector with Cu Kα (λ = 1.54178 Å) for the structure of **3**. The diffraction images were processed and scaled using Rigaku Oxford Diffraction software.[14] The structure was solved with SHELXT and was refined against F^2 on all data by full-matrix least squares with SHELXL.[15] All non-hydrogen atoms were refined anisotropically. Hydrogen atoms were included in the model at geometrically calculated positions and refined using a riding model. The isotropic displacement parameters of all hydrogen atoms were fixed to 1.2 times the U value of the atoms to which they are linked (1.5 times for methyl groups). The full details of the X-ray structure determination are included in the .cif.

*X-ray Structure of **3***

Table S14. Crystal data and structure refinement for **3**.

Empirical formula	$C_{53}H_{61}FeNiOP_2$
Formula weight	890.56
Temperature/K	566.3
Crystal system	Monoclinic
Space group	$P2_1/c$
a/Å	14.2235(10)
b/Å	16.3932(11)
c/Å	19.5487(14)
α/°	90
β/°	98.0230(10)
γ/°	90
Volume/Å^3	4513.5(5)
Z	4
ρ_{calc}g/cm^3	1.309
μ/mm^{-1}	4.044
F(000)	1880.0
Crystal size/mm^3	0.2 × 0.2 × 0.2
Radiation	CuKα (λ = 1.54178)
2Θ range for data collection/°	6.276 to 135.932
Index ranges	$-17 \leq h \leq 17$, $-19 \leq k \leq 19$, $-23 \leq l \leq 22$
Reflections collected	158320
Independent reflections	8172 [R_{int} = 0.0478, R_{sigma} = 0.0157]

Data/restraints/parameters	8172/0/531
Goodness-of-fit on F^2	1.052
Final R indexes [I>=2σ (I)]	R_1 = 0.0273, wR_2 = 0.0734
Final R indexes [all data]	R_1 = 0.0321, wR_2 = 0.0751
Largest diff. peak/hole / e Å^{-3}	0.62/-0.49

Table S15. Fractional Atomic Coordinates ($\times 10^4$) and Equivalent Isotropic Displacement Parameters (Å$^2\times 10^3$) for **3**. U_{eq} is defined as 1/3 of the trace of the orthogonalised U_{IJ} tensor.

Atom	***x***	***y***	***Z***	**U(eq)**
Ni1	2523.7(2)	6857.0(2)	4749.8(2)	17.26(8)
Fe1	2490.0(2)	4300.8(2)	5062.9(2)	15.55(7)
P1	2677.1(3)	5886.1(2)	3995.5(2)	16.72(9)
P2	2281.0(3)	6178.0(2)	5686.3(2)	16.59(9)
C1	2601.8(11)	8027(1)	4520.8(8)	18.5(3)
C2	3469.0(11)	8456.6(10)	4552.7(8)	18.4(3)
C3	3490.3(12)	9295.6(10)	4429.4(9)	20.3(3)
C4	2660.0(12)	9751.1(10)	4265.6(8)	20.2(3)
C5	1803.8(12)	9336.7(10)	4233.9(9)	21.6(4)
C6	1768.5(11)	8498.6(10)	4359.5(8)	19.6(3)
C7	4401.8(11)	8004.9(10)	4764.7(9)	20.4(3)
C8	4809.4(13)	8218.3(11)	5510.8(9)	27.5(4)
C9	5136.0(12)	8146.4(11)	4276.7(10)	28.8(4)
C10	2723.6(13)	10664.3(10)	4129.5(9)	23.5(4)
C11	1829.5(13)	11137.2(11)	4227.9(11)	32.3(4)
C12	2985.0(17)	10830.0(12)	3412.7(11)	38.1(5)
C13	804.0(12)	8080(1)	4296.3(9)	22.6(4)
C14	87.6(13)	8512.4(12)	4684.9(11)	32.6(4)
C15	399.1(13)	7965.6(11)	3534.6(10)	28.4(4)
C16	3067.2(11)	4878.1(10)	4300.8(8)	18.2(3)
C17	3775.5(11)	4740.5(10)	4888.1(8)	19.0(3)
C18	3849.4(12)	3886.3(10)	5016.9(9)	22.5(4)
C19	3191.5(12)	3486.9(10)	4513.1(9)	22.8(4)
C20	2713.0(12)	4088.3(10)	4071.2(9)	20.8(3)
C21	1889.6(11)	5123.5(9)	5647.4(8)	16.9(3)
C22	2260.9(12)	4443.3(10)	6064.5(9)	20.0(3)
C23	1797.9(12)	3723.6(10)	5782.8(9)	22.6(4)
C24	1140.6(12)	3941.5(10)	5201.7(9)	21.7(4)
C25	1192.5(11)	4801.8(10)	5111.2(8)	17.7(3)
C26	3533.2(11)	6150.8(10)	3412.5(8)	18.3(3)
C27	4406.0(12)	5769.6(11)	3440.4(9)	24.5(4)
C28	5039.0(12)	6002.6(11)	2995.7(10)	27.8(4)

C29	4794.9(12)	6606.6(11)	2512.3(9)	26.3(4)
C30	3923.8(13)	6985.4(11)	2477.6(9)	26.8(4)
C31	3297.6(12)	6770.8(10)	2931.8(9)	24.5(4)
C32	1622.4(11)	5637.2(9)	3376.8(8)	18.3(3)
C33	729.7(11)	5896.4(10)	3496.5(9)	19.8(3)
C34	-75.6(12)	5691.1(10)	3041.6(9)	24.1(4)
C35	4.0(13)	5223.4(11)	2464.8(9)	25.5(4)
C36	892.6(12)	4969.1(10)	2334.3(9)	24.0(4)
C37	1700.9(12)	5176.8(10)	2784.1(8)	21.3(3)
C38	1385.8(11)	6692.1(10)	6116.3(8)	19.1(3)
C39	1503.3(14)	7527.4(11)	6243.7(10)	31.2(4)
C40	861.4(15)	7951.6(12)	6578.5(11)	35.5(5)
C41	86.4(13)	7559.9(11)	6776.0(9)	28.8(4)
C42	-42.6(13)	6735.7(12)	6649.0(9)	28.4(4)
C43	609.4(12)	6302.1(10)	6321.6(9)	23.4(4)
C44	3292.4(11)	6144.6(10)	6379.0(8)	19.3(3)
C45	4199.9(11)	6295.4(10)	6219.2(9)	20.9(3)
C46	4984.9(12)	6259.7(11)	6732.3(9)	25.4(4)
C47	4864.1(13)	6085.2(11)	7407.7(10)	28.5(4)
C48	3960.8(13)	5953.2(11)	7571.7(9)	27.8(4)
C49	3176.5(12)	5979.4(10)	7061.8(9)	23.7(4)
O1	2790.7(9)	4117.1(7)	1702.8(6)	28.1(3)
C50	2687.2(14)	4584.5(12)	1087.5(10)	30.7(4)
C51	3025.1(19)	5431.4(13)	1240.3(11)	47.6(6)
C52	2505.1(14)	3298.6(11)	1590.8(10)	30.5(4)
C53	2542.9(17)	2865.0(13)	2264.4(11)	43.7(5)

Table S16. Anisotropic Displacement Parameters ($Å^2 \times 10^3$) for **3**. The Anisotropic displacement factor exponent takes the form: $-2\pi^2[h^2a^{*2}U_{11}+2hka^*b^*U_{12}+\ldots]$.

Atom	$\mathbf{U^{11}}$	$\mathbf{U^{22}}$	$\mathbf{U^{33}}$	$\mathbf{U^{23}}$	$\mathbf{U^{13}}$	$\mathbf{U^{12}}$
Ni1	18.68(15)	12.45(14)	20.33(15)	1.94(11)	1.56(11)	-0.63(10)
Fe1	17.66(14)	11.62(13)	17.68(14)	0.97(10)	3.51(10)	1.28(10)
P1	16.8(2)	16.9(2)	16.7(2)	2.20(15)	2.96(15)	0.37(15)
P2	18.3(2)	13.51(19)	18.0(2)	-1.13(15)	2.60(16)	-0.74(15)
C1	21.5(8)	16.5(8)	17.7(8)	1.0(6)	2.9(6)	0.1(6)
C2	20.7(8)	17.1(8)	17.8(8)	1.9(6)	3.9(6)	0.6(6)
C3	21.1(8)	17.7(8)	22.4(9)	1.6(6)	4.1(7)	-2.3(6)
C4	26.1(9)	15.8(8)	18.6(8)	1.0(6)	3.1(7)	0.2(7)
C5	21.9(8)	19.2(8)	23.1(9)	2.4(7)	0.6(7)	4.4(6)
C6	20.8(8)	18.8(8)	19.4(8)	1.2(6)	2.8(6)	0.1(6)

C7	18.6(8)	16.0(8)	26.4(9)	2.9(7)	2.9(7)	0.9(6)
C8	25.1(9)	25.5(9)	30.5(10)	1.6(8)	-0.7(7)	4.0(7)
C9	24.3(9)	27.5(10)	36.1(11)	7.6(8)	8.9(8)	4.9(7)
C10	26.7(9)	14.7(8)	28.3(9)	2.3(7)	1.4(7)	0.2(7)
C11	34.4(10)	16.2(9)	45.2(12)	2.6(8)	1.6(9)	4.1(8)
C12	58.9(14)	21.7(10)	35.4(11)	7.7(8)	12.9(10)	-0.6(9)
C13	20.7(8)	17.6(8)	29.1(9)	3.1(7)	1.7(7)	1.5(7)
C14	23.6(9)	35.5(11)	39.3(11)	-2.4(9)	7.0(8)	-0.8(8)
C15	26.6(9)	22.2(9)	34.1(10)	-0.5(8)	-3.8(8)	0.3(7)
C16	19.0(8)	18.8(8)	17.7(8)	0.4(6)	6.7(6)	1.3(6)
C17	16.6(8)	19.5(8)	21.6(8)	0.1(7)	4.7(6)	0.7(6)
C18	22.0(8)	20.8(9)	25.6(9)	3.0(7)	6.0(7)	7.6(7)
C19	27.0(9)	15.3(8)	27.6(9)	-2.9(7)	9.6(7)	4.0(7)
C20	22.0(8)	21.5(8)	19.5(8)	-1.8(7)	5.2(7)	0.9(7)
C21	18.3(8)	15.1(8)	18.2(8)	-0.1(6)	5.8(6)	1.2(6)
C22	23.0(8)	19.4(8)	18.2(8)	2.4(6)	5.2(7)	1.5(7)
C23	30.2(9)	14.7(8)	24.8(9)	4.5(7)	10.2(7)	0.7(7)
C24	23.0(8)	18.5(8)	25.0(9)	-1.8(7)	7.9(7)	-4.6(7)
C25	16.4(8)	17.7(8)	19.9(8)	0.9(6)	5.6(6)	0.9(6)
C26	19.7(8)	17.8(8)	17.6(8)	-0.7(6)	3.2(6)	-2.9(6)
C27	23.8(9)	24.4(9)	25.2(9)	4.4(7)	2.9(7)	1.2(7)
C28	20.4(9)	31.2(10)	32.9(10)	2.1(8)	7.3(7)	3.1(7)
C29	26.3(9)	29.7(10)	24.8(9)	0.0(7)	10.4(7)	-6.2(7)
C30	32.9(10)	23.6(9)	24.7(9)	5.9(7)	6.7(8)	-2.8(7)
C31	23.4(9)	22.5(9)	28.6(9)	3.6(7)	6.8(7)	2.2(7)
C32	20.0(8)	17.0(8)	18.1(8)	5.0(6)	3.0(6)	-0.3(6)
C33	23.1(8)	16.4(8)	20.5(8)	3.5(6)	4.8(7)	0.2(6)
C34	19.6(8)	21.4(9)	31.5(10)	7.2(7)	4.3(7)	1.0(7)
C35	24.6(9)	25.0(9)	25.3(9)	3.9(7)	-2.4(7)	-6.2(7)
C36	29.4(9)	21.7(9)	20.6(9)	0.9(7)	2.6(7)	-3.4(7)
C37	22.9(8)	21.6(8)	19.8(8)	2.6(7)	4.7(7)	0.3(7)
C38	22.2(8)	17.5(8)	17.3(8)	-0.7(6)	1.2(6)	2.6(6)
C39	37(1)	19.9(9)	39.3(11)	-5.1(8)	14.8(9)	-3.7(8)
C40	49.8(12)	18.8(9)	40.1(12)	-7.6(8)	13.6(9)	3.7(8)
C41	33.5(10)	30(1)	23.5(9)	-2.6(8)	6.2(8)	13.1(8)
C42	25.4(9)	33(1)	28.3(10)	-0.7(8)	8.5(8)	2.6(8)
C43	25.9(9)	19.3(8)	25.4(9)	-2.0(7)	5.5(7)	0.2(7)
C44	21.4(8)	14.6(8)	21.3(8)	-1.6(6)	0.7(7)	-0.9(6)
C45	23.8(8)	18.1(8)	21.3(8)	-2.0(7)	4.7(7)	-0.9(7)
C46	19.8(8)	25.5(9)	30.4(10)	-4.8(7)	2.2(7)	-1.0(7)
C47	28.2(9)	27(1)	27.5(10)	-1.7(8)	-6.3(8)	0.5(7)
C48	36.4(10)	25.6(9)	20.2(9)	1.3(7)	0.0(8)	-4.1(8)

C49	25.4(9)	23.2(9)	22.8(9)	-1.6(7)	4.9(7)	-4.3(7)
O1	37.6(7)	22.7(6)	23.4(6)	-3.3(5)	2.2(5)	-3.2(5)
C50	35.8(10)	30.6(10)	26.5(10)	-1.4(8)	6.9(8)	-0.7(8)
C51	77.4(17)	32.8(11)	35.9(12)	0.7(9)	19.4(11)	-11.2(11)
C52	38.7(11)	24.5(9)	28.1(10)	-6.8(8)	3.8(8)	-5.2(8)
C53	61.6(14)	29.5(11)	36.5(12)	1.9(9)	-5(1)	-9.8(10)

Table S17. Bond Lengths for **3**.

Atom	Atom	Length/Å	Atom	Atom	Length/Å
Ni1	P1	2.2012(5)	C17	C18	1.424(2)
Ni1	P2	2.2103(5)	C18	C19	1.420(2)
Ni1	C1	1.9762(16)	C19	C20	1.420(2)
Fe1	C16	2.0325(16)	C21	C22	1.438(2)
Fe1	C17	2.0382(16)	C21	C25	1.439(2)
Fe1	C18	2.0632(16)	C22	C23	1.424(2)
Fe1	C19	2.0568(16)	C23	C24	1.413(2)
Fe1	C20	2.0377(17)	C24	C25	1.425(2)
Fe1	C21	2.0313(16)	C26	C27	1.384(2)
Fe1	C22	2.0426(17)	C26	C31	1.393(2)
Fe1	C23	2.0569(16)	C27	C28	1.390(3)
Fe1	C24	2.0614(17)	C28	C29	1.379(3)
Fe1	C25	2.0341(16)	C29	C30	1.379(3)
P1	C16	1.8171(16)	C30	C31	1.388(2)
P1	C26	1.8323(16)	C32	C33	1.389(2)
P1	C32	1.8367(17)	C32	C37	1.400(2)
P2	C21	1.8144(16)	C33	C34	1.390(2)
P2	C38	1.8268(17)	C34	C35	1.381(3)
P2	C44	1.8337(16)	C35	C36	1.388(3)
C1	C2	1.414(2)	C36	C37	1.389(2)
C1	C6	1.413(2)	C38	C39	1.398(2)
C2	C3	1.397(2)	C38	C43	1.383(2)
C2	C7	1.525(2)	C39	C40	1.383(3)
C3	C4	1.396(2)	C40	C41	1.377(3)
C4	C5	1.388(2)	C41	C42	1.381(3)
C4	C10	1.525(2)	C42	C43	1.393(2)
C5	C6	1.398(2)	C44	C45	1.392(2)
C6	C13	1.523(2)	C44	C49	1.394(2)
C7	C8	1.533(2)	C45	C46	1.394(2)
C7	C9	1.527(2)	C46	C47	1.385(3)
C10	C11	1.524(2)	C47	C48	1.384(3)

C10	C12	1.523(3)	C48	C49	1.389(2)
C13	C14	1.528(2)	O1	C50	1.416(2)
C13	C15	1.531(2)	O1	C52	1.410(2)
C16	C17	1.436(2)	C50	C51	1.486(3)
C16	C20	1.438(2)	C52	C53	1.491(3)

Table S18. Bond Angles for **3**.

Atom	Atom	Atom	Angle/°	Atom	Atom	Atom	Angle/°
P1	Ni1	P2	103.426(19)	C11	C10	C4	113.97(15)
C1	Ni1	P1	122.42(5)	C12	C10	C4	111.31(15)
C1	Ni1	P2	134.15(5)	C12	C10	C11	109.90(16)
C16	Fe1	C17	41.30(6)	C6	C13	C14	113.97(14)
C16	Fe1	C18	69.18(7)	C6	C13	C15	110.26(14)
C16	Fe1	C19	69.14(7)	C14	C13	C15	110.72(14)
C16	Fe1	C20	41.39(7)	P1	C16	Fe1	121.87(8)
C16	Fe1	C22	141.64(7)	C17	C16	Fe1	69.56(9)
C16	Fe1	C23	175.22(7)	C17	C16	P1	123.61(12)
C16	Fe1	C24	135.09(7)	C17	C16	C20	106.52(14)
C16	Fe1	C25	107.93(6)	C20	C16	Fe1	69.50(9)
C17	Fe1	C18	40.63(7)	C20	C16	P1	129.68(12)
C17	Fe1	C19	68.27(7)	C16	C17	Fe1	69.14(9)
C17	Fe1	C22	112.77(7)	C18	C17	Fe1	70.63(9)
C17	Fe1	C23	143.47(7)	C18	C17	C16	108.79(15)
C17	Fe1	C24	175.30(6)	C17	C18	Fe1	68.74(9)
C19	Fe1	C18	40.33(7)	C19	C18	Fe1	69.59(9)
C19	Fe1	C23	111.87(7)	C19	C18	C17	107.79(15)
C19	Fe1	C24	114.33(7)	C18	C19	Fe1	70.08(9)
C20	Fe1	C17	68.81(7)	C18	C19	C20	108.38(15)
C20	Fe1	C18	68.34(7)	C20	C19	Fe1	68.98(9)
C20	Fe1	C19	40.59(7)	C16	C20	Fe1	69.11(9)
C20	Fe1	C22	176.72(7)	C19	C20	Fe1	70.43(9)
C20	Fe1	C23	136.48(7)	C19	C20	C16	108.52(15)
C20	Fe1	C24	110.35(7)	P2	C21	Fe1	120.36(8)
C21	Fe1	C16	110.35(6)	C22	C21	Fe1	69.76(9)
C21	Fe1	C17	108.48(7)	C22	C21	P2	128.97(12)
C21	Fe1	C18	135.50(7)	C22	C21	C25	106.87(14)
C21	Fe1	C19	175.83(7)	C25	C21	Fe1	69.38(9)
C21	Fe1	C20	141.46(7)	C25	C21	P2	123.78(12)
C21	Fe1	C22	41.33(6)	C21	C22	Fe1	68.92(9)
C21	Fe1	C23	69.00(6)	C23	C22	Fe1	70.22(10)

C21	Fe1	C24	69.11(6)	C23	C22	C21	108.05(14)
C21	Fe1	C25	41.45(6)	C22	C23	Fe1	69.13(9)
C22	Fe1	C18	110.81(7)	C24	C23	Fe1	70.11(9)
C22	Fe1	C19	136.81(7)	C24	C23	C22	108.66(14)
C22	Fe1	C23	40.65(7)	C23	C24	Fe1	69.77(10)
C22	Fe1	C24	68.32(7)	C23	C24	C25	108.07(14)
C23	Fe1	C18	114.78(7)	C25	C24	Fe1	68.62(9)
C23	Fe1	C24	40.12(7)	C21	C25	Fe1	69.17(9)
C24	Fe1	C18	143.81(7)	C24	C25	Fe1	70.68(9)
C25	Fe1	C17	134.90(7)	C24	C25	C21	108.35(14)
C25	Fe1	C18	175.41(6)	C27	C26	P1	122.60(13)
C25	Fe1	C19	142.71(7)	C27	C26	C31	119.08(15)
C25	Fe1	C20	112.08(7)	C31	C26	P1	118.31(12)
C25	Fe1	C22	69.04(7)	C26	C27	C28	120.47(16)
C25	Fe1	C23	68.29(7)	C29	C28	C27	120.20(17)
C25	Fe1	C24	40.70(6)	C30	C29	C28	119.70(16)
C16	P1	Ni1	119.46(5)	C29	C30	C31	120.45(16)
C16	P1	C26	102.75(7)	C30	C31	C26	120.08(16)
C16	P1	C32	101.43(7)	C33	C32	P1	120.18(13)
C26	P1	Ni1	112.46(5)	C33	C32	C37	118.98(15)
C26	P1	C32	101.28(7)	C37	C32	P1	120.83(12)
C32	P1	Ni1	116.97(5)	C32	C33	C34	120.60(16)
C21	P2	Ni1	121.85(5)	C35	C34	C33	120.17(16)
C21	P2	C38	103.26(7)	C34	C35	C36	119.82(16)
C21	P2	C44	101.94(7)	C35	C36	C37	120.30(16)
C38	P2	Ni1	110.38(5)	C36	C37	C32	120.10(16)
C38	P2	C44	101.49(7)	C39	C38	P2	117.41(13)
C44	P2	Ni1	115.44(6)	C43	C38	P2	123.80(13)
C2	C1	Ni1	123.34(12)	C43	C38	C39	118.80(16)
C6	C1	Ni1	120.64(12)	C40	C39	C38	120.44(17)
C6	C1	C2	115.88(15)	C41	C40	C39	120.36(17)
C1	C2	C7	119.37(14)	C40	C41	C42	119.83(17)
C3	C2	C1	121.49(15)	C41	C42	C43	120.10(17)
C3	C2	C7	119.05(14)	C38	C43	C42	120.47(16)
C4	C3	C2	121.86(15)	C45	C44	P2	119.04(13)
C3	C4	C10	119.73(15)	C45	C44	C49	119.12(15)
C5	C4	C3	117.21(15)	C49	C44	P2	121.84(13)
C5	C4	C10	123.06(15)	C44	C45	C46	120.39(16)
C4	C5	C6	121.72(15)	C47	C46	C45	120.07(16)
C1	C6	C13	119.30(14)	C48	C47	C46	119.74(16)
C5	C6	C1	121.83(15)	C47	C48	C49	120.49(17)
C5	C6	C13	118.84(14)	C48	C49	C44	120.18(16)

C2	C7	C8	110.30(14)	C52	O1	C50	112.92(14)
C2	C7	C9	113.65(14)	O1	C50	C51	110.02(16)
C9	C7	C8	111.03(14)	O1	C52	C53	110.04(15)

Table S19. Torsion Angles for **3**.

A	B	C	D	Angle/°	A	B	C	D	Angle/°
Ni1	P1	C16	Fe1	47.23(11)	C16	P1	C32	C37	-63.47(14)
Ni1	P1	C16	C17	-38.15(15)	C16	C17	C18	Fe1	-58.78(11)
Ni1	P1	C16	C20	136.09(13)	C16	C17	C18	C19	0.04(18)
Ni1	P1	C26	C27	110.02(14)	C17	C16	C20	Fe1	60.02(11)
Ni1	P1	C26	C31	-68.83(14)	C17	C16	C20	C19	0.42(18)
Ni1	P1	C32	C33	-16.04(15)	C17	C18	C19	Fe1	-58.29(11)
Ni1	P1	C32	C37	164.78(11)	C17	C18	C19	C20	0.22(18)
Ni1	P2	C21	Fe1	44.29(11)	C18	C19	C20	Fe1	-59.18(11)
Ni1	P2	C21	C22	131.88(13)	C18	C19	C20	C16	-0.40(19)
Ni1	P2	C21	C25	-40.01(15)	C20	C16	C17	Fe1	-59.98(11)
Ni1	P2	C38	C39	-50.02(15)	C20	C16	C17	C18	-0.28(18)
Ni1	P2	C38	C43	130.19(13)	C21	P2	C38	C39	178.24(14)
Ni1	P2	C44	C45	-20.24(15)	C21	P2	C38	C43	-1.55(16)
Ni1	P2	C44	C49	159.20(12)	C21	P2	C44	C45	114.01(13)
Ni1	C1	C2	C3	-175.82(13)	C21	P2	C44	C49	-66.55(15)
Ni1	C1	C2	C7	0.8(2)	C21	C22	C23	Fe1	58.72(11)
Ni1	C1	C6	C5	176.32(13)	C21	C22	C23	C24	-0.42(19)
Ni1	C1	C6	C13	-5.8(2)	C22	C21	C25	Fe1	-59.97(11)
Fe1	C16	C17	C18	59.70(11)	C22	C21	C25	C24	0.09(17)
Fe1	C16	C20	C19	-59.60(11)	C22	C23	C24	Fe1	58.54(12)
Fe1	C17	C18	C19	58.82(11)	C22	C23	C24	C25	0.47(19)
Fe1	C18	C19	C20	58.51(11)	C23	C24	C25	Fe1	58.77(11)
Fe1	C19	C20	C16	58.79(11)	C23	C24	C25	C21	-0.35(18)
Fe1	C21	C22	C23	-59.53(11)	C25	C21	C22	Fe1	59.73(10)
Fe1	C21	C25	C24	60.06(11)	C25	C21	C22	C23	0.20(18)
Fe1	C22	C23	C24	-59.14(12)	C26	P1	C16	Fe1	172.52(9)
Fe1	C23	C24	C25	-58.06(11)	C26	P1	C16	C17	87.14(14)
Fe1	C24	C25	C21	-59.12(11)	C26	P1	C16	C20	-98.62(16)
P1	C16	C17	Fe1	115.40(12)	C26	P1	C32	C33	-138.63(13)
P1	C16	C17	C18	175.10(12)	C26	P1	C32	C37	42.19(14)
P1	C16	C20	Fe1	-114.98(14)	C26	C27	C28	C29	-1.3(3)
P1	C16	C20	C19	-174.59(12)	C27	C26	C31	C30	1.6(3)
P1	C26	C27	C28	-178.76(14)	C27	C28	C29	C30	0.8(3)
P1	C26	C31	C30	-179.53(13)	C28	C29	C30	C31	0.9(3)

P1	C32	C33	C34	-178.14(12)	C29	C30	C31	C26	-2.1(3)
P1	C32	C37	C36	177.69(13)	C31	C26	C27	C28	0.1(3)
P2	C21	C22	Fe1	-113.24(13)	C32	P1	C16	Fe1	-82.98(10)
P2	C21	C22	C23	-172.77(12)	C32	P1	C16	C17	-168.36(13)
P2	C21	C25	Fe1	113.45(12)	C32	P1	C16	C20	5.88(17)
P2	C21	C25	C24	173.51(12)	C32	P1	C26	C27	-124.33(14)
P2	C38	C39	C40	-178.83(15)	C32	P1	C26	C31	56.83(15)
P2	C38	C43	C42	179.82(13)	C32	C33	C34	C35	0.2(2)
P2	C44	C45	C46	-178.82(13)	C33	C32	C37	C36	-1.5(2)
P2	C44	C49	C48	179.51(13)	C33	C34	C35	C36	-1.0(3)
C1	C2	C3	C4	-0.3(3)	C34	C35	C36	C37	0.6(3)
C1	C2	C7	C8	-103.95(17)	C35	C36	C37	C32	0.7(3)
C1	C2	C7	C9	130.62(16)	C37	C32	C33	C34	1.1(2)
C1	C6	C13	C14	132.73(17)	C38	P2	C21	Fe1	168.86(9)
C1	C6	C13	C15	-102.03(17)	C38	P2	C21	C22	-103.54(15)
C2	C1	C6	C5	0.5(2)	C38	P2	C21	C25	84.56(14)
C2	C1	C6	C13	178.42(14)	C38	P2	C44	C45	-139.60(13)
C2	C3	C4	C5	0.4(2)	C38	P2	C44	C49	39.84(15)
C2	C3	C4	C10	-179.45(15)	C38	C39	C40	C41	-1.5(3)
C3	C2	C7	C8	72.72(19)	C39	C38	C43	C42	0.0(3)
C3	C2	C7	C9	-52.7(2)	C39	C40	C41	C42	1.0(3)
C3	C4	C5	C6	-0.1(2)	C40	C41	C42	C43	0.0(3)
C3	C4	C10	C11	-157.95(16)	C41	C42	C43	C38	-0.5(3)
C3	C4	C10	C12	77.1(2)	C43	C38	C39	C40	1.0(3)
C4	C5	C6	C1	-0.4(3)	C44	P2	C21	Fe1	-86.12(10)
C4	C5	C6	C13	-178.35(15)	C44	P2	C21	C22	1.47(17)
C5	C4	C10	C11	22.2(2)	C44	P2	C21	C25	-170.42(13)
C5	C4	C10	C12	-102.8(2)	C44	P2	C38	C39	72.88(15)
C5	C6	C13	C14	-49.3(2)	C44	P2	C38	C43	-106.91(15)
C5	C6	C13	C15	75.94(19)	C44	C45	C46	C47	-1.0(3)
C6	C1	C2	C3	-0.1(2)	C45	C44	C49	C48	-1.1(2)
C6	C1	C2	C7	176.46(14)	C45	C46	C47	C48	-0.5(3)
C7	C2	C3	C4	-176.95(15)	C46	C47	C48	C49	1.2(3)
C10	C4	C5	C6	179.83(16)	C47	C48	C49	C44	-0.4(3)
C16	P1	C26	C27	-19.72(16)	C49	C44	C45	C46	1.7(2)
C16	P1	C26	C31	161.44(13)	C50	O1	C52	C53	-174.49(16)
C16	P1	C32	C33	115.71(13)	C52	O1	C50	C51	-178.44(17)

*Crystallographic Information for (dppf)Ni^{II}(2,4,6-^{i}Pr$_3$C$_6$H$_2$)(Br) (**9**) (CCDC: 1815573)*

Single crystals of **9** were grown from a concentrated toluene solution at -15 °C. Low-temperature diffraction data (ω-scans) were collected on a Rigaku SCX Mini diffractometer coupled to a Rigaku Mercury275R CCD with Mo Kα radiation (λ = 0.71073 Å) for the structure of **9** (Figure S26). The diffraction images were processed and scaled using Rigaku CryAlisPro software.[14] The structure was solved with SHELXT and was refined against F^2 on all data by full-matrix least squares with SHELXL.[14] All non-hydrogen atoms were refined anisotropically. Hydrogen atoms were included in the model at geometrically calculated positions and refined using a riding model. The isotropic displacement parameters of all hydrogen atoms were fixed to 1.2 times the U value of the atoms to which they are linked (1.5 times for methyl groups). The residual density is abnormally high and likely due to disorder that was not modelled in this refinement. The high residual density could possibly be a result of whole molecule disorder; however, a reasonable model was not obvious. Despite this, we believe that the connectivity of the first coordination sphere of the nickel unit is valid and unperturbed by the unresolved electron density. Also, several low angle reflections were recorded improperly and subsequently omitted from the least square refinement. The full details of the X-ray structure determination are included in the .cif.

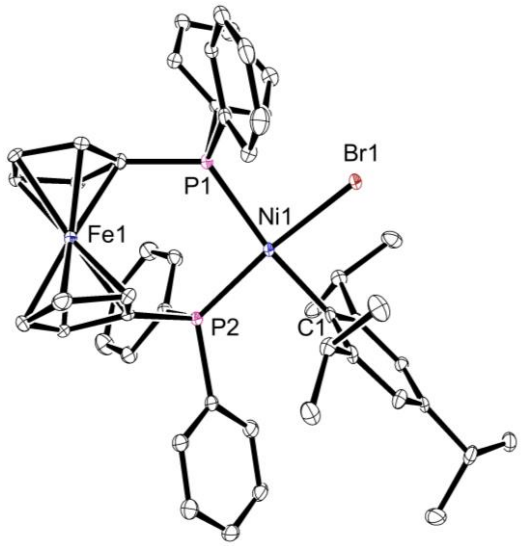

Figure S26. ORTEP of **9** with ellipsoids drawn at 50% probability. Hydrogen atoms and solvent of crystallization have been omitted for clarity.

*X-ray Structure of **9***

Table S20. Crystal data and structure refinement for **9**.

Empirical formula	$C_{63}H_{67}BrFeNiP_2$
Formula weight	1080.57
Temperature/K	293(2)
Crystal system	Triclinic
Space group	P-1
a/Å	10.4283(5)
b/Å	13.6108(6)
c/Å	19.5796(10)
α/°	77.340(4)
β/°	81.336(4)
γ/°	88.445(4)
Volume/Å^3	2680.5(2)
Z	2
ρ_{calc}g/cm^3	1.339
μ/mm^{-1}	1.466
F(000)	1128.0
Crystal size/mm^3	0.2 × 0.2 × 0.2
2Θ range for data collection/°	3.95 to 50.084
Index ranges	$-12 \le h \le 12$, $-16 \le k \le 16$, $-23 \le l \le 23$
Reflections collected	37772
Independent reflections	9484 [R_{int} = 0.0907, R_{sigma} = 0.0778]
Data/restraints/parameters	9484/0/621
Goodness-of-fit on F^2	1.022
Final R indexes [I>=2σ (I)]	R_1 = 0.0828, wR_2 = 0.2072
Final R indexes [all data]	R_1 = 0.1116, wR_2 = 0.2321
Largest diff. peak/hole / e Å^{-3}	4.67/-0.61

Table S21. Fractional Atomic Coordinates (×10^4) and Equivalent Isotropic Displacement Parameters (Å^2×10^3) for **9**. U_{eq} is defined as 1/3 of the trace of the orthogonalised U_{IJ} tensor.

Atom	***x***	***y***	***z***	**U(eq)**
Br1	4265.7(6)	7438.1(5)	3375.0(4)	22.1(2)
Ni1	6269.8(7)	8195.1(6)	2832.2(4)	15.9(2)
Fe1	10129.7(8)	7689.5(7)	3330.9(5)	19.1(2)
P1	7188.1(15)	6722.5(12)	3361.7(9)	17.1(4)
P2	8018.1(15)	9029.2(12)	2302.8(9)	16.1(4)
C1	5260(6)	9344(5)	2417(3)	18.9(14)
C2	4743(6)	9331(5)	1800(3)	18.4(14)
C3	3974(6)	10139(5)	1524(3)	18.2(13)
C4	3690(6)	10943(5)	1840(4)	22.2(15)

C5	4191(6)	10920(5)	2473(3)	22.1(14)
C6	4975(6)	10134(5)	2755(3)	19.8(14)
C7	4955(6)	8445(5)	1442(3)	22.3(14)
C8	3661(7)	7896(5)	1483(4)	31.4(17)
C9	5624(7)	8710(5)	667(4)	28.6(16)
C10	2923(7)	11850(5)	1537(4)	28.1(16)
C11	2004(7)	11650(6)	1050(4)	31.5(17)
C12	3867(8)	12716(6)	1143(5)	47(2)
C13	5410(7)	10137(5)	3466(3)	23.2(15)
C14	4310(8)	9799(6)	4078(4)	36.9(19)
C15	5980(7)	11139(6)	3514(4)	31.0(17)
C16	8916(6)	6528(5)	3405(4)	19.2(14)
C17	9946(6)	6546(5)	2833(4)	20.1(14)
C18	11139(6)	6451(5)	3103(4)	24.3(15)
C19	10881(6)	6348(5)	3840(4)	22.3(15)
C20	9512(6)	6392(5)	4035(4)	22.0(14)
C21	9303(6)	8947(4)	2835(3)	17.6(13)
C22	10683(6)	8987(4)	2609(4)	21.4(14)
C23	11304(7)	8946(5)	3204(4)	27.0(16)
C24	10336(7)	8868(5)	3811(4)	29.3(17)
C25	9107(6)	8872(5)	3586(4)	21.0(14)
C26	6829(6)	5635(5)	2992(3)	18.9(14)
C27	7534(6)	4744(5)	3141(4)	22.9(15)
C28	7268(7)	3928(5)	2871(4)	26.8(16)
C29	6317(7)	3991(5)	2436(4)	30.2(17)
C30	5638(7)	4875(5)	2266(4)	27.0(16)
C31	5897(6)	5696(5)	2548(4)	22.5(15)
C32	6599(6)	6406(5)	4317(4)	21.1(14)
C33	6233(6)	7199(5)	4646(4)	23.4(15)
C34	5887(7)	7014(6)	5379(4)	33.7(18)
C35	5894(7)	6049(6)	5783(4)	34.2(18)
C36	6252(6)	5251(6)	5457(4)	27.0(16)
C37	6615(6)	5426(5)	4722(4)	22.3(15)
C38	8026(6)	10399(5)	1952(3)	20.4(14)
C39	8736(6)	11031(5)	2220(4)	24.6(15)
C40	8794(7)	12071(6)	1940(4)	33.5(18)
C41	8123(7)	12477(5)	1380(4)	32.6(18)
C42	7418(7)	11844(5)	1103(4)	29.7(17)
C43	7372(7)	10812(5)	1390(4)	26.5(16)
C44	8763(6)	8579(5)	1518(3)	19.4(14)
C45	9748(7)	9128(5)	1027(4)	24.6(15)
C46	10355(8)	8720(6)	470(4)	35.5(18)

C47	9997(7)	7805(6)	385(4)	30.5(17)
C48	9020(7)	7251(6)	867(4)	30.6(17)
C49	8398(6)	7639(5)	1431(4)	22.2(14)
C50	444(11)	4608(8)	1601(7)	76(4)
C51	1453(9)	4954(6)	975(6)	49(2)
C52	2523(9)	5553(7)	1009(5)	52(2)
C53	3467(10)	5819(7)	445(6)	55(3)
C54	3448(9)	5503(7)	-189(5)	47(2)
C55	2424(10)	4896(7)	-224(5)	54(2)
C56	1443(9)	4654(7)	361(5)	48(2)
C57	-2226(8)	2390(6)	4720(4)	35.7(18)
C58	-901(7)	2502(6)	4280(4)	31.0(17)
C59	-370(8)	1730(6)	3960(4)	37.1(19)
C60	847(8)	1834(6)	3549(5)	42(2)
C61	1546(8)	2737(7)	3441(5)	43(2)
C62	1028(7)	3492(6)	3752(4)	35.1(18)
C63	-179(7)	3372(6)	4176(4)	27.6(16)

Table S22. Anisotropic Displacement Parameters ($Å^2 \times 10^3$) for **9**. The Anisotropic displacement factor exponent takes the form: $-2\pi^2[h^2a^{*2}U_{11}+2hka^*b^*U_{12}+\ldots]$.

Atom	$\mathbf{U_{11}}$	$\mathbf{U_{22}}$	$\mathbf{U_{33}}$	$\mathbf{U_{23}}$	$\mathbf{U_{13}}$	$\mathbf{U_{12}}$
Br1	10.7(3)	22.6(4)	28.5(4)	2.3(3)	0.0(3)	-0.5(2)
Ni1	9.2(4)	16.5(4)	20.0(4)	-0.7(3)	-0.6(3)	0.6(3)
Fe1	11.8(5)	18.2(5)	27.0(5)	-4.0(4)	-3.4(4)	0.7(4)
P1	11.5(8)	16.8(8)	22.0(9)	-2.1(7)	-2.0(6)	0.3(6)
P2	10.9(8)	15.8(8)	19.8(9)	-1.5(7)	0.0(6)	0.4(6)
C1	9(3)	23(3)	24(4)	-6(3)	2(3)	-1(2)
C2	15(3)	18(3)	19(3)	-2(3)	2(3)	0(2)
C3	15(3)	21(3)	17(3)	-1(3)	-1(3)	1(3)
C4	8(3)	21(3)	33(4)	1(3)	0(3)	0(3)
C5	19(3)	27(4)	20(3)	-6(3)	-2(3)	8(3)
C6	10(3)	26(3)	24(4)	-8(3)	-1(3)	0(3)
C7	21(4)	27(4)	18(3)	-3(3)	-3(3)	0(3)
C8	35(4)	24(4)	36(4)	-12(3)	3(3)	-7(3)
C9	34(4)	24(4)	27(4)	-7(3)	-1(3)	8(3)
C10	18(4)	29(4)	35(4)	-3(3)	-6(3)	10(3)
C11	17(4)	34(4)	37(4)	3(3)	-3(3)	3(3)
C12	35(5)	26(4)	77(7)	11(4)	-28(5)	-5(3)
C13	22(4)	26(4)	22(4)	-6(3)	-3(3)	5(3)
C14	30(4)	53(5)	30(4)	-12(4)	-4(3)	-9(4)
C15	23(4)	37(4)	35(4)	-15(3)	-1(3)	-4(3)

C16	12(3)	18(3)	28(4)	-6(3)	-2(3)	3(2)
C17	18(3)	17(3)	25(4)	-7(3)	0(3)	4(3)
C18	12(3)	17(3)	41(4)	-1(3)	-2(3)	0(3)
C19	20(3)	12(3)	33(4)	1(3)	-10(3)	5(3)
C20	18(3)	16(3)	28(4)	4(3)	-2(3)	-2(3)
C21	16(3)	10(3)	26(4)	0(3)	-7(3)	0(2)
C22	15(3)	13(3)	34(4)	1(3)	-6(3)	1(2)
C23	14(3)	18(3)	48(5)	-4(3)	-7(3)	-3(3)
C24	33(4)	20(3)	39(4)	-8(3)	-14(3)	2(3)
C25	18(3)	18(3)	26(4)	-4(3)	-4(3)	5(3)
C26	16(3)	22(3)	17(3)	-3(3)	3(3)	-3(3)
C27	18(3)	21(3)	27(4)	-2(3)	-2(3)	2(3)
C28	19(4)	25(4)	33(4)	-5(3)	5(3)	1(3)
C29	30(4)	28(4)	34(4)	-11(3)	-1(3)	1(3)
C30	23(4)	33(4)	25(4)	-8(3)	-2(3)	-3(3)
C31	17(3)	22(3)	26(4)	-1(3)	1(3)	2(3)
C32	11(3)	28(4)	24(4)	-5(3)	-2(3)	0(3)
C33	19(3)	22(3)	28(4)	-2(3)	-5(3)	3(3)
C34	25(4)	49(5)	30(4)	-18(4)	0(3)	8(3)
C35	16(4)	58(5)	25(4)	-2(4)	-1(3)	-4(3)
C36	17(4)	39(4)	21(4)	4(3)	-4(3)	-4(3)
C37	12(3)	24(3)	27(4)	4(3)	-4(3)	-2(3)
C38	13(3)	20(3)	24(4)	-3(3)	5(3)	2(3)
C39	19(4)	23(4)	28(4)	-3(3)	3(3)	3(3)
C40	22(4)	30(4)	46(5)	-9(4)	5(3)	2(3)
C41	23(4)	21(4)	46(5)	-1(3)	9(3)	3(3)
C42	21(4)	29(4)	31(4)	8(3)	-1(3)	7(3)
C43	19(4)	29(4)	26(4)	2(3)	1(3)	0(3)
C44	18(3)	20(3)	21(3)	-5(3)	-2(3)	0(3)
C45	21(4)	26(4)	22(4)	-2(3)	6(3)	1(3)
C46	29(4)	45(5)	30(4)	-10(4)	8(3)	-5(3)
C47	24(4)	42(4)	25(4)	-15(3)	5(3)	6(3)
C48	32(4)	29(4)	33(4)	-13(3)	-2(3)	-1(3)
C49	19(3)	24(3)	23(4)	-6(3)	2(3)	-1(3)
C50	55(7)	50(6)	117(10)	-29(7)	18(7)	0(5)
C51	40(5)	29(4)	77(7)	-9(5)	-11(5)	0(4)
C52	51(6)	43(5)	64(6)	-24(5)	5(5)	-5(4)
C53	55(6)	41(5)	71(7)	-21(5)	-2(5)	-16(4)
C54	42(5)	49(5)	54(6)	-17(5)	-4(4)	-6(4)
C55	57(6)	58(6)	54(6)	-14(5)	-26(5)	6(5)
C56	40(5)	41(5)	66(6)	-10(5)	-15(5)	1(4)
C57	32(4)	47(5)	29(4)	-8(4)	-6(3)	-7(4)

C58	29(4)	36(4)	30(4)	-6(3)	-12(3)	5(3)
C59	31(4)	45(5)	38(5)	-10(4)	-10(4)	0(4)
C60	33(5)	37(5)	63(6)	-29(4)	-11(4)	10(4)
C61	23(4)	52(5)	55(6)	-20(4)	1(4)	4(4)
C62	27(4)	35(4)	44(5)	-8(4)	-8(4)	-4(3)
C63	27(4)	32(4)	27(4)	-10(3)	-10(3)	5(3)

Table S23. Bond Lengths for **9**.

Atom	**Atom**	**Length/Å**	**Atom**	**Atom**	**Length/Å**
Br1	Ni1	2.3509(10)	C22	C23	1.405(10)
Ni1	P1	2.3006(18)	C23	C24	1.425(11)
Ni1	P2	2.1712(17)	C24	C25	1.415(10)
Ni1	C1	1.956(6)	C26	C27	1.400(9)
Fe1	C16	2.019(6)	C26	C31	1.388(9)
Fe1	C17	2.036(6)	C27	C28	1.381(10)
Fe1	C18	2.059(7)	C28	C29	1.390(10)
Fe1	C19	2.074(6)	C29	C30	1.382(10)
Fe1	C20	2.040(6)	C30	C31	1.399(10)
Fe1	C21	2.014(6)	C32	C33	1.390(9)
Fe1	C22	2.041(6)	C32	C37	1.396(9)
Fe1	C23	2.079(7)	C33	C34	1.393(10)
Fe1	C24	2.059(7)	C34	C35	1.378(11)
Fe1	C25	2.019(6)	C35	C36	1.390(11)
P1	C16	1.825(6)	C36	C37	1.402(10)
P1	C26	1.854(7)	C38	C39	1.382(10)
P1	C32	1.838(7)	C38	C43	1.387(10)
P2	C21	1.805(6)	C39	C40	1.400(10)
P2	C38	1.840(6)	C40	C41	1.394(11)
P2	C44	1.836(7)	C41	C42	1.392(11)
C1	C2	1.400(9)	C42	C43	1.392(10)
C1	C6	1.384(9)	C44	C45	1.403(9)
C2	C3	1.401(9)	C44	C49	1.397(9)
C2	C7	1.519(9)	C45	C46	1.391(10)
C3	C4	1.375(9)	C46	C47	1.361(11)
C4	C5	1.410(10)	C47	C48	1.392(10)
C4	C10	1.512(9)	C48	C49	1.392(10)
C5	C6	1.395(9)	C50	C51	1.489(14)
C6	C13	1.529(9)	C51	C52	1.419(13)
C7	C8	1.543(10)	C51	C56	1.353(13)
C7	C9	1.540(9)	C52	C53	1.356(13)

C10	C11	1.518(10)	C53	C54	1.403(13)
C10	C12	1.547(10)	C54	C55	1.387(13)
C13	C14	1.528(10)	C55	C56	1.401(14)
C13	C15	1.530(10)	C57	C58	1.506(11)
C16	C17	1.426(9)	C58	C59	1.399(11)
C16	C20	1.439(9)	C58	C63	1.380(10)
C17	C18	1.416(9)	C59	C60	1.390(12)
C18	C19	1.405(10)	C60	C61	1.405(11)
C19	C20	1.424(9)	C61	C62	1.364(11)
C21	C22	1.439(9)	C62	C63	1.392(11)
C21	C25	1.435(9)			

Table S24. Bond Angles for **9**.

Atom	Atom	Atom	Angle/°	Atom	Atom	Atom	Angle/°
P1	Ni1	Br1	85.99(5)	C14	C13	C15	110.2(6)
P2	Ni1	Br1	174.43(6)	P1	C16	Fe1	121.6(3)
P2	Ni1	P1	99.51(6)	C17	C16	Fe1	70.0(4)
C1	Ni1	Br1	86.24(18)	C17	C16	P1	128.0(5)
C1	Ni1	P1	172.03(19)	C17	C16	C20	106.3(6)
C1	Ni1	P2	88.29(19)	C20	C16	Fe1	70.0(4)
C16	Fe1	C17	41.2(3)	C20	C16	P1	125.6(5)
C16	Fe1	C18	69.0(2)	C16	C17	Fe1	68.8(4)
C16	Fe1	C19	69.1(3)	C18	C17	Fe1	70.7(4)
C16	Fe1	C20	41.5(3)	C18	C17	C16	108.8(6)
C16	Fe1	C22	136.4(3)	C17	C18	Fe1	68.9(4)
C16	Fe1	C23	175.9(3)	C19	C18	Fe1	70.7(4)
C16	Fe1	C24	140.0(3)	C19	C18	C17	108.6(6)
C16	Fe1	C25	109.7(3)	C18	C19	Fe1	69.6(4)
C17	Fe1	C18	40.4(3)	C18	C19	C20	107.9(6)
C17	Fe1	C19	67.7(3)	C20	C19	Fe1	68.5(3)
C17	Fe1	C20	68.5(3)	C16	C20	Fe1	68.5(4)
C17	Fe1	C22	110.5(3)	C19	C20	Fe1	71.0(4)
C17	Fe1	C23	138.5(3)	C19	C20	C16	108.5(6)
C17	Fe1	C24	178.6(3)	P2	C21	Fe1	127.5(3)
C18	Fe1	C19	39.7(3)	C22	C21	Fe1	70.2(3)
C18	Fe1	C23	113.2(3)	C22	C21	P2	128.5(5)
C19	Fe1	C23	114.8(3)	C25	C21	Fe1	69.4(3)
C20	Fe1	C18	67.8(3)	C25	C21	P2	124.7(5)
C20	Fe1	C19	40.5(3)	C25	C21	C22	106.7(6)
C20	Fe1	C22	177.8(3)	C21	C22	Fe1	68.2(4)

C20	Fe1	C23	142.2(3)	C23	C22	Fe1	71.5(4)
C20	Fe1	C24	113.0(3)	C23	C22	C21	108.5(6)
C21	Fe1	C16	107.4(3)	C22	C23	Fe1	68.6(4)
C21	Fe1	C17	110.0(3)	C22	C23	C24	108.4(6)
C21	Fe1	C18	140.0(3)	C24	C23	Fe1	69.1(4)
C21	Fe1	C19	176.6(3)	C23	C24	Fe1	70.6(4)
C21	Fe1	C20	136.6(3)	C25	C24	Fe1	68.2(4)
C21	Fe1	C22	41.6(2)	C25	C24	C23	108.0(6)
C21	Fe1	C23	68.6(3)	C21	C25	Fe1	69.0(4)
C21	Fe1	C24	69.1(3)	C24	C25	Fe1	71.2(4)
C21	Fe1	C25	41.7(3)	C24	C25	C21	108.4(6)
C22	Fe1	C18	112.8(3)	C27	C26	P1	119.9(5)
C22	Fe1	C19	141.3(3)	C31	C26	P1	121.2(5)
C22	Fe1	C23	39.9(3)	C31	C26	C27	118.9(6)
C22	Fe1	C24	68.1(3)	C28	C27	C26	120.3(6)
C24	Fe1	C18	139.6(3)	C27	C28	C29	120.4(7)
C24	Fe1	C19	113.2(3)	C30	C29	C28	120.1(7)
C24	Fe1	C23	40.3(3)	C29	C30	C31	119.4(7)
C25	Fe1	C17	139.4(3)	C26	C31	C30	120.9(6)
C25	Fe1	C18	178.0(3)	C33	C32	P1	117.4(5)
C25	Fe1	C19	138.5(3)	C33	C32	C37	119.9(6)
C25	Fe1	C20	110.2(3)	C37	C32	P1	122.5(5)
C25	Fe1	C22	69.2(3)	C32	C33	C34	120.0(7)
C25	Fe1	C23	68.2(3)	C35	C34	C33	120.6(7)
C25	Fe1	C24	40.6(3)	C34	C35	C36	119.8(7)
C16	P1	Ni1	125.4(2)	C35	C36	C37	120.3(7)
C16	P1	C26	100.2(3)	C32	C37	C36	119.4(7)
C16	P1	C32	98.0(3)	C39	C38	P2	120.6(5)
C26	P1	Ni1	112.9(2)	C39	C38	C43	118.7(6)
C32	P1	Ni1	110.6(2)	C43	C38	P2	120.6(5)
C32	P1	C26	107.7(3)	C38	C39	C40	121.4(7)
C21	P2	Ni1	114.6(2)	C41	C40	C39	119.3(7)
C21	P2	C38	99.4(3)	C42	C41	C40	119.6(7)
C21	P2	C44	104.1(3)	C41	C42	C43	120.1(7)
C38	P2	Ni1	122.6(2)	C38	C43	C42	120.9(7)
C44	P2	Ni1	112.4(2)	C45	C44	P2	121.4(5)
C44	P2	C38	101.3(3)	C49	C44	P2	119.2(5)
C2	C1	Ni1	119.5(5)	C49	C44	C45	119.3(6)
C6	C1	Ni1	120.7(5)	C46	C45	C44	119.4(7)
C6	C1	C2	119.7(6)	C47	C46	C45	121.4(7)
C1	C2	C3	119.0(6)	C46	C47	C48	120.0(7)
C1	C2	C7	121.4(6)	C49	C48	C47	120.0(7)

C3	C2	C7	119.6(6)	C48	C49	C44	120.1(6)
C4	C3	C2	122.8(6)	C52	C51	C50	121.5(10)
C3	C4	C5	117.0(6)	C56	C51	C50	121.7(9)
C3	C4	C10	124.1(6)	C56	C51	C52	116.6(9)
C5	C4	C10	118.9(6)	C53	C52	C51	120.8(10)
C6	C5	C4	121.6(6)	C52	C53	C54	122.1(9)
C1	C6	C5	120.0(6)	C55	C54	C53	117.7(9)
C1	C6	C13	121.7(6)	C54	C55	C56	119.0(9)
C5	C6	C13	118.1(6)	C51	C56	C55	123.7(9)
C2	C7	C8	110.6(5)	C59	C58	C57	120.9(7)
C2	C7	C9	114.9(6)	C63	C58	C57	121.1(7)
C9	C7	C8	109.4(6)	C63	C58	C59	118.0(7)
C4	C10	C11	114.4(6)	C60	C59	C58	121.1(8)
C4	C10	C12	109.4(6)	C59	C60	C61	119.5(7)
C11	C10	C12	109.9(6)	C62	C61	C60	119.5(8)
C6	C13	C15	114.5(6)	C61	C62	C63	120.6(7)
C14	C13	C6	111.1(6)	C58	C63	C62	121.3(7)

SXI. References

1. Evans, D. F. 400. The Determination of the Paramagnetic Susceptibility of Substances in Solution by Nuclear Magnetic Resonance. *J. Chem. Soc.* **1959**, 2003-2005.

2. Melvin, P. R.; Nova, A.; Balcells, D.; Dai, W.; Hazari, N.; Hruszkewycz, D. P.; Shah, H. P.; Tudge, M. T. Design of a Versatile and Improved Precatalyst Scaffold for Palladium-Catalyzed Cross-Coupling: $(\eta^3\text{-1-}^t\text{Bu-indenyl})_2(\mu\text{-Cl})_2\text{Pd}_2$. *ACS Catal.* **2015**, *5*, 3680-3688.

3. (a) Kuroda, J.-i.; Inamoto, K.; Hiroya, K.; Doi, T. N-Heterocyclic Carbene Derived Nickel–Pincer Complexes: Efficient and Applicable Catalysts for Suzuki–Miyaura Coupling Reactions of Aryl/Alkenyl Tosylates and Mesylates. *Eur. J. Org. Chem.* **2009**, *2009*, 2251-2261; (b) Ackermann, L.; Gschrei, C. J.; Althammer, A.; Riederer, M. Cross-Coupling Reactions of Aryl and Vinyl Chlorides Catalyzed by a Palladium Complex Derived From an Air-Stable *H*-Phosphonate. *Chem. Commun.* **2006**, 1419-1421.

4. (a) Quasdorf, K. W.; Antoft-Finch, A.; Liu, P.; Silberstein, A. L.; Komaromi, A.; Blackburn, T.; Ramgren, S. D.; Houk, K. N.; Snieckus, V.; Garg, N. K. Suzuki-Miyaura Cross-Coupling of Aryl Carbamates and Sulfamates: Experimental and Computational Studies. *J. Am. Chem. Soc.* **2011**, *133*, 6352-6363; (b) Quasdorf, K. W.; Riener, M.; Petrova, K. V.; Garg, N. K. Suzuki-Miyaura Coupling of Aryl Carbamates, Carbonates, and Sulfamates. *J. Am. Chem. Soc.* **2009**, *131*, 17748-17749; (c) Giffin, N. A.; Makramalla, M.; Hendsbee, A. D.; Robertson, K. N.; Sherren, C.; Pye, C. C.; Masuda, J. D.; Clyburne, J. A. C. Anhydrous TEMPO-H: Reactions of a Good Hydrogen Atom Donor with Low-Valent Carbon Centres. *Org. Biomol. Chem.* **2011**, *9*, 3672-3680.

5. Jin, D.; Schmeier, T. J.; Williard, P. G.; Hazari, N.; Bernskoetter, W. H. Lewis Acid Induced β-Elimination from a Nickelalactone: Efforts toward Acrylate Production from CO_2 and Ethylene. *Organometallics* **2013**, *32*, 2152-2159.

6. Stoll, S.; Schweiger, A. EasySpin, A Comprehensive Software Package for Spectral Simulation and Analysis in EPR. *J. Magn. Reson.* **2006**, *178*, 42-55.

7. Tasker, S. Z.; Standley, E. A.; Jamison, T. F. Recent Advances in Homogeneous Nickel Catalysis. *Nature* **2014**, *509*, 299-309.

8. Mohadjer Beromi, M.; Nova, A.; Balcells, D.; Brasacchio, A. M.; Brudvig, G. W.; Guard, L. M.; Hazari, N.; Vinyard, D. J. Mechanistic Study of an Improved Ni Precatalyst for Suzuki–Miyaura Reactions of Aryl Sulfamates: Understanding the Role of Ni(I) Species. *J. Am. Chem. Soc.* **2017**, *139*, 922-936.

9. Zhao, Q.; Li, C.; Senanayake, C. H.; Tang, W. An Efficient Method for Sterically Demanding Suzuki–Miyaura Coupling Reactions. *Chem. Eur. J.* **2013**, *19*, 2261-2265.

10. Pilloni, G.; Toffoletti, A.; Bandoli, G.; Longato, B. Homoleptic Complexes of Cobalt(0) and Nickel(0,I) with 1,1'-Bis(diphenylphosphino)ferrocene (dppf): Synthesis and Characterization. *Inorg. Chem.* **2006**, *45*, 10321-10328.

11. Yin, G.; Kalvet, I.; Englert, U.; Schoenebeck, F. Fundamental Studies and Development of Nickel-Catalyzed Trifluoromethylthiolation of Aryl Chlorides: Active Catalytic Species and Key Roles of Ligand and Traceless MeCN Additive Revealed. *J. Am. Chem. Soc.* **2015**, *137*, 4164-4172.

12. Zweier, J. L.; Kuppusamy, P. Electron Paramagnetic Resonance Measurements of Free Radicals in the Intact Beating Heart: A Technique for Detection and Characterization of Free Radicals in Whole Biological Tissues. *Proc. Natl. Acad. Sci. U.S.A.* **1988**, *85*, 5703-5707.

13. Mohadjer Beromi, M.; Nova, A.; Balcells, D.; Brasacchio, A. M.; Brudvig, G. W.; Guard, L. M.; Hazari, N.; Vinyard, D. J. Mechanistic Study of an Improved Ni Precatalyst for Suzuki–

Miyaura Reactions of Aryl Sulfamates: Understanding the Role of Ni(I) Species. *J. Am. Chem. Soc.* **2017**, *139*, 922-936.
14. Weix, D. J. Methods and Mechanisms for Cross-Electrophile Coupling of Csp^2 Halides with Alkyl Electrophiles. *Acc. Chem. Res.* **2015**, *48*, 1767-1775.
15. Sheldrick, G. M. A Short History of SHELX. *Acta Cryst.* **2008**, *A64*, 112-122.